DEVELOPMENT OF Mg BASED NANOCOMPOSITES WITH IMPROVED PROPERTIES

Ph.D. Thesis

Priyanka Meena
ID: 2014RMT9510

DEPARTMENT OF METALLURGICAL AND MATERIALS ENGINEERING
MALAVIYA NATIONAL INSTITUTE OF TECHNOLOGY JAIPUR

March 2019

DEVELOPMENT OF Mg BASED NANOCOMPOSITES WITH IMPROVED PROPERTIES

Submitted in
fulfillment of the requirements for the degree of

Doctor of Philosophy

by

Priyanka Meena
(2014RMT9510)

Under the Supervision of

Dr. V. K. Sharma
MNIT Jaipur

Dr. Ramvir Singh
UoR Jaipur

DEPARTMENT OF METALLURGICAL AND MATERIALS ENGINEERING
MALAVIYA NATIONAL INSTITUTE OF TECHNOLOGY JAIPUR

March 2019

This thesis is dedicated to

My Father: Late O.P. Meena

My Mother: Smt. Nirmala Meena

My Husband: Mr. Ravindra Kumar Meena

My Brothers: Mr. Ravi Meena and Mr. Rohit Meena

DECLARATION

I, **Priyanka Meena**, declare that this thesis titled, **"Development of Mg based nanocomposites with improved properties"** and the work presented in it are my own. I confirm that:

- This work was done wholly or mainly while in candidature for a research degree at this institution.
- Where any part of this thesis has previously been submitted for a degree or any other qualification at this institution or any other university, this has been clearly stated.
- Where I have consulted the published work of others, this is always clearly attributed.
- Where I have quoted from the work of others, the source is always given. With the exception of such quotations, this thesis is entirely my own work.
- I have acknowledged all main sources of help.
- Where the thesis is based on work done by myself, jointly with others, I have made clear exactly what was done by others and what I have contributed myself.

Date: **Priyanka Meena**
(2014RMT9510)

CERTIFICATE

This is to certify that the thesis entitled **"Development of Mg Based Nanocomposites with Improved Properties"** being submitted by **Ms. Priyanka Meena (2014RMT9510)** is a bonafide research work carried out under my supervision and guidance in fulfillment of the requirement for the award of the degree of **Doctor of Philosophy** in the Department of **Metallurgical and Materials Engineering,** Malaviya National Institute of Technology, Jaipur, India. The matter embodied in this thesis is original and has not been submitted to any other University or Institute for the award of any other degree.

Dr. Ramvir Singh
Associate Professor
Deptt. of Physics
UoR, Jaipur, India

Dr. V. K. Sharma
Associate Professor & HOD
Deptt. of Met. & Mats. Engg.
MNIT, Jaipur, India

Place: Jaipur

Date:

ACKNOWLEDGEMENT

I find words falling short in expressing the multitude of ever flowing gratitude to my supervisors **Dr. V.K. Sharma** and **Dr. Ramvir Singh** for their impetus, able and continual guidance throughout the research work, without their constant support and encouragements, completion of the thesis would not have been possible. I am grateful to **Prof. I.P. Jain**, Center for non-conventional energy resources, UoR, Jaipur who has been a constant source of inspiration for me. Besides helping me in experimental work, his constructive criticism has helped me compile my work in the present form and also thankful to **Prof. Mridula Jain,** Punjab University Chandigarh for helping me in improving the language of my thesis. I would like to express my sincere thanks to **Dr. Sumanta Kumar Meher, Dr. Ajaya Kumar Pradhan and Prof. Awadhesh Kumar Bhardwaj** for being in my DREC committee as well as for their encouragement, analytical insights and recommendations. I further extend my thanks to all the staff members of **Materials Research Center (MNIT Jaipur), ACMS (IIT Kanpur) and IIT Jodhpur** for providing characterization facilities. Thanks are also due to the **Director DMRL, Hyderabad** for providing material processing facility. I express my deep appreciation to my friends and co-workers **Dr. Mukesh Jangir, Mr. Arun Kumar, Mr. Devesh Kumar, Mr. Ankit Goyal, Ms. Nitika Khundan,** and all the post graduate students of the department of Metallurgical and Materials Engineering, MNIT Jaipur for their moral support and help. I would like to extend my sincere thanks to all the faculty and staff members of MNIT, Jaipur for their support during my Ph.D. I would like to thank **my dear mother, my husband Mr. Ravindra Kumar Meena, my elder brothers and my other family members** for their unconditional support. Last but not least, I would like to thank God Almighty, my Lord for giving me the will power and strength to make this far when I didn't see a light. Without him, this thesis would have not been possible.

Priyanka Meena

ABSTRACT

Hydrogen energy has established itself as the fuel of 21st century as its combustion does not lead to pollution. A lot of work is in progress all over the world for hydrogen production, storage and applications. Among different metal hydrides, magnesium hydrides are considered as an important class of materials for hydrogen storage. Magnesium is used because it is the most promising material for hydrogen storage. However, magnesium is not practicable for applications due to its slow hydrogenation/dehydrogenation kinetics and high thermodynamic stability (ΔH= -75 kJ/mol).

In the present thesis, four nanocomposites-MgH_2-x wt% $La_{23}Nd_{7.8}Ti_{1.1}Ni_{33.9}Co_{32.9}Al_{0.65}$, MgH_2-xwt%FeTi, MgH_2-xwt%NiMnAl and MgH_2-xwt% $NiMn_{9.3}Al_{4.0}Co_{14.1}Fe_{3.6}$ have been examined. The effect of these alloys has been studied for hydrogenation/dehydrogenation kinetics of MgH_2. All types of alloys were prepared by arc-melting method in argon atmosphere. Nanocomposites were mechanically milled for 10 hrs at 300 rpm under 0.1 MPa argon pressure. Different characterization studies like XRD, SEM, EDS, TGA and DSC have been carried out.

Hydrogen sorption properties of MgH_2- xwt% $La_{23}Nd_{8.5}Ti_{1.1}Ni_{33.9}Co_{32.9}Al_{0.65}$ (x=10, 25 & 50) nanocomposites resulted insignificant reduction in onset temperature of desorption. A reduction in activation energy by 98 kJ/mol has been observed for the addition of x=25 wt% of $La_{23}Nd_{8.5}Ti_{1.1}Ni_{33.9}Co_{32.9}Al_{0.65}$, which improves hydrogen storage capacity. TGA studies have revealed higher desorption temperature for milled MgH_2 as compared to MgH_2-xwt% FeTi. Activation energy was found to be 177.90, 215.69, 162.46 and 87.93 kJ/mol for milled MgH_2 and MgH_2-x wt% FeTi (10, 25 &50) nanocomposites, respectively. It indicates 89.97 kJ/mol reduction in activation energy for 50 wt% FeTi additives which results in an improvement in hydrogen storage capacity. DSC studies have shown that by increasing the concentration of NiMnAl in MgH_2 from 25 to 50 wt%, onset temperature of hydrogen absorption decreases by about 40°C.Onset temperature as low as 180°C was observed for MgH_2–50wt% $NiMn_{9.3}Al_{4.0}Co_{14.1}Fe_{3.6}$ nanocomposites which is about 80°C lower than that of the as-milled MgH_2 giving 131.34 KJ/mol activation energy. Structural analysis has shown tetragonal, orthorhombic and monoclinic phases for MgH_2, $Al_{60}Mn_{11}Ni_4$ and

Mg_2NiH_4, respectively. DSC studies have revealed a single broad exothermic peak in the temperature range 48°C– 353°C after the addition of $NiMn_{9.3}Al_{4.0}Co_{14.1}Fe_{3.6}$ in MgH_2. The results of present studies for hydrogen storage for such types of nanocomposites have been found to be better than previous ones. It is a step forward in the usage of hydrogen energy for stationary and mobile applications.

CONTENTS

LIST OF TABLES

LIST OF FIGURES

LIST OF ABBREVIATIONS

BM	Ball Milling
BPR	Ball-to-Powder Mass-Charge Ratio
wt%	Weight Percent
TM	Transition Metal
H	Hour
H/M	Hydrogen/Metal
MA	Mechanical Alloying
Mm	Mischmetal
Mg	Magnesium
MgH_2	Magnesium Hydride
RT	Room Temperature
XRD	X-Ray Diffraction
SEM	Scanning Electron Microscope
EDS	Energy Dispersive X-ray Spectroscopy
BSE	Back Scattered Electron
TGA	Thermogarvimetric Analysis
DTA	Differential Thermal Analysis
DSC	Differential Scanning Calorimetry
PCI	Pressure-Composition-Isotherms
HCS	Hydriding Combustion Synthesis
RS	Rapid Solidification

Chapter-1

INTRODUCTION

The Hydrogen became interesting in the means of environmental concerns because of the fossil fuels detrimental emission. A call for more proficient energy source also has amplified the various technologies for use of hydrogen such as in hydrogen fuel cells or hydrocarbons as a fuel. This chapter represents the numerous benefits of hydrogen as an energy prime.

1.1 Why Hydrogen

Based on the literature and facts, the abundance of hydrogen element in the universe is high (~75 at. %) with good properties such as non toxicity and high volatility. However, it is less in the earth's atmosphere but available in the huge amount in the form of chemically bound H_2O [1-3]. Hydrogen atom has only one electron and one proton, being the first element in the periodic table. It exists in molecular H_2 form in nature, as a gas but can be liquefied and solidified at 14K and 21K respectively. Solid hydrogen behaves as molecular insulator and can be transforming into atomic solid at high pressure which is simple metal. For production of energy, hydrogen can be utilized as a gas or liquid or in the form of solid hydrocarbons. Dissociation of H_2O or solid hydrocarbon can release hydrogen which may be used to produce synthetic fuels. Nuclear fission and fusion processes produce enormous amount of energy.

It was observed that the chemical energy of hydrogen per unit mass (142 $MJKG^{-1}$) found to be three time higher than any other chemically derived fuel such as, liquid hydrocarbons (47 $MJKG^{-1}$).Hydrogen obtained, as a synthetic clean fuel while burned with oxygen. This leads the highly exothermic reaction i.e. oxidation reaction of hydrogen, which has two leading benefits over traditional processes. First, a clean nontoxic fuel combustion i.e. no production of CO_2 while use of air-hydrogen mixture. Second, the gain of high energy per electron due to higher ratio of

nucleon over electrons, which leads high energy per unit mass for hydrogen. Despite having tremendous advantages, hydrogen not going to be used for energy application now days. The main hurdle in the use of hydrogen currently is its production and storage, which needs further research to overcome these problems.

1.2 Where will Hydrogen Come From?

Deficiency of energy and increase of environmental degradation have gained our attention towards the energy crisis in near future.

Hydrogen is a considerable energy source over the conventional fuel present in, harvested from natural resources, and identified as potential energy source for various ecofriendly technologies. However, there is discrepancy in the occurrence of hydrogen in the environment. Since the production of hydrogen by Fujishima and Honda in 1972, using photocatalytic water splitting by supply of electric current to water, hydrogen became a prominent future for energy applications. However, the production of hydrogen using this technique is limited yet, due to small-scale production. Unfortunately, there is yet a need of cost effective and economical process for the large-scale production of hydrogen. Presently, the half of the production of hydrogen is from gasification and thermos-catalytic reaction of natural gases, which are the precursor materials.

The next largest resources for the production of hydrogen are heavy oils, naphtha and coal. The occurrence of these natural resources shown in figure 1.1. Ultimately, water is the most and largest source for the production of hydrogen and used for the production of gas using fossil fuel during the process called, stream reforming.

Following reaction shows the production of half to total hydrogen obtained from natural resources:-

$$3CH_4 + 6H_2O \rightarrow 12\ H_2 + 3CO_2 \qquad (1.1)$$

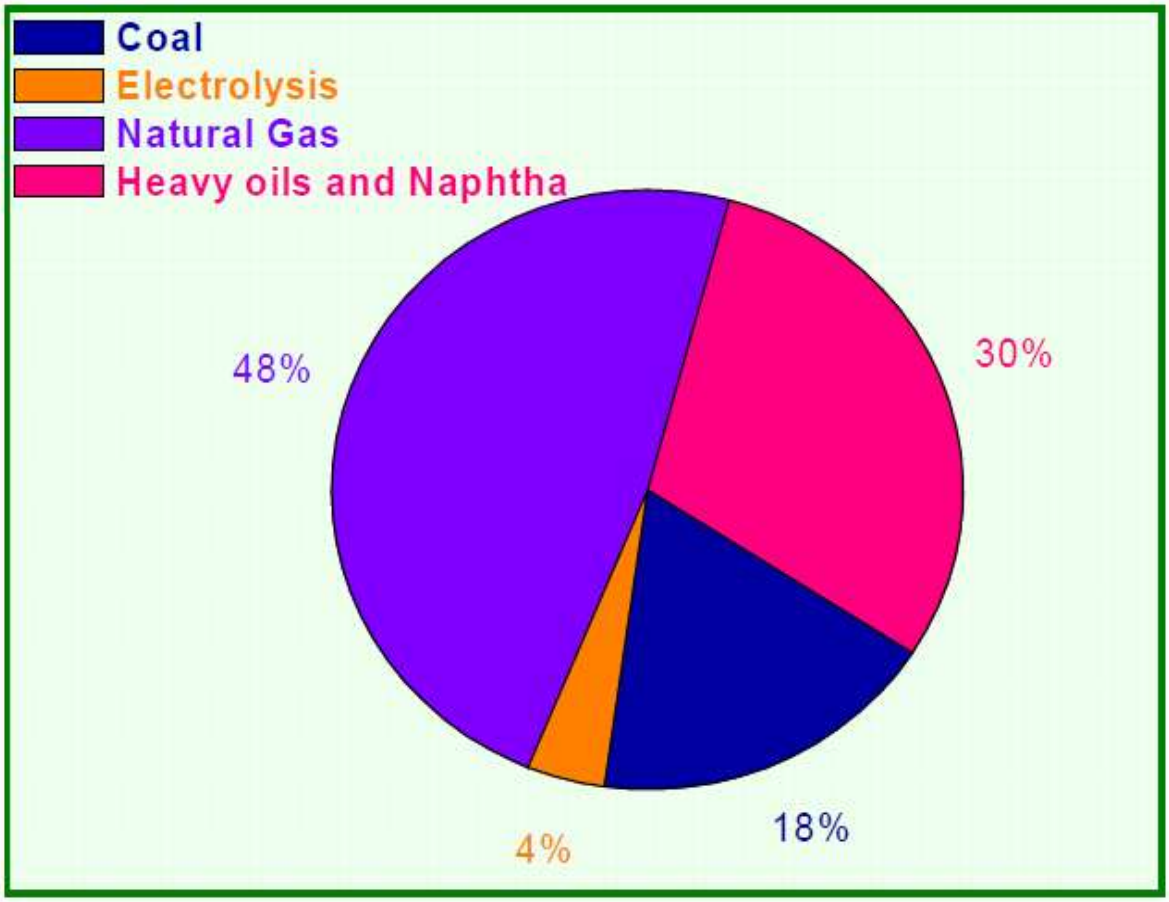

Figure 1.1 – Sources of global energy

Figure 1.2 states that the wind and biomass, out of numerous energy sources, are the least expensive sources of energy generation [4].Thus, it would be similar cost pattern for the production of hydrogen by direct electrolysis. The study of biological production of hydrogen is on top recently. Certain types of green algae yield hydrogen in the occurrence of sunlight (biologists have known of these algae for some time).

In 2001, researchers used spinach plant to produce hydrogen by manipulating photosynthetic process but resulted the immature laboratory experiments. Intense study continues to a better thoughtful of the way to improve these hydrogen production methods [5].

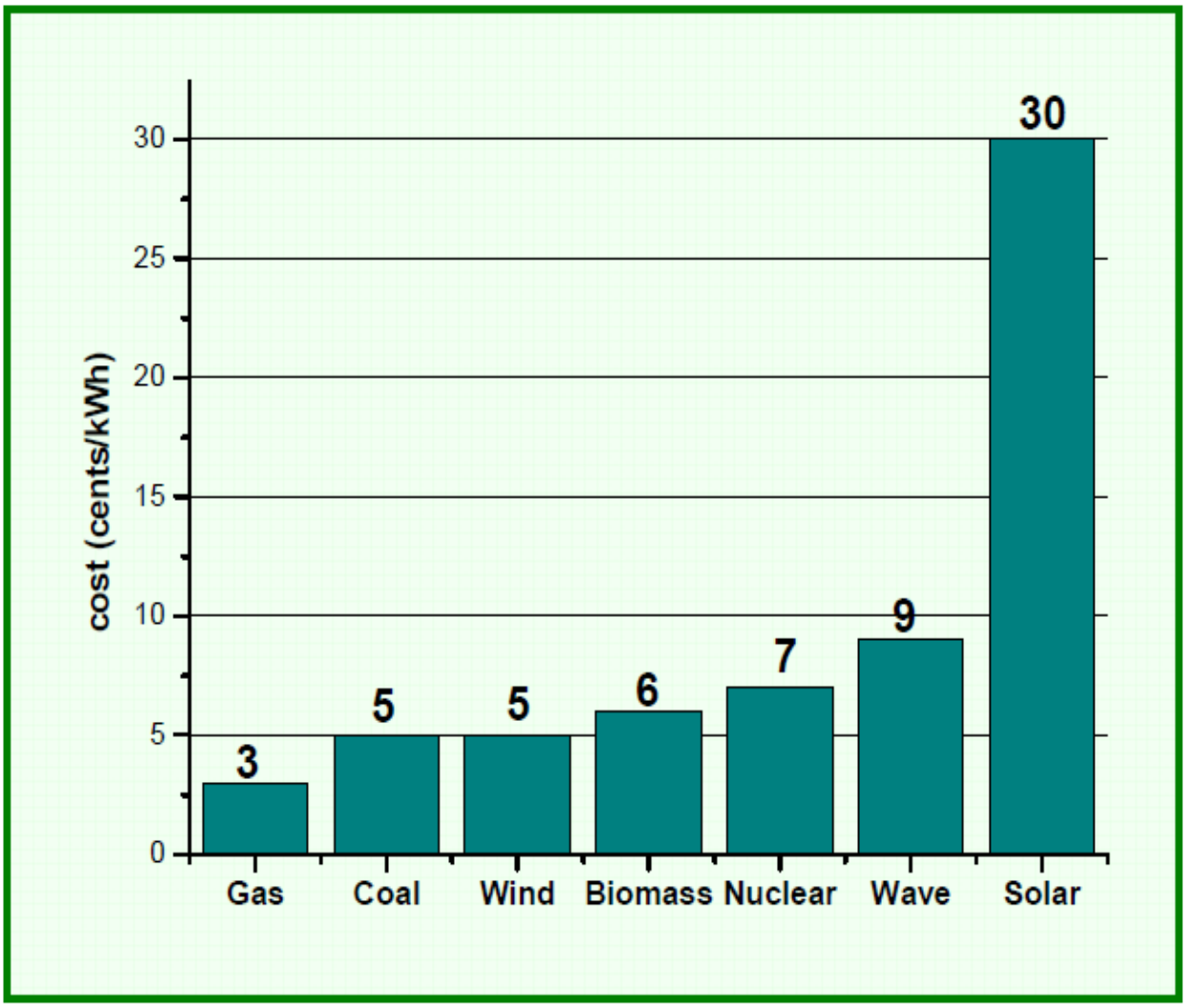

Figure 1.2 – Typical costs for electricity generation

Hydrogen thus formed can be utilized as compressed or as liquid hydrogen stored in appropriate containers for use on-board the vehicles, or hydrogen can be used in the form metal/compound hydrides or as adsorbed hydrogen gas on solids.

It can also be produced by decomposition or reaction of hydrogen containing species on-board. Even though each technique requires characteristics, none of these methods satisfies all the necessities with respect to proficiency, size, weight, cost, and safety for passage usages. The next section deals with the process of hydrogen storage in different forms.

1.3 Hydrogen Storage Technologies

1.3.1 Liquid hydrogen

Hydrogen can be liquefied with 11 $KWhKg^{-1}$ energy [10], which is 28% of total energy content of hydrogen. The liquid hydrogen can be stored and, in fact, has been effectively used as fuel in space technology. In the past many years, liquid hydrogen been used in the space technology as a fuel [9].

The gravimetric energy density of liquid hydrogen involved the storage container is about 25.9 wt% (13.8 KWh/Kg) and the volumetric energy density about 2760 KWh/m^3 [11]. The advances in insulation techniques and pressurization of the vessel will mark these statistics to some extent [12].The storing containers lose energy owing to boiling hydrogen that is triggered by thermal conductivity. The boil-off losses differ from 0.06% per day of large vessels to 3% per day of small vessels [13].The boil-off losses can be compact over proper insulation.

1.3.3 Metallic hydrides

Storage of hydrogen as gas (under pressure) or as liquid involve some physical difficulties and may be hazardous at times. Hence the study of metal hydrides becomes an option. Many intermetallic elements absorb large quantity of hydrogen gas when exposed to it at definite pressure and temperature.

The hydrogen atoms dispersed through the intermetallic lattice and form corresponding metallic hydrides (viz. intermetallic).This hydrogen can be released under specific conditions and can be utilized for energy production. However, appropriate intermetallic matrix must be proficient in absorbing and releasing hydrogen.

1.3.4 Complex hydrides

A certain number of transition metals produce hydrides with some elements of sets IA and IIA in the periodic table. The transition metals stabilize the composite of hydrogen. For instance,

Mg_2NiH_4 is made while Mg territories two electrons to the $[NiH4]^{-4}$ complex. The first entirely categorized member was K_2ReHg, which was described in 1964 [14].

The kinetics of hydride multiplexes inclines to be gentler as compared to the outdated interstitial hydrides subsequently the decomposition and formation of the hydride complex, involves some metal diffusion. Hydrogen desorption furthermore needed, typically, a high temperature above 150˚C. In spite of these drawbacks, the lager hydrogen volume marks such materials as potential applicant for hydrogen storage. For instance, the extreme capability of Mg_2FeH_6 is 5.5 wt% [15]. Also, some non-transition metals form complex hydrides. These contain, for instance, alterable two-step reaction of $NaAlH_4$ [15, 16]:

$$NaAlH_4 \leftrightarrow 1/3\ Na_3AlH_6 + 2/3\ Al + H_2 \leftrightarrow NaH + Al + 3/2\ H_2 \qquad (1.5)$$

The maximum hydrogen capability of this reaction is 5.6 wt%. Efforts have also been made to improve the hydrogen reversibility NaAlH by ball milling with or without additives [17, 18].

1.3.5 Hydrogen in carbon structures

Hydrogen could be stored as molecular hydrogen in single wall or multiwall nanotubes by chemisorptions or physisorption. The trapping of hydrogen by such nanomaterials are still rare and needs to be investigated [19, 20], however, density function calculations have given insights into the mechanisms involved [19,21].

The advantages of hydrogen storage in carbon nanotubes are comparable to that in complex hydrides where one can store more hydrogen by weight percentage as compared to in metal hydrides. Moreover, the hydrogen absorption/desorption kinetics in nano-phase resources are better than complex hydrides with kinetics a like to metal hydride. Carbon nano-tubes are predictable to store somewhere from 4.2 % to 65% of their own weight of hydrogen.

Considerable interest has arisen on recent reports over the use of carbon nano-fibers [22] and carbon nano-tubes [23] now the anticipation appears to have calmed down to some extent

[24].Other forms may also be considered for hydrogen storage resolution, like graphite nanofibers [22],fullerenes[15,25] and actuated carbon. Between these choices, hydrogen storage properties of high surface area activated carbon have been widely studied [23, 26].

1.3.6 Zeolites

Zeolites are naturally occurring microporous inorganic compounds and form a candidate for hydrogen storage just like the carbon nanotubes. The pore size in zeolites is 0.3-1.0 nm and hydrogen molecules can diffuse in if the temperature and pressure are increased. However, most of pores are smaller than the kinetic size of a hydrogen molecule which renders zeolites mostly insufficient for H_2 storage [27, 28].

The hydrogen storage capacity of zeolites is quite poor and cyclic stability of zeolites also has not been studied much 0.1-0.8 wt % of hydrogen is absorbed at high temperature and pressure (200-300˚C; 100-600 Bar). Ernst et al [28] suggested that a potential in zeolites might exist if there is modification in synthesis techniques. However, this is yet to be observed.

1.3.7 Glass Spheres

Hollow glass spheres of diameter 25µm to 500 µm and with a wall thickness of about 1 µm are permeable to hydrogen at high temperature of 200-400˚C and pressure 200-490 bar [30]. The hydrogen remains trapped inside the spheres even after cooling to ambient temperature.

The storage capacity of spheres is about 5-6 wt% .This trapped hydrogen can be released by heating the spheres or by crushing them. There is always a risk of accidental crushing if not controlled properly. This makes the glass spheres as storage option non feasible.

1.4 Metal Hydride

Although there is a number of approaches for hydrogen storage as deliberated in the earlier section, the most applied method for on board application is ‘Metal Hydride’.

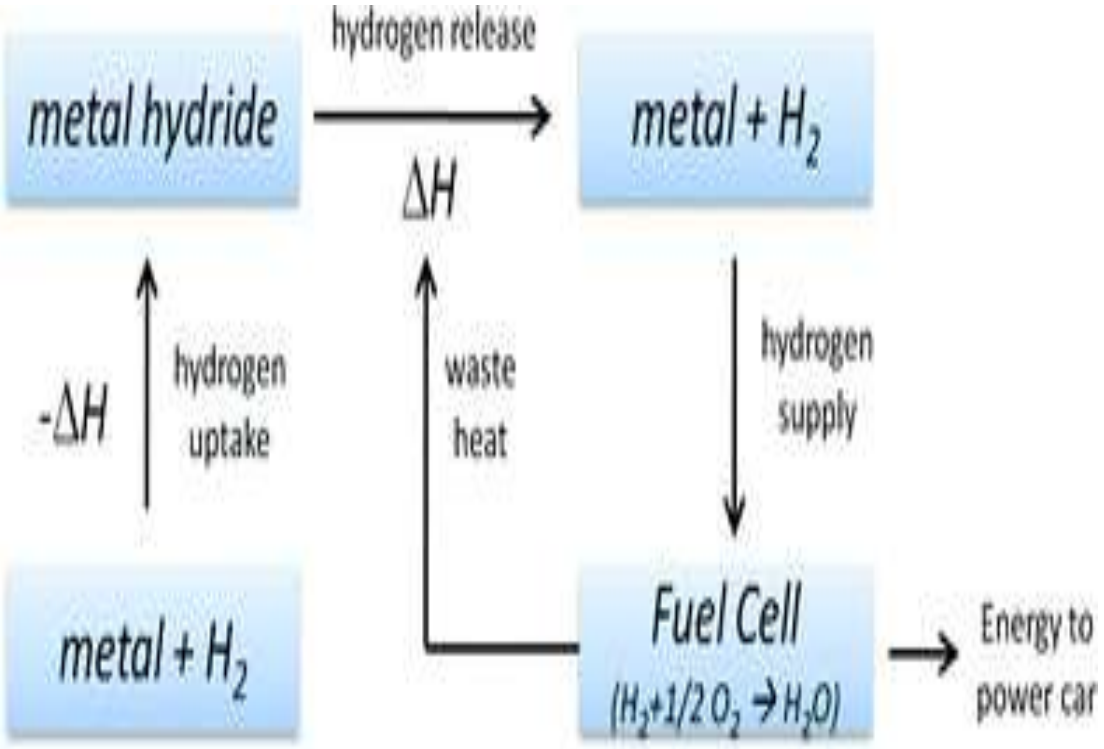

Figure1.3. Principle of a metal hydride tank for the reversible storage of hydrogen[36]

Adsorption of Hydrogen to form metal hydride is an exothermic reaction. In a fuel cell this heat is utilized to release hydrogen from the hydride on demand.

Formation of metal hydride

Metal hydrides are typically formed by simply exposing the metal to hydrogen gas. Hydride development is represented by the following equation:

$$M_{solid} + X/2H_2 \leftrightarrow MH_{x(solid)} + Heat\ (\beta phase)$$

Where M = Metal element or alloy

x=ratio of hydrogen to metal

When hydrogen is introduced, molecular hydrogen is detached at the metal surface into atomic hydrogen. The atomic hydrogen then dissolves in the crystal lattice of the metal to form a solid

solution (α phase). Further growth in hydrogen pressure above the substrate lead to more dissolved hydrogen. There is, then formation of β-phase, due to nucleation, and growth of hydride and of lattice.

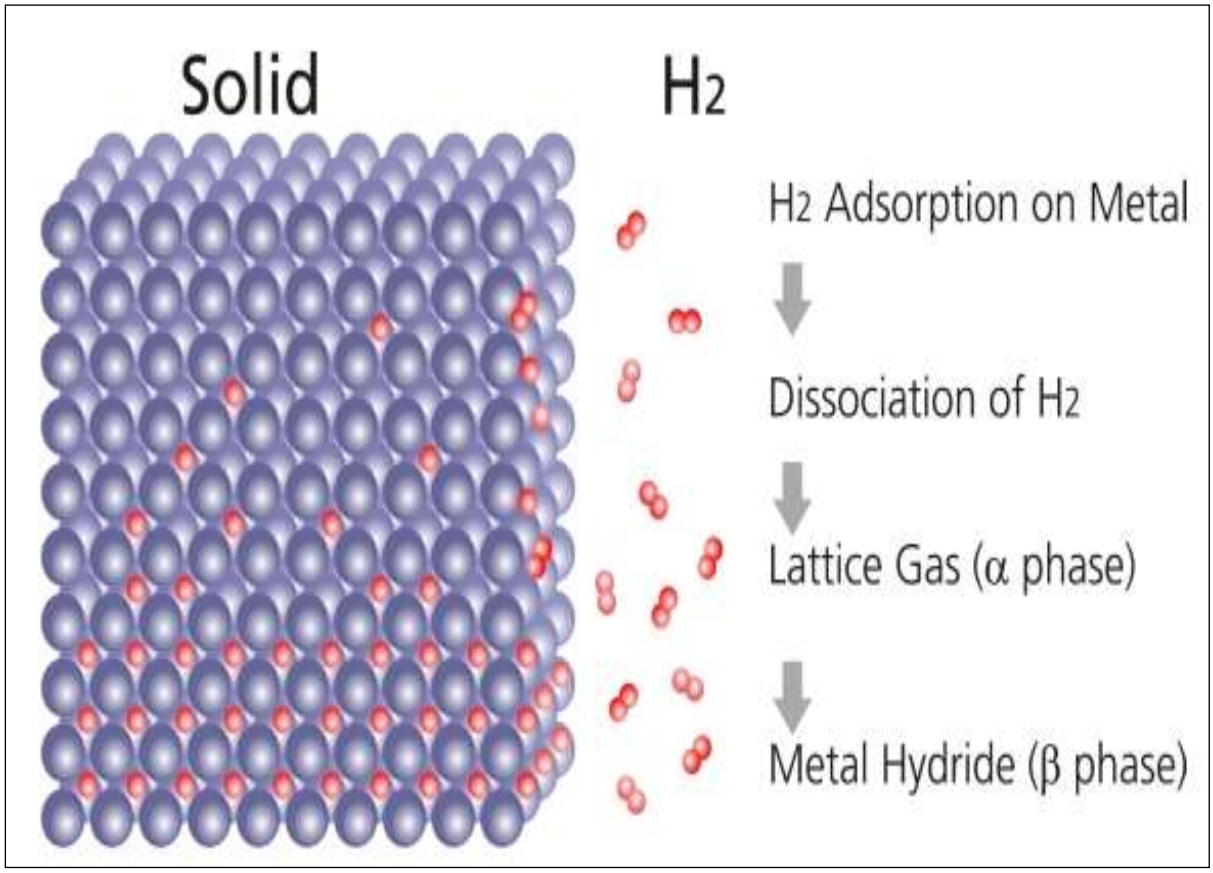

Fig. 1.4: Schematic diagram of metal hydride formation [37]

The α and β phase coexist in the plateau pressure region. The hydrogen absorption procedure is exothermic and a certain extent of heat is released through the hydrogen absorption depending upon the host material.

Thermodynamics aspect of Metal Hydride

The thermodynamic behavior as well as the capacity of a metal hydride considered by its Pressure-Composition Isotherm. A plot between hydrogen pressure and hydrogen to the metal ratio at a constant temperature called pressure-composition isotherm or PCT curve.

These PCI are widely used to determine key properties of the different hydrides.

- The length of the plateau regulates how much quantity of hydrogen can be stored and improved by means of a small change in pressure.

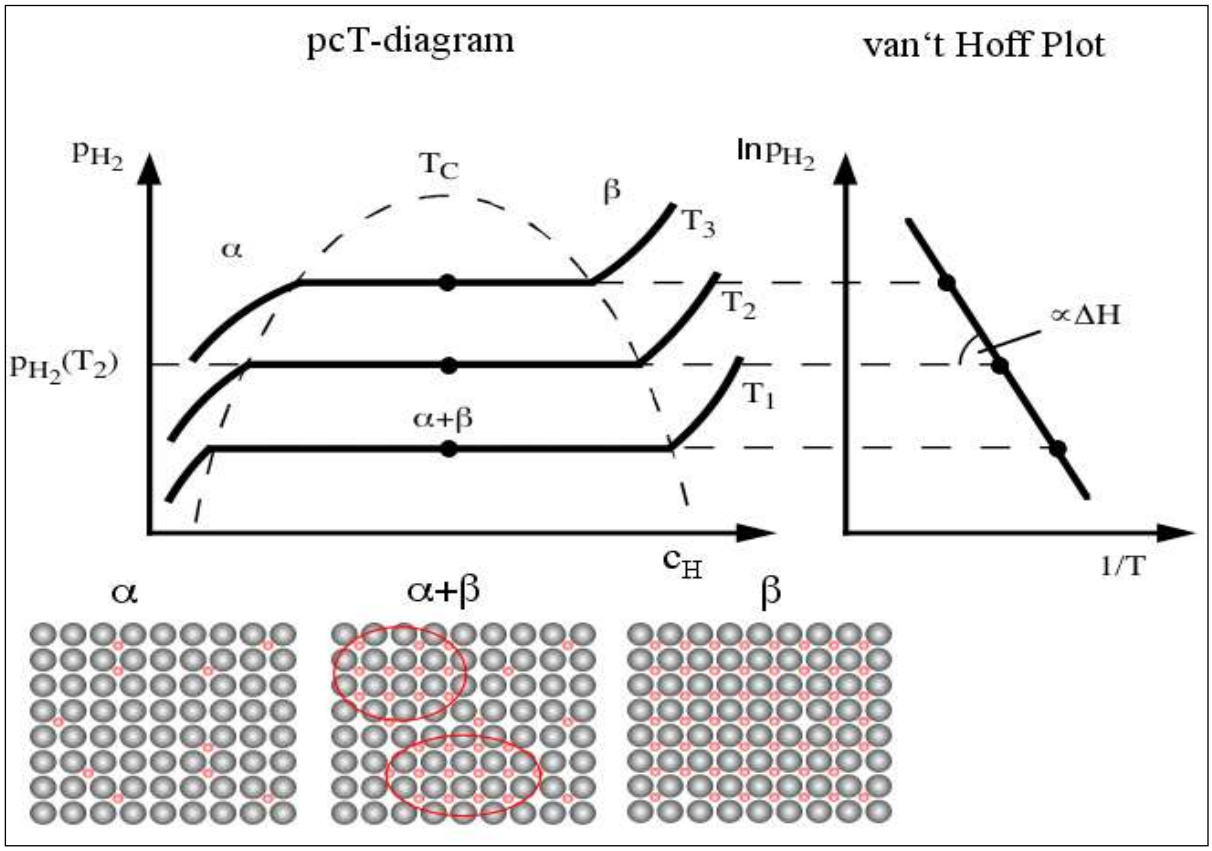

Fig-1.5. Schematic PC isotherms and van't Hoff plot [37]

- The plateau pressure will rise with temperature according to the Vant's Hoff equation and vanish at the critical temperature Tc. (Figure 1.5)

$$\text{Ln}\ (P_{H2}/P_o) = \Delta H/RT - \Delta S/R$$

Where

R = gas constant

T = absolute temperature

P_o= reference pressure of 1 bar

ΔH= enthalpy of formation of the hydride

ΔS= entropy of the formation of the hydride

The enthalpy of hydride development can be easily determined from the slope of the Van't Hoff plot.

Kinetics aspects

For practical hydrogen storage uses, kinetic study of metal hydride is important.
Hydrogen captivation reaction is composed of several different steps, which includes [38, 39]:

(i) Physisorption of hydrogen molecules.
(ii) Dissociation of the hydrogen molecule and chemisorptions
(iii) Surface penetration of hydrogen atoms
(iv) Diffusion of hydrogen atoms over the hydride layer
(v) Hydride development at the metal/hydride interface

Desorption proceeds via inverse scheme, starting with the decay of the hydride phase monitored by bulk and sub surface diffusion. Consequently, two H recombine to form the H_2 molecule, which finally desorbs. Each of the reaction has a specific rate. The complete kinetics limited by the slowest step, which is called rate-limiting step.

The hydride nucleation and growth or diffusion is the rate-limiting step in most of the cases [39]. Generally, for separation of the H_2 molecule requires an extra amount of energy, which called activation energy. The dehydrogenation/rehydrogenation kinetics studies of metal hydride based on the research carried out under Isothermal and Non-Isothermal condition.

Isothermal dehydrogenation/rehydrogenation kinetics is accomplished by means of Sieverts type apparatus, which allows precise volumetric determination of the volume of hydrogen evolved at preferred temperature and pressure. In order to gain comprehensive statistics about

the kinetics of the reactions, the activation energy (E_a) for a reaction is estimated using the Arrhenius equation [40].

$$K(T) = A\ exp^{(-Ea/RT)}$$

Where K is the temperature reliant on reaction rate constant, A is a pre-exponential factor, E_a is the apparent activation energy, R is the gas constant, and T is absolute temperature.

On the other hand, the kinetic investigation of solid state reaction under non-isothermal conditions by using thermal study method analysis technique such as Thermogravimetric Analysis (TGA) which allows determining the hydrogen content.

The peak or glance gives the statistics about variation in thermal possessions of the sample. The difference in peak temperature used to define the activation energy. The activation vitalities calculated by plotting a curve between ln k and $1/RT_p$ using the following equation,

$$lnk = -\frac{E_a}{RT_P} + a$$

Where, $k = \beta/T_p^2$

β = heating rate, in ˚C/min

T_p= peak temperature

E_a= activation energy of desorption

R = gas constant

Limitation of MgH_2 for practical application

MgH_2 is thermodynamically also stable, require a raised temperature for absorption and desorption. The enthalpy and entropy of MgH_2 development are about -74.5 KJ/(mol) and -13.5 J/(K mol)correspondingly, which are not adjacent to the target value.

On the other hand, the MgH_2 also suffers from meagre absorption/desorption kinetics, the origin generally ascribed to the following barriers:

(i) Magnesium is very subtle to oxidation. Through oxidation, a inert layer of MgO formed over magnesium surface, which creates a surface blockade. This increase deceptive activation energy for both absorption and desorption.

(ii) Incomplete separation rate of hydrogen molecules at Mg surface

(iii) Measured dispersion of hydrogen molecules, which is due to the nucleation of the MgH_2 in the surface of the Mg.

1.5 Objectives of the Present Research Work:

In order to improve the hydrogenation properties of MgH_2, the investigation will focus on the following specific objectives:

- Preparing the alloy and doped MgH_2 by ball milling with varying concentration of doping material.
- Investigating the structural and morphological changes induced in the samples during milling.
- Measuring the hydrogen content.
- Understanding the influence of transition metal based alloyson dehydrogenation/ hydrogenation properties of MgH_2.

1.6 Thesis Outline

The remainder of the thesis is organized as follows:

Chapter 2: A review of previous literature providing summary of work done by otherscientist and the knowledge already available regarding the present research on structural, thermal and P-C-T isotherms of various types of intermetallic compounds by various investigators.

Chapter 3: Deals with the description of the principles of the techniques and experimental setups utilized for the present work such as arc melting and ball milling respectively. Various characterization techniques such as x-ray diffraction (XRD), scanning electron microscopy (SEM), energy dispersivespectroscopy,differential scanning calorimetry (DSC) and thermo gravimetric analysis (TGA) used for reported materials have been discussed.

Chapter 4: In current chapter, discussion has given about the results based on study of influence of MgH_2-x wt% $La_{23}Nd_{8.5}Ti_{1.1}Ni_{33.9}Co_{32.9}Al_{0.65}$ (x=10, 25 & 50) additive on the hydrogenation/dehydrogenation properties of as-milled MgH_2 with various concentrations.

Chapter 5: In the present chapter hydrogen kinetics studies of MgH_2-FeTi nano composites have discussed.

Chapter 6: Deals with the hydrogenation/dehydrogenation behavior of the nano composite (MgH_2- NiMnAl) was examined through differential scanning calorimetry (DSC) and thermogravimetric analysis (TGA) respectively.

Chapter 7: The current chapter discusses the results based on the study of the influence MgH_2-x wt%$NiMn_{9.3}Al_{4.0}Co_{14.1}Fe_{3.6}$(x=10, 25 & 50) additive on the hydrogenation properties of ball milled MgH_2 with various concentrations.

Chapter 8: Provides a summary of the findings of the research work outlines specific conclusions drawn from the experimental and analytical efforts and suggests ideas and directions for the future scope.

The next chapter briefly presents/discuss the literature review of various research papers on structural, thermal and P-C-T isotherms of a series of experimental alloy material. The specific objectives of this work are clearly outlined in the next chapter.

*****

Chapter-2

LITERATURE REVIEW

Since the last decade, Hydrogen storage alloys have become a field of research area and a lot of work has been done in this area. This becomes very important to discuss the major works related to the nanocomposites and their properties. The purpose of literature review is to provide background information on the issues to be considering in this thesis and to emphasize the relevance of the present study. Various aspects of nanocomposites have been considered with reference to development as well as their characterizations. Existing literature related to the structural, thermal and P-C-T isotherms of the composites have been reviewed. Knowledge gap in the earlier works has been presented to outline the need and objectives of the present work.

The chapter includes brief reviews:

2.1 Study based on effect of intermetallic compound on hydrogenation/dehydrogenation properties of MgH_2

2.1.1 Study based on effect of MgH_2-$LaNi_5$ type alloys on structural, thermal and PCT-isotherms.

2.1.2 Study based on effect of MgH_2-FeTi alloy nanocomposites.

2.1.3 Study based on effect of MgH_2-NiMnAl nanocomposites.

2.1.4 Study based on effect of MgH_2-Ni based alloy nanocomposites.

At the end of this chapter a summary of the literature survey and the objectives of the present research work are outlined.

2.1 Study Based on Effect of Intermetallic Compound on Hydrogenation/Dehydrogenation Properties of MgH_2

The literature study reveals that various intermetallic compound studies based on effect of intermetallic compound on hydrogenation/dehydrogenation properties of MgH_2. These composite find lot of application in transportation. This part of literature study discusses about the effect of various alloys on MgH_2.

2.1.1 Study based on effect of MgH_2- $La_{23}Nd_{7.8}Ti_{1.1}Ni_{33.9}Co_{32.9}Al_{0.65}$ on structural, thermal and PCT-isotherms.

Jain et al. [51] fabricated the P–C–T isotherms of La $_{(28.9)}$ $Ni_{(67.5)}Si_{(3.55)}$ by substitution of Ni by Si in $LaNi_5$ at various temperatures. The saturation value of H/M of above alloy is about 1.0 for P–C–T at ambient temperature (293 K).

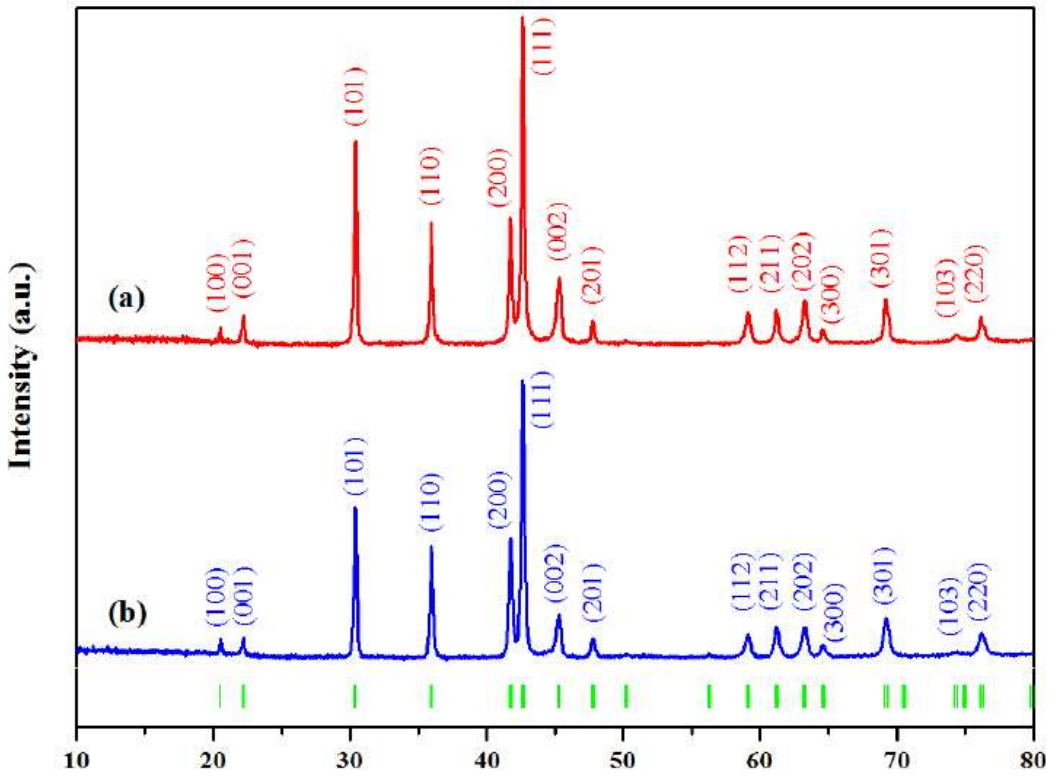

Figure 2.1. XRD profiles of $MmNi_{4.22}Co_{0.48}Mn_{0.15}Al_{0.15}$ alloy (a) before hydrogen activation (b) after 30 H/D cycles

The H/M values were found to be 0.9, 0.85, 0.8 and equilibrium pressures were 1.01×10^5; 1.41×10^5; 1.71×10^5; 2.12×10^5 Pa for P–C–T isotherms at 313, 323, 333 K, respectively. The results show that the wt% of hydrogen in the alloy was about 1.75% and the maximum amount of hydrogen released by the alloy is in the temperature range 313–343 K.

2.1.2 Study based on effect of MgH_2-FeTi nanocomposites.

This part of literature study discuss about the the effect of various concentration of FeTi added MgH_2. **Mandal et al. [67]** synthesized Mg-40% FeTi and found a storage capacity of ~3-3.6 wt% at room temperature (27°C). This is the highest known capacity exhibited by any hydrogen storage material at ambient conditions.

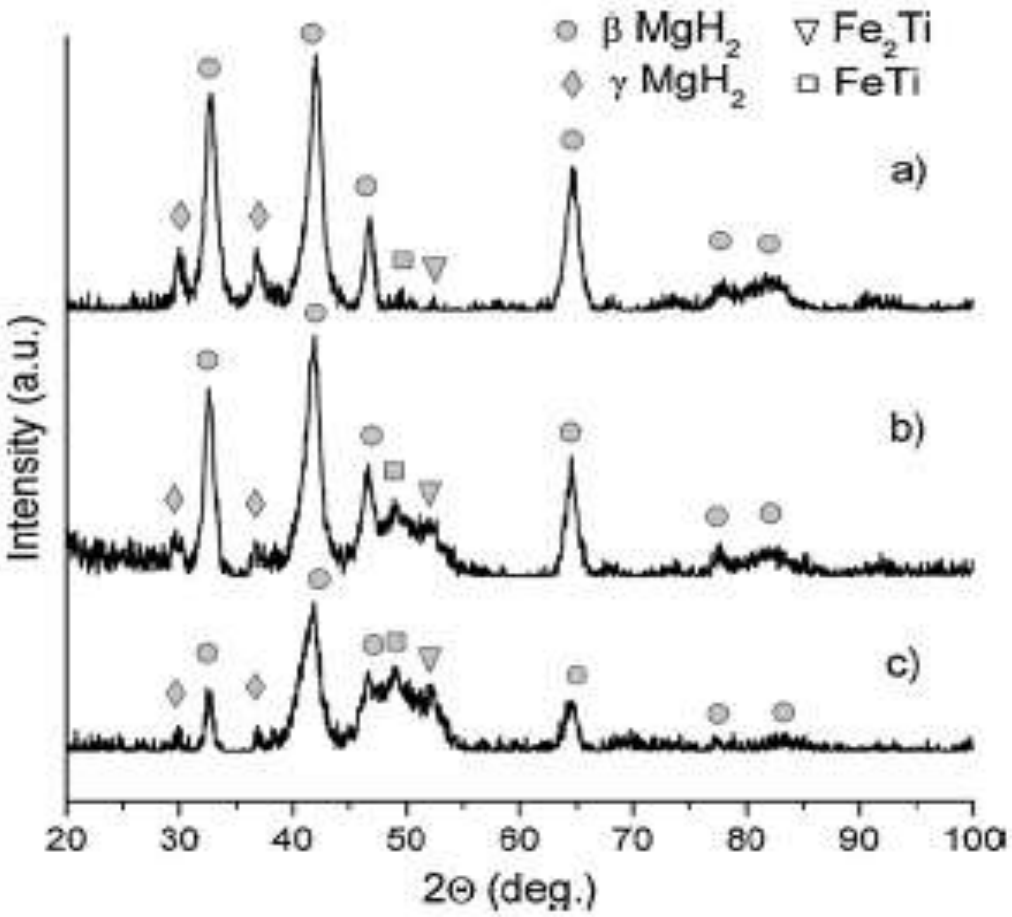

Figure 2.2. XRD patterns of MgH_2–$FeTiH_x$ composites after milling for 10 h with (a) 10 wt% $FeTiH_x$, (b) 30 wt% $FeTiH_x$ and (c) 50 wt% $FeTiH_x$

Figure 2.2 showing the XRD patterns of the 10, 30 and 50 wt% $FeTiH_x$ composites after milling confirms that the microstructure comprises primarily MgH_2 and FeTi with a small amount of minority intermetallic Fe_2Ti.

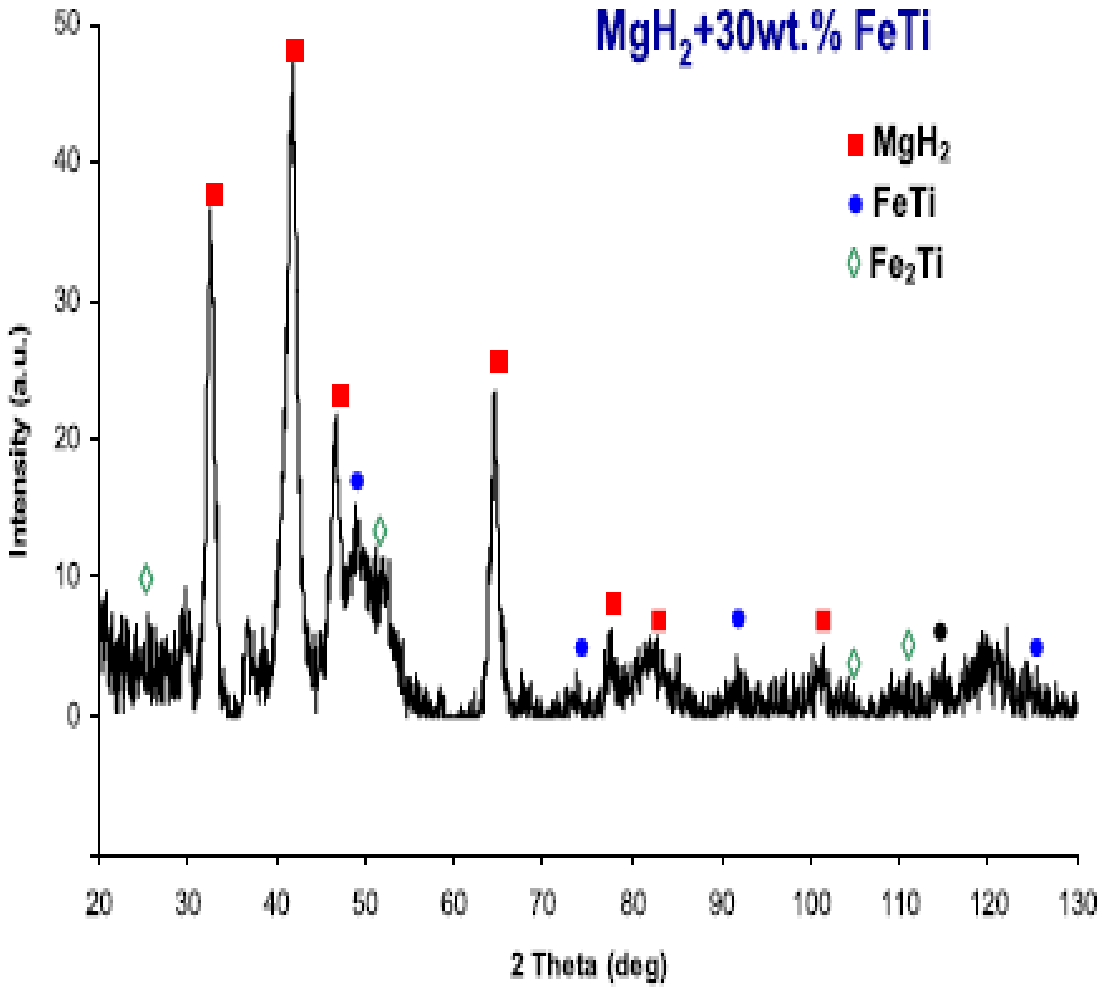

Figure 2.3. XRD patterns of the MgH_2-FeTi composites after milling

2.1.3 Study based on effect of MgH_2-NiMnAl nanocomposites

Deledda et al. [76] reported the ball milling techniques to introduce both fluorine and catalytic transition metals (Fe, Ni) into MgH_2 nanograined powders. XRD was carried out to follow the structural evolution upon milling and the thermal stability against H-desorption was investigated

by DSC and TG analysis. The latter showed that fluorine additions with the Fe catalyst effectively decrease the desorption temperature to about 500 K. Outcomes on the absorption/desorption kinetics, which was calculated by volumetric techniques, are presented and discussed with respect to both the simultaneous catalytic activity of Fe or Ni with F and the effect of solid-state processes which may occur upon mechanical alloying.

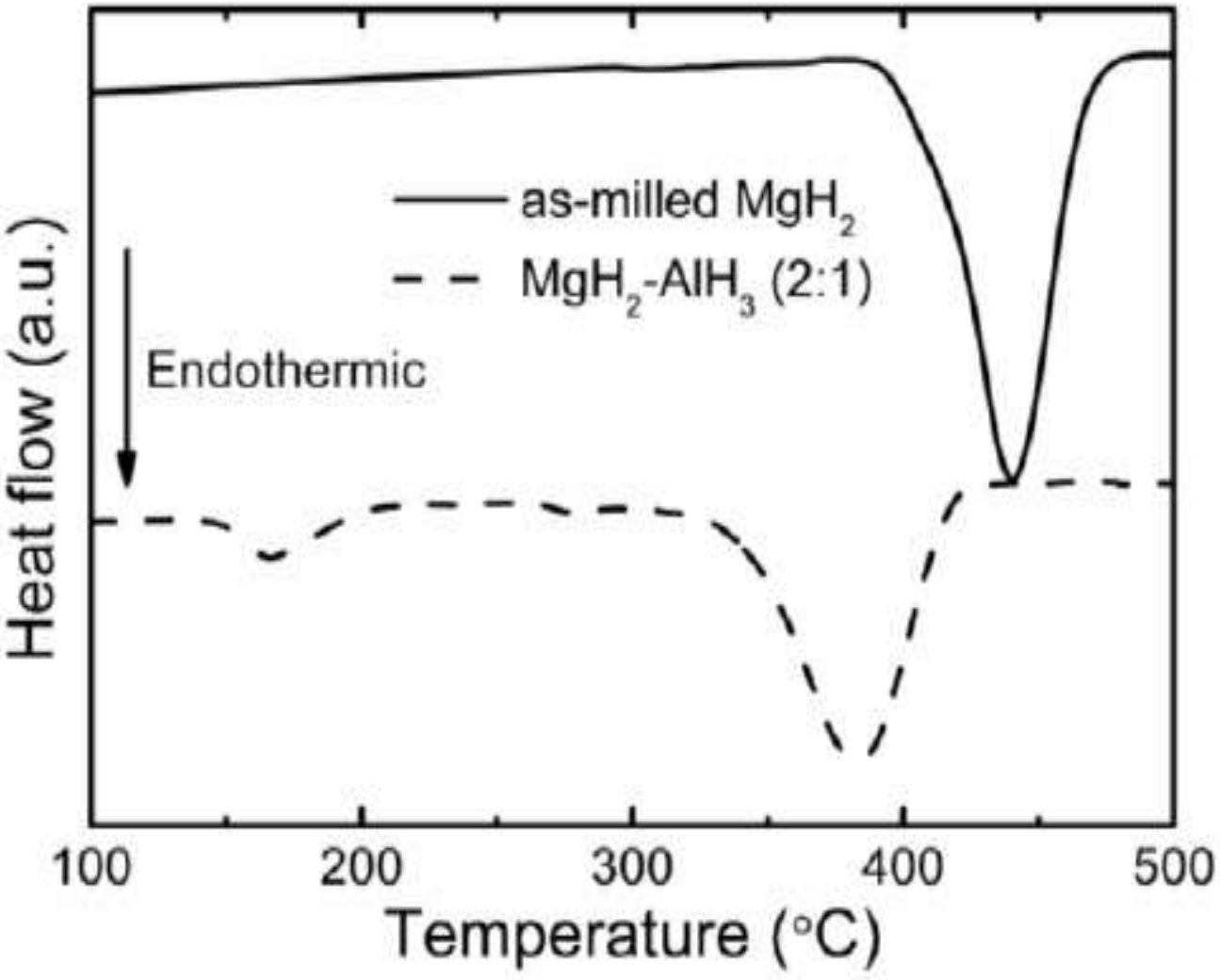

Figure 2.4. DSC traces of the as-milled and the MgH_2-AlH_3 composite

2.1.4 Study based on effect of MgH_2- $NiMn_{9.3}Al_{4.0}Co_{14.1}Fe_{3.6}$ nanocomposites

G. Liang et al. [83] studied for hydrogen storage of MgH_2 –Tm (Ti, V, Mn, Fe, Ni) nanocomposites prepared by mechanical milling. The titanium and vanadium are better catalysts than Ni for hydrogen absorption and desorption. The composite with Ti or V additives represents very rapid desorption kinetics above 523K and absorption kinetics at temperature as low as 302K. The 3d-metal additives could significantly reduce the activation energy of hydrogen desorption.

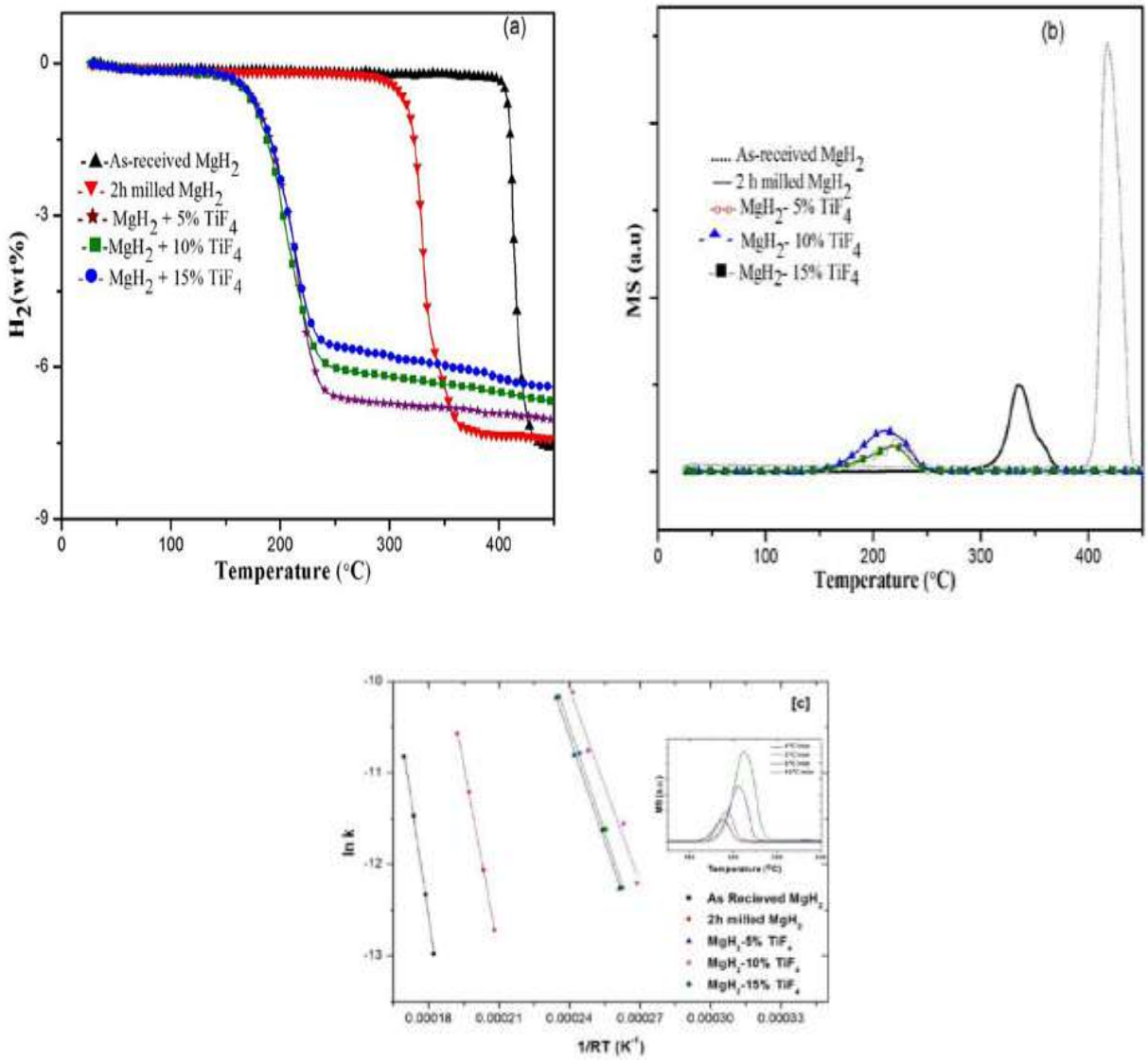

Figure 2.5. (a) TG (b) TDMS (c) Kissinger plot for dehydrogenation of the as-received MgH_2, 2 h milled MgH_2 and MgH_2- x wt% TiF_4 (x= 5, 10, 15) samples

Zhang et al. [98] investigated the effect of the Ni morphology (including size and shape) on the desorption performance of MgH_2, in which a modified wet chemical route was used to control the morphology of Ni. A well-distinguished desorption behavior was found by introducing the as synthesized Ni-based catalysts into MgH_2, evidencing the existence of the morphology-dependent effect of the catalytic phase. Among them, graphene sheets (GS) supported by Ni (Ni_6GS_4) exhibited the best catalytic performance with respect to a lowered MgH_2 onset desorption temperature of 225 ˚C (the undoped MgH_2 initiated to desorb hydrogen at 308˚C) and a saturated hydrogen desorption capacity of 6.74 wt%.

Table 2.1 summarizes the use of different metal hydrides used for hydrogen storage with their characteristics.

Table 2.1. List of different Metal hydrides for hydrogen storage

Name	Method	Temperature (˚C)	Pressure (bar)	Kinetics (min)	Hydrogen content (wt %)	Ref. No.
Mg- 5wt% $FeTi_{1.2}$	BM	T_{abs} and T_{des}:400	P_{abs}:30 P_{des}:1	No data	2.70	[100]
MgH_2-50 wt% $LaNi_5$	BM	T_{des}:250-300	P_{abs} and P_{des}:10-15	t_{abs}:3.33	4.10	[101]
Mg–Mg_2Ni	BM	T_{abs}: 300	P_{abs}: 12	t_{abs}: 83	3.60	[102]
30 wt% Mg- $MmNi_5$-x ($CoAlMn)_x$	BM	T_{abs}: 15	P_{abs}:6	t_{abs}:83	2.30	[103,104]
65 wt% MgH_2–35 wt% Mg_2NiH_4	BM	T_{des}: 220–240	P_{des}: 0.5	t_{abs}: 10	5.00	[105]

MgH_2-Mg_2FeH_6	Mixing	T_{abs} and T_{des}:350-525	P_{abs} and P_{des}:3.6-93.7	t_{abs} and t_{des}:90-1440	5.00	[106]
MgH_2-5 mol% Al_2O_3	BM	T_{abs}: 300	P_{abs}: 15	t_{abs}: 67	4.49	[107]
MgH_2- 1at% Al	BM	T_{abs}: 180	P_{abs}:0.6	t_{abs}:420	7.30	[108]
Mg-30 wt% $LaNi_{2.28}$	BM	T_{abs}: 280	P_{abs}: 30	t_{abs}: 1.6	5.40	[109]
Mg-20 wt% Mm (La, Nd, Ce)	BM (Pellet form)	T_{abs}:300 T_{des}:480	P_{abs}:10 P_{des}:1	t_{abs}:10 t_{des}:5	3.50	[110]

2.2 Essential Qualities of Hydrogen Storage Systems

Specific criteria have been established by the U.S. Department of Energy (DOE) for commercial application of hydrogen storage systems which are [111]:

- High gravimetric capacity
- High volumetric capacity
- Operation temperature approximately in the range 60˚C-120˚C.
- Reversibility and cyclability
- Safety Requirements
- Cheap and environmental friendly storage

U.S Department of Energy decided target parameters for On-board hydrogen storage are shown in Table 1.2.

Table 2.2. Technical system targets for on-board hydrogen storage [111]

Storage Parameter	Units	2020	2025	Ultimate
Gravimetric Capacity Usable, specific-energy from H_2 (net useful energy/max system mass)	kWh/kg (kg H_2/kg system)	1.5 (0.045)	1.8 (0.055)	2.2 (0.065)
Volumetric Capacity Usable energy density from H_2 (net useful energy/max system volume)	kWh/L (kg H_2/L system)	1.0 (0.030)	1.3 (0.040)	1.7 (0.050)
Storage System Cost Fuel cost	$/kWh net ($/kg H2) $/gge at pump	10 333 4	9 300 4	8 266 4
Operating ambient temperature	ºC	-40/60 (sun)	-40/60 (sun)	-40/60 (sun)
Min/max delivery temperature	ºC	-40/85	-40/85	-40/85
Operational cycle life (1/4 tank to full)	Cycles	1,500	1,500	1,500
Min delivery pressure from storage system	bar (abs)	5	5	5
Max delivery pressure from storage system	bar (abs)	12	12	12
System fill time	Min	3–5	3–5	3–5

The safety aspect related to the hydrogen storage system is very important as it has connection with the societal acceptance.

Chapter Summary

This chapter has provided

- An exhaustive review of research works on various aspects of alloys.
- The objectives of the present work.

The next chapter describes the materials and methods used for the processing of the composites, the experimental planning, structural, thermal and PCT isotherm properties.

*****

Chapter-3

MATERIALS AND METHODOLOGY

This section portrays all the experimental approaches used for sample preparation, characterization and the hydrogen storage properties of the materials. The bulk alloys were prepared with the help of arc melting Furnace and characterized by XRD technique. The morphology of the alloys and elemental composition were obtained by Scanning Electron Microscopy and with techniques. The hydrogen absorption properties such as hydrogen concentration (P-C-T isotherm) and Kinetics of the alloys were studied using a Sievert type.

3.1. Alloys preparation by arc melting

Arc melting furnace have been used for the preparation of alloys under inert atmosphere and homogeneity have been obtained by three times re-melting process. The purity of all the constituent metals was found to be more than 99.5%.

The figure 3.1 shows a arc furnace set-up at DMRL, Hyderabad. A pile of small ingots of constituent metal was kept in carbide crucible placed on a water-cooled copper hearth at a temperature of 1550-1600 ^{0}C and vacuum of 10^{-5} mbar. Before that oxygen and other reaction gases were removed from the chamber by flushing it thrice with high purity argon gas at 0.4 bar pressure.

An arc was applied on titanium getter to melt and then arc was directed to the crucible to melt the pile of elements.

Samples were cool down to room temperature after which removed from crucible and were weighed to ensure that there were no material losses.

Figure 3.1.Arc Furnace at DMRL, Hyderabad

3.2. Preparation of Nanocomposites

3.2.1. Glove box

Magnesium hydride is highly reactive towards oxidation forming MgO. So inert environment is required to prevent oxidation of the samples, which were provided by the Glove Box as shown in figure 3.2.

Figure 3.2. Glove Box

Sample synthesis condition

Sample synthesis conditions are tabulated in table 3.3 and sample specifications are as follows:

The following four series have been prepared using base material (MgH_2):

(a) MgH_2 - x wt% (x=10, 25 & 50) $La_{23}Nd_{7.8}Ti_{1.1}Ni_{33.9}Co_{32.9}Al_{0.65}$
(b) MgH_2 - x wt% (x=10, 25 & 50) NiMnAl
(c) MgH_2 - x wt% (x=10, 25 & 50) FeTi
(d) MgH_2 - x wt% (x=10, 25 & 50) $NiMn_{9.3}Al_{4.0}Co_{14.1}Fe_{3.6}$

3.2.2. Ball milling

The Ball milling or mechanical milling is a widely used technique which allows the modification of chemical, structural composition and the size of the crystallites. It is used to harvest nanocrystalline powders at room temperature [99, 100].

The Fig. 3.3 and 3.4 shows the Ball Milling machine which was used for the sample preparation.

During the process, powdered particles periodically trapped between colliding balls, followed by plastically deformation.

The effect of the milling depends on the milling parameters and conditions such as ball to powder mass ratio, rotation speed, number of balls, milling time [101].

The powders processed by energetic ball milling become amorphous for short duration [101,102] and then produce a nano-crystallization.

The particle size reduces rapidly in the early hours of the milling.

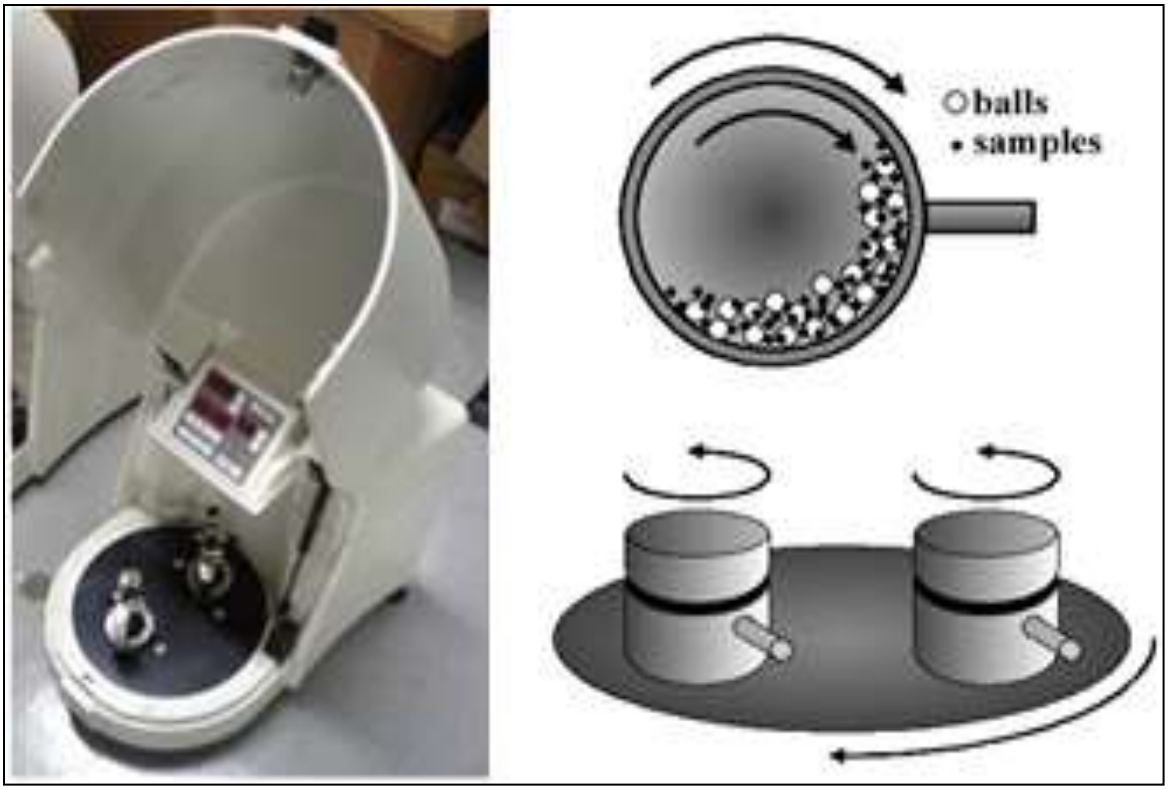

Figure 3.3: Fritsch P7 ball milling

Figure 3.4. Ball mill machine

The specifications of ball mill machine used for the preparation of samples shown in table 3.2 and 3.3.MA is a better technique for the preparation of Mg-based hydrogen storage materials in comparison to other conventional metallurgical processes, such as melting, because of the low miscibility of MgH_2 with most transition metals, low melting point (923K) and high vapor pressure [103].

Table 3.1. Specification of FRITSCH P7 ball mill machine

Model	FRITSCH P7
Size reduction principle	Impact, friction
No. of grinding station	2
Speed ratio	1:2
Sun wheel speed	100 - 800 rpm
Material of grinding tools	Stainless steel ball of dia. 0.1-15 mm
Grinding jar size	12 ml and 45 ml
Power	880 W

Table 3.2.Specification of retsch PM 100 ball mill machine

Model	Planetary Ball Mill PM 100
Size reduction principle	Impact, friction
No. of grinding station	1
Speed ratio	1:2
Sun wheel speed	100 - 650 rpm
Material of grinding tools	Stainless steel ball of dia. 5mm & 10 mm
Grinding jar size	250 ml
Power	1250 W

Table 3.3. Milling parameters of nanocomposites

Milling Parameters	
Powder mass	5 grams
Ball to powder weight ratio	10:1
Atmosphere	Argon
Speed	300 rpm
Milling time	10 hour
Interval	15 hour
Interval brake	5 min.

3.3 Structural Characterization

The structural and morphological characterization of bulk samples were performed using X- ray Diffraction technique and Scanning Electron Microscopy (SEM). X-ray Photoelectron spectroscopy used to determine the composition and chemical state of surface constituents.

3.3.1 X-ray diffraction

Powder XRD (X-ray Diffraction) is the most widely used non-destructive analytical to obtain structural information about crystalline solids. It can indirectly reveal the details of the internal structure of matter at the order of 10^{-8} cm in size [105].The nature of the powders, whether crystalline or amorphous, can be determined using XRD.

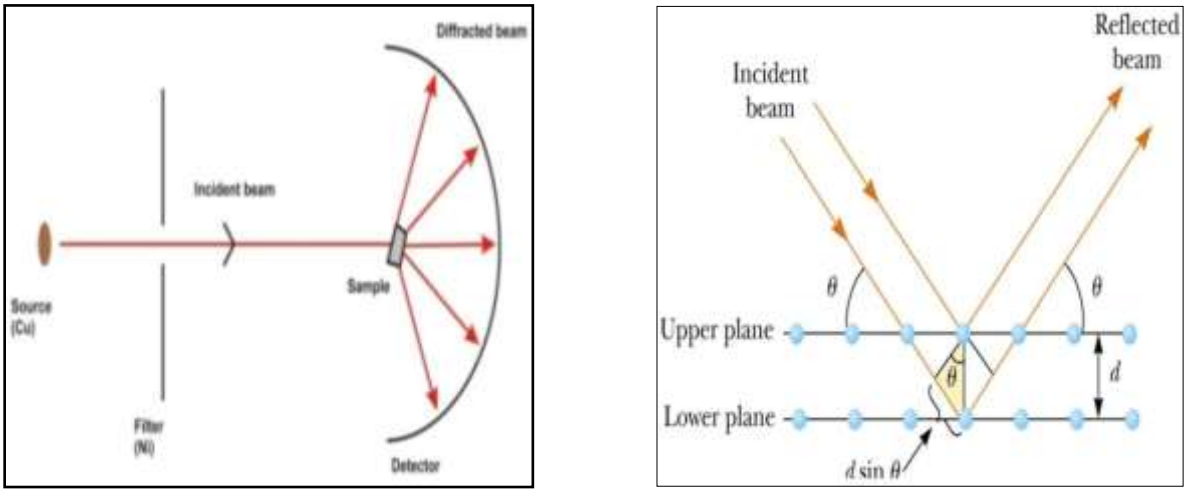

Figure 3.5.Reflection of X-ray from two planes of atom in a solid[106]

Bragg's law can describe diffraction as follows:

$$n\lambda = 2d \sin \theta$$

Where d is the interplanar spacing, θ is the Bragg angle, n is the order of reflection, and λ is the X-ray wavelength. X-ray diffraction is based on constructive interference of monochromatic X-rays and a crystalline sample.

A cathode ray tube, filtered to produce monochromatic radiation, collimated to concentrate, and directed toward the sample, generates these X-rays. When X-rays is incident on the crystal and X-ray photon, collide with electrons. Some photon from the incident beam reflected away from the direction where they originally travel.

The wavelength of these scattered X-rays did not change, and only the momentum transferred. These scattered X-rays from different atoms can interface with each other and the resultant intensity distribution strongly modulated. The interaction of the incident rays with the sample results in constructive interference of diffracted rays when conditions satisfy Bragg's Law. These diffracted X-rays are then detected, processed and counted [107].

Analysis of the position of the diffraction effect leads immediately to a knowledge of the size, shape and orientation of the unit cell. To locate the position of the individual atoms in the lattice, the intensities needs to be measured and analyzed [108].

X-ray diffraction is an indispensable tool for crystalline materials. A powder XRD is most common and prime instrument used by solid-state scientists. The powdered sample in the form of compact flat pack was exposed to a monochromatic beam of X-ray and the diffracted beam collected in a range of angles (two theta with respect to incident beam).

The intensity corresponding to a constructive interference of the diffracted beam from a crystallographic plane observed as peak, corresponding to the Bragg angle (theta). In all other angles, a background obtained. A typical block diagram of powder diffractometer given in figure 3.6 [109].

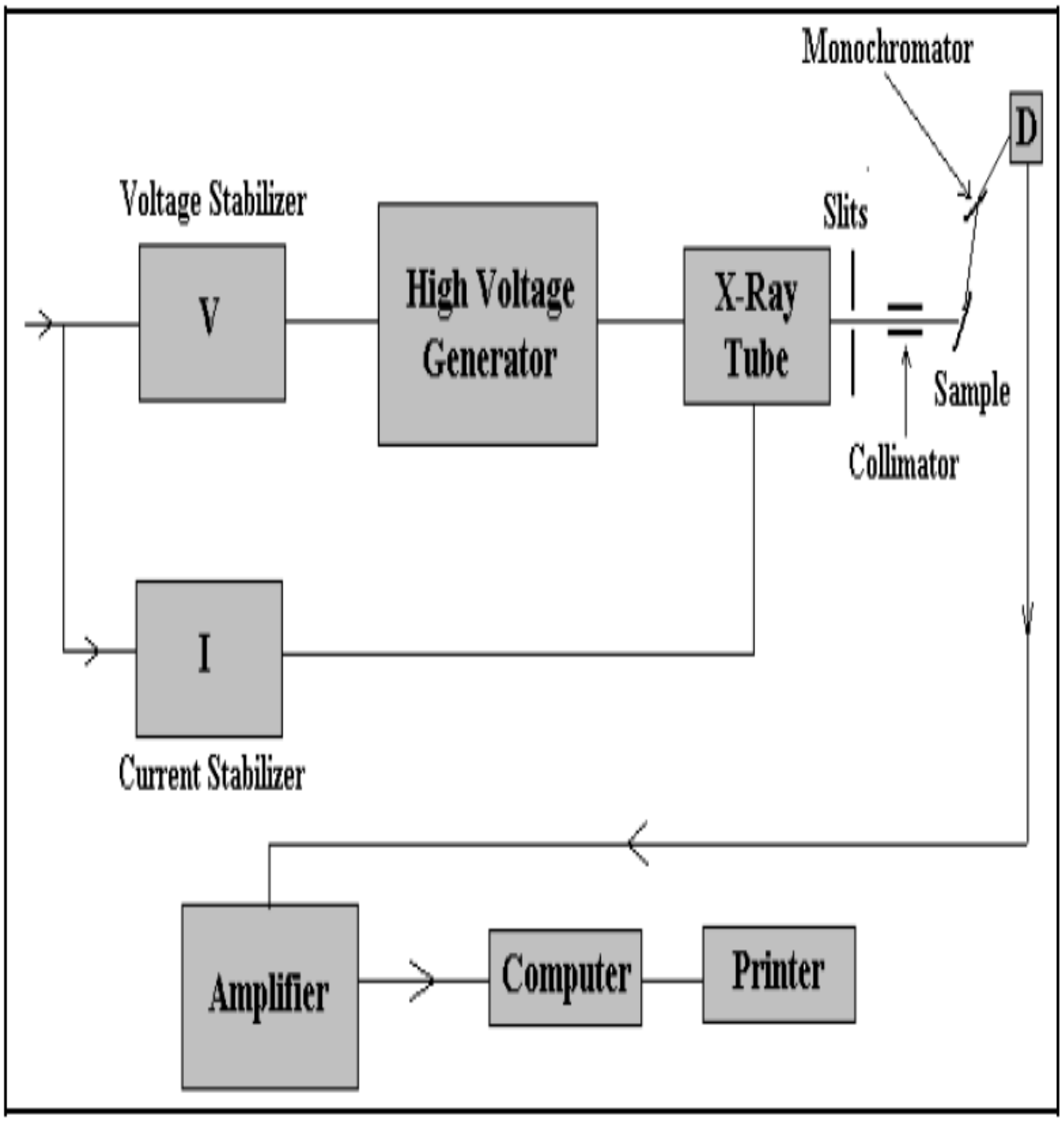

Figure 3.6.A typical block diagram of a Powder XRD unit

The prime components of a powder diffractometer are the source of X-ray, usually called X-ray tube, and the sample chamber and a goniometer for measuring the angles followed by an X-ray detector for measuring the intensity of diffracted X-ray beam.

Figure 3.7. X-ray Diffractometer unit

Specifications of the powder diffractometer

A photograph of the entire unit is shown in figure 2.4. XRD spectra of all samples were taken by using The X-Ray Diffractometer (Panalytical X Pert Pro) with CuK_α (λ=1.5418 Å) for Bragg angle 10° to 90°. The tube was operated at 45 kV, 40 mA with a scanning rate of 0.02°/ sec. The

peaks of the XRD patterns were searched by computer programming using Powder X Software.

Table 3.4: XRD parameters

Parameters	Values
Model	Panalytical X Pert Pro
V/A	45Kv/40 Ma
Radiation	CuKα
Theta Range	10°-90°
Scan Speed	0.02/ sec
Step Size	0.02

3.4.3 Dynamic type apparatus

A simple and user-friendly experimental apparatus for the study of hydrogen storage in metal compounds based on volumetric technique Known as Sievert type system [113]. In this system, a calibrated volume filled with a He-gas to a certain pressure and subsequently, the He-gas introduced to the sample holder containing the sample. The amount of hydrogen absorbed by the sample calculated based on the change of pressure. For each value of initial pressure, a certain quantity of hydrogen absorbed obtained and after no. of cycles with different initial pressure, a complete PCT curve for a given temperature obtained.

Unlike Sievert type apparatus, the instrument used in this work is dynamic PCT system, in which hydrogen continuously flows into the system through Mass Flow Controller (MFC) until the desired maximum pressure reached.

The apparatus allows the study of hydrogen absorption and desorption kinetics keeping the pressure constant in the reaction chamber as well as the determination of pressure- composition isotherm of metal- hydrogen system. A series of isotherm measured at different temperatures could used to calculate thermodynamic properties of the hydrogen solid- system: for example, the heat or enthalpy of hydride formation and decomposition [114] or isostatic enthalpy of adsorption [115, 116].

3.4.3.1 Schematic of dynamic PCT system

The schematic of the apparatus used for dynamic PCT measurements, given in figure 2.5. It divided into two parts: The first is the volume v_1 that includes the volume occupied by measuring part i.e. from inlet of hydrogen to the opening of the sample holder, containing SS tubes, Mass Flow Controller and pressure transducers. This volume kept at room temperature during the entire measurement. The second volume v_2, is the volume of the sample holder that contains the sample. This part kept inside a furnace and heated to the desired temperature up to a maximum limit of 500^oC.

A TC positioned in the tabular oven in contact with SC and controlled with a proportional integrative and derivative (PID) system monitors the sample temperature. The pressure in the system monitored by pressure gauge capable to measure 0.1 bars to100 bars. The system evacuated up to 10^{-6} mbar by a turbo pump (Model: Varian TPS-compact). During the experimental run data automatically saved using data acquisition software developed by Syscon, Bangalore.

The apparatus also connected to a He cylinder, which is used to fill the system before measurements and after the periodic maintenance operation in order to check any possible leak.

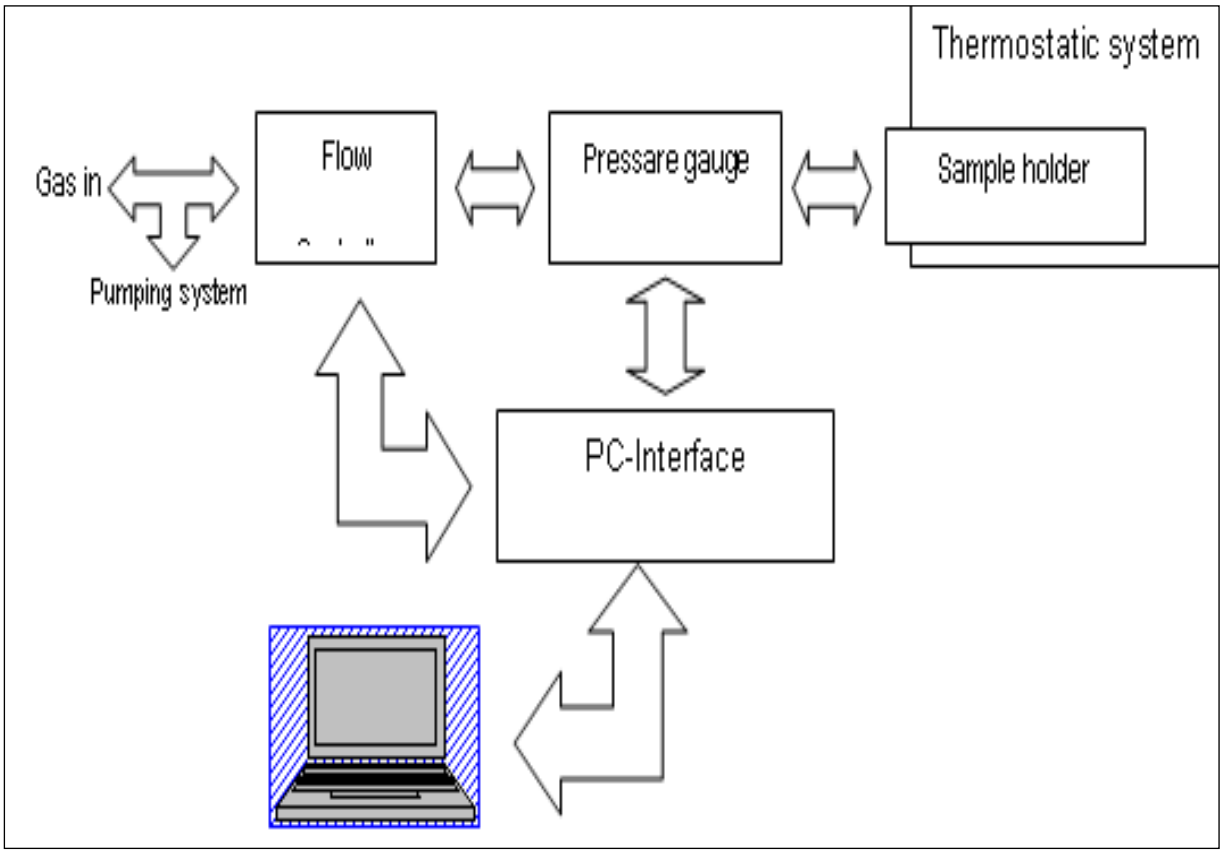

Figure 3.13 Schematic diagrams of Dynamic PCT apparatus

Calculation of absorbed hydrogen volume

To calculate the quantity of hydrogen absorbed, the following steps have to take into account:

1. **Calibration of the system volume**

The total volume of the system could measured by entering hydrogen into the system with a known flow. The total volume of hydrogen entered into the system through MFC with a constant flow f would be the integration of the flow with respect to time t at normal conditions i.e.

$$v = \int_0^t f dt \quad \text{..... (1)}$$

Where t is the required time to increase the pressure of system by 1 bar. Thus, the above volume considered as the volume of the system at room temperature. So we can write;

$$v_{system} = \int_0^t f dt = v_1 + v_2 \text{..... (2)}$$

2. Calculation of quantity of absorbed hydrogen:

First we will consider the case of the empty sample holder. The total hydrogen entered into the system to reach the condition of required pressure P will be:

$$v_{empty} = P.v_{system} \text{..... (3)}$$

Now if a known quantity of material placed in the sample holder, it will absorb a certain volume of hydrogen, let us say $v_{absorbed}$. Thus the total volume of hydrogen entered into the system to reach upto pressure P will be the sum of v_{empty} and $v_{absorbed}$ i.e.

$$v_{filled} = v_{empty} + v_{absorbed} \text{..... (4)}$$

We can calculate this volume filled by the integration of the flow with respect to time also i.e.

$$v_{filled} = \int_0^{t_1} f\ dt \text{..... (5)}$$

Where t_1 is the time taken by the system to reach the desired pressure P.

By combining eqn. (3) – (5):

$$\int_0^{t_1} f\ dt = P.v_{system} + v_{absorbed}$$

or,

$$v_{absorbed} = \int_0^{t_1} f\ dt - P.v_{system} \text{.....(6)}$$

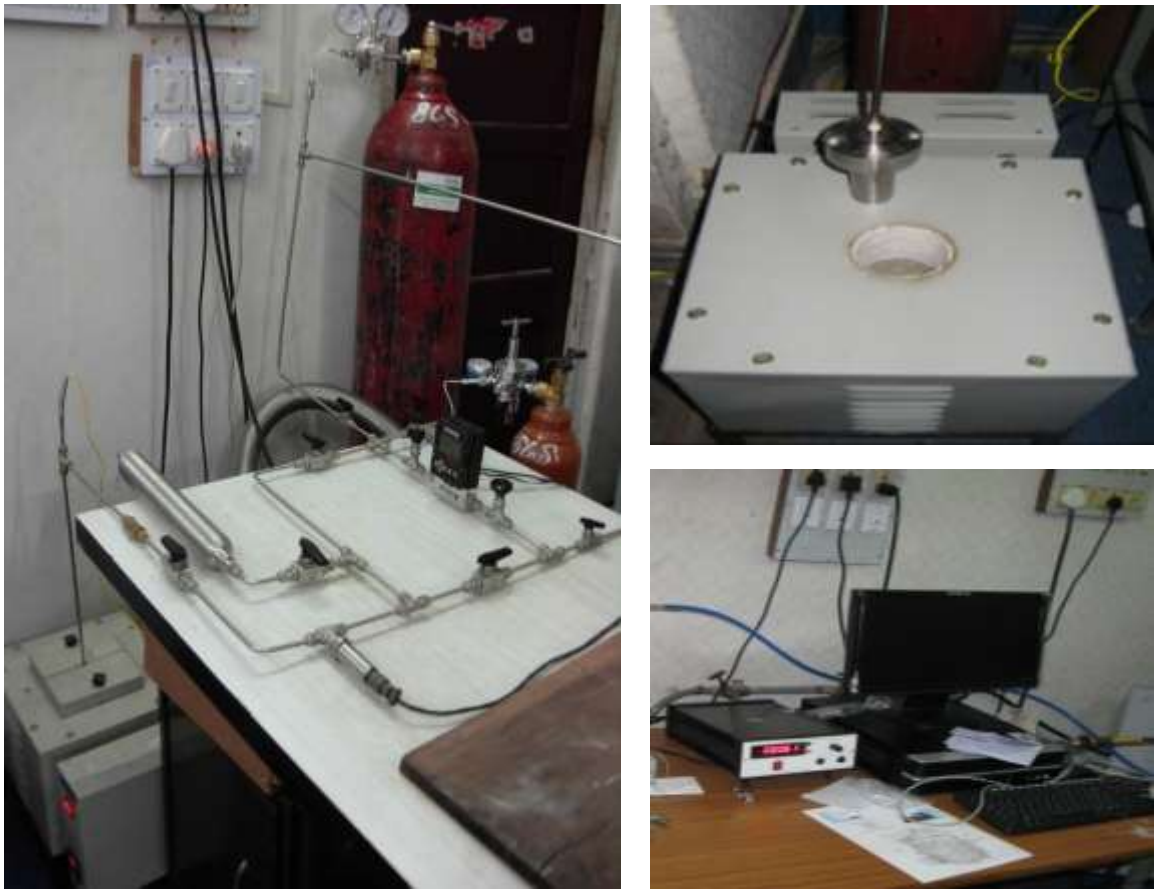

Figure 3.14. P-C-T isotherm measuring apparatus

A complete set of PCI measurements can be divided into two processes:

(a) Activation process

Since the handling of material after milling was done in open air, there may be a thin oxide layer on the surface of the material, which can prevent hydrogen to enter into the material. Thus, an activation procedure needed before real PCI measurement recorded. To activate the material, the whole system is evacuated to 10^{-6} torr vacuum and then heated the sample holder at 300°C for 2 hrs. The sample was introduced to 10 bar hydrogen and left in the same condition for 2 hrs.

Again the vacuum is made and 5 cycles of absorption and desorption were carried out to ensure the removal of the oxide layer and the repeatability of the data.

The hydrogen absorption and desorption as shown in figure 3.15.

Figure 3.15. Experimental set up of hydrogen absorption and desorption

The experimental procedure of hydrogen absorption/desorption is as follows:

Before starting the process all the valves except V8 should be open to make complete vacuum in the whole system during heating of the sample holder then close all the valves.

Now below is the process to start absorption / desorption one by one:

1. Absorption

a. Open V1, V2, V3 and all other valve should remain close including V5 & V6.

b. Put the file name you want to save with and press ok.

c. Open the regulator and set the pressure about 30 bar.

d. Open V4 and close immediately within no time.

2. Desorption

Can be done in two ways:

[I]. Through MFC:

a. Close all the valves 1st. set the flow value at 30 ml/min (the maximum).

b. Now open V1, V3, V5 and V6.

c. Start rotary pump open the valve between rotary pump and valve V7.

d. Put the file name and press ok.

e. Open valve V7 and V2 to reach the pressure upto 0 bar as indicated in the pressure meter and close valve V2 immediately. in this case the hydrogen will follow the path sample holder-valve V1- valve V3-Valve V5-MFC_Valve V6-Valve V7-rotary pump.

f. With the help of time and flow you can calculate the kinetics curve.

[II]. MFC not included:

Since our MFC has a limitation of 30 ml/min - the highest flow. So if the kinetics is fast (which usually be the case for 300 or 350 ˚C) MFC will reach to its threshold value and kinetics will not be real, in that case you will have to be dependent on the pressure readings, which is more complicated.

a. Close all the valves including V5 and V6.

b. Open V1 & V2.

c. Put the file name and click Ok to save.

d. Start rotary pump open the valve between rotary pump and valve V7.

e. Open valve V7 to reach the pressure upto 0 bar as indicated in the pressure meter and close it immediately.

f. Pressure will start to increase again which means sample is desorbing hydrogen, this pressure rise will give you the chance to calculate the amount of hydrogen desorbed w.r.t. time.

g. If the pressure reach to the equilibrium pressure (as noted from desorption PCT curve), then point (e) should repeat again.

(b) PCI measurement

To make PCI curves the sample holder heated to the desired temperature under dynamic vacuum. Then hydrogen is allowed to enter in to the system with a fixed flow of 5 sccm till the desired pressure reached. During desorption hydrogen is pumped out with the same flow until the pressure reached up to 0.01 bar. The cycle repeated at different temperatures. This gives a complete set of PCI curves for a range of temperatures.

The next chapter briefly presents/discuss the effect of $La_{23}Nd_{7.8}Ti_{1.1}Ni_{33.9}Co_{32.9}Al_{0.65}$alloy doping in MgH_2 for hydrogen storage.

*****

Chapter-4

EFFECT OF $La_{23}Nd_{7.8}Ti_{1.1}Ni_{33.9}Co_{32.9}Al_{0.65}$ DOPING IN MgH_2 FOR HYDROGEN STORAGE

Introduction

In the current chapter are discussed the results based on study the influence MgH_2-x wt% $La_{23}Nd_{8.5}Ti_{1.1}Ni_{33.9}Co_{32.9}Al_{0.65}$ (x=10, 25 and 50 wt%) additive on the hydrogenation properties of ball milled MgH_2 with various concentrations. Nanocomposites were characterized by x-ray diffraction (XRD), scanning electron microscopy (SEM) with EDS analysis, differential scanning calorimetry (DSC) and thermo gravimetric analysis (TGA).

There are several approaches have been used to improve dehydrating temperature and kinetics of MgH_2 for the production of nano-dimensional structures such as alloy formation [117-121], high energy ball milling [122], formation of oxide-halides [123-126],metal hybrids [127-130] and incorporation of various metals [131-136].

4.1 Structural Characterization by XRD

The average crystallite size was calculated using debye scherer formula,

$$\boldsymbol{D = \frac{0.9\lambda}{\beta \cos\theta}}$$

Where λ is the X-ray wavelength, β is the line broadening at half the maximum intensity in radian, θ is the Bragg angle. Using Debye Scherer formula, the values of average crystallites size for the as-received MgH_2, as-milled MgH_2, MgH_2-10 wt% $La_{23}Nd_{7.8}Ti_{1.1}Ni_{33.9}Co_{32.9}Al_{0.65}$, MgH_2-25 wt% $La_{23}Nd_{7.8}Ti_{1.1}Ni_{33.9}Co_{32.9}Al_{0.65}$, MgH_2-50 wt% $La_{23}Nd_{7.8}Ti_{1.1}Ni_{33.9}Co_{32.9}Al_{0.65}$ nanocomposites are estimated to be about 48.382 nm, 43.061 nm, 26.911nm, 32.282 nm and 33.244 nm respectively (Table 4.1).

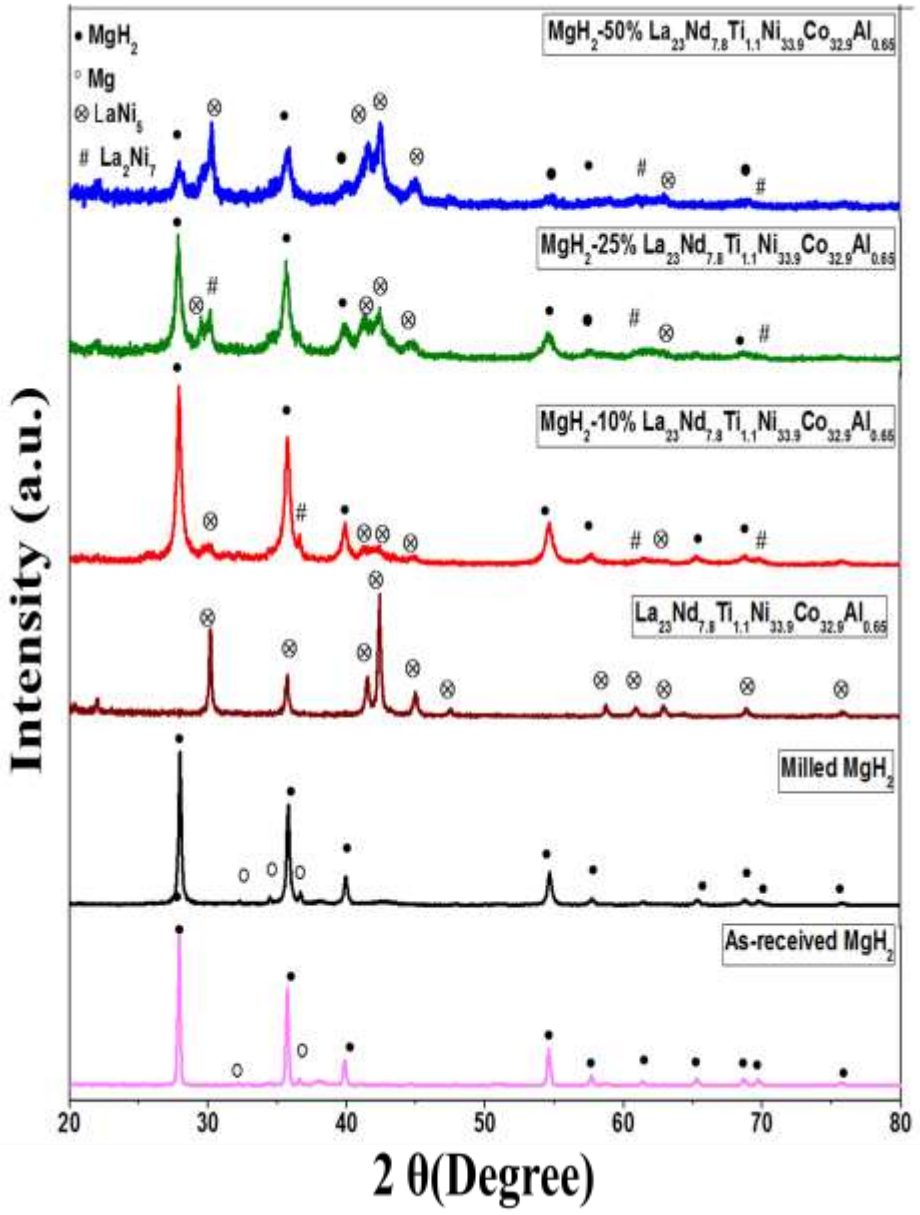

Figure 4.1. XRD pattern of MgH_2-x wt% (10, 25 & 50) $La_{23}Nd_{7.8}Ti_{1.1}Ni_{33.9}Co_{32.9}Al_{0.65}$ nanocomposites

Table 4.1.The crystallographic data for MgH_2 -x wt% $La_{23}Nd_{7.8}Ti_{1.1}Ni_{33.9}Co_{32.9}Al_{0.65}$ (x =10, 25 & 50) nanocomposites

Sample	Phase	Space group (No.)	Lattice parameters *a*[Å]	*c*[Å]	Volume V[Å ^{3}]	D_{avg} (nm)
x=10	MgH_2	$P4_2/mnm$ (136)	4.517	3.020	61.63	
	$LaNi_5$	P6/mmm (191)	5.017	3.981	86.78	32.3
	La_2Ni_7	P63/mmc (194)	5.053	24.62	544.40	
x=25	MgH_2	$P4_2/mnm$ (136)	4.517	3.020	61.63	
	$LaNi_5$	P6/mmm (191)	5.017	3.981	86.78	26.9
	La_2Ni_7	P63/mmc (194)	5.053	24.62	544.40	
x=50	MgH_2	$P4_2/mnm$ (136)	4.517	3.020	61.63	
	$LaNi_5$	P6/mmm (191)	5.017	3.981	86.78	33.2
	La_2Ni_7	P63/mmc (194)	5.053	24.62	544.40	

4.2 Morphological Characterization by SEM with EDS

The elemental composition of the alloy has been studied by EDS technique at different sites of the ingots was found almost same at all the sites as shown in figure 4.2.

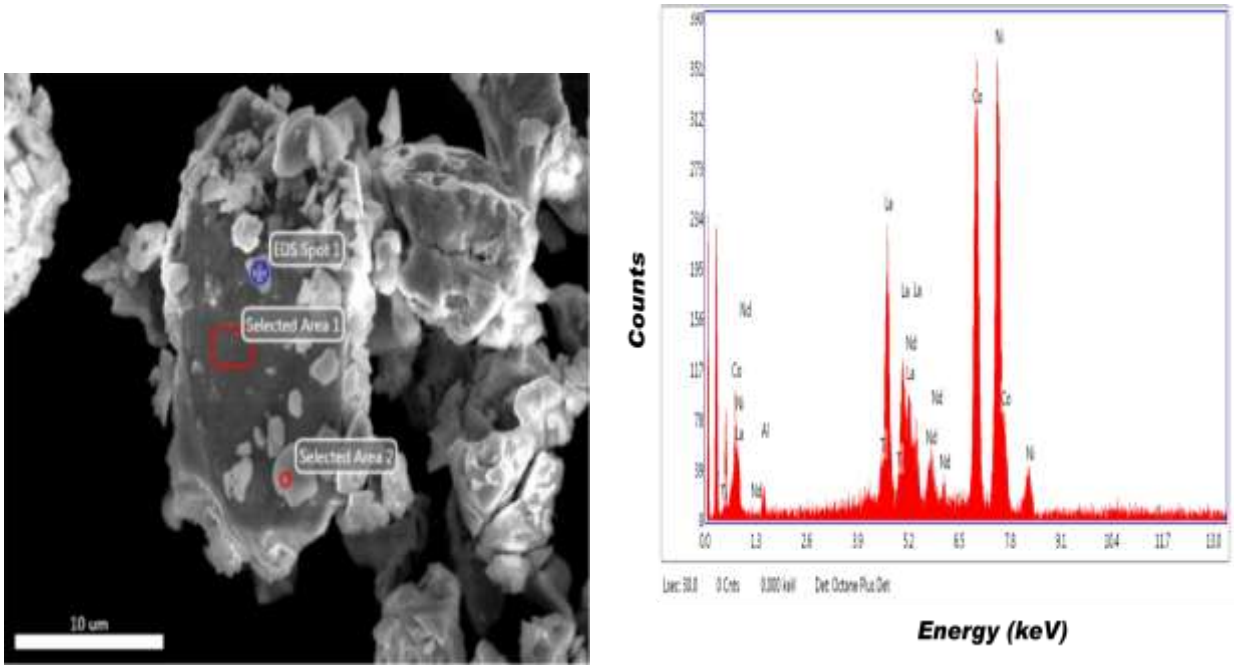

Figure 4.2.EDS analysis of $La_{23}Nd_{7.8}Ti_{1.1}Ni_{33.9}Co_{32.9}Al_{0.65}$

The elemental percentage of the alloy is shown in Table 4.3.

Table 4.2 -Results of EDS analysis (in weight) for $La_{23}Nd_{8.5}Ti_{1.1}Ni_{33.9}Co_{32.9}Al_{0.65}$

% Weight						
Area	**La**	**Nd**	**Ti**	**Ni**	**Co**	**Al**
1	**20.21**	**10.99**	**1.71**	**33.29**	**31.33**	**0.47**
2	**21.85**	**9.58**	**1.50**	**31.69**	**31.35**	**0.03**
EDS spot 1	**23.56**	**7.83**	**1.47**	**32.60**	**33.88**	**0.66**
Present material	**23**	**8.5**	**1.1**	**33.9**	**32.9**	**0.65**
EDS confirms composition of material under study						

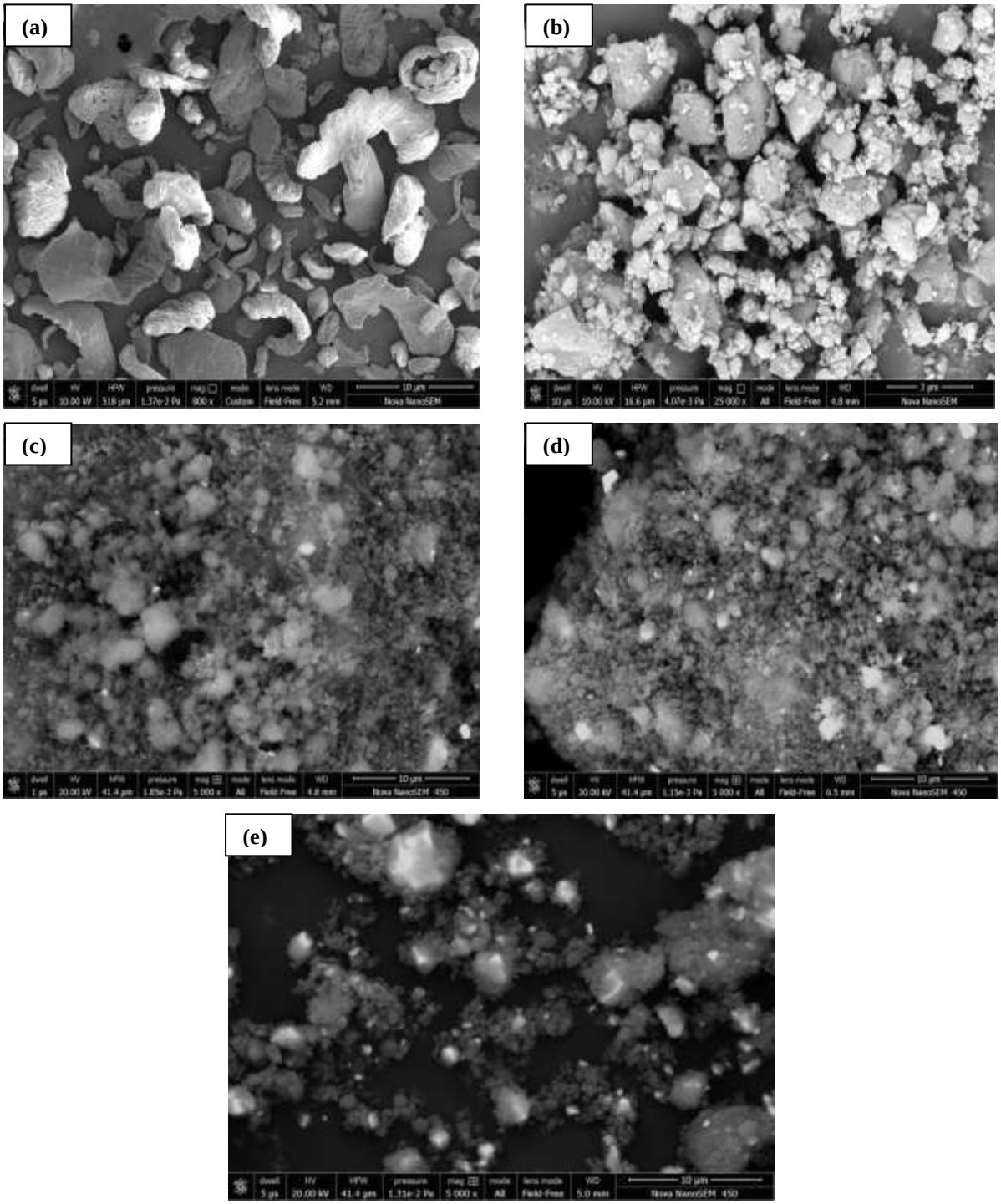

Figure 4.3.SEM analysis (BSE images) for the nanocomposites: (a) as-received MgH_2 (b)as-milled MgH_2 (c) MgH_2-10 wt% $La_{23}Nd_{7.8}Ti_{1.1}Ni_{33.9}Co_{32.9}Al_{0.65}$(d) MgH_2-25 wt% $La_{23}Nd_{7.8}Ti_{1.1}Ni_{33.9}Co_{32.9}Al_{0.65}$ (e) MgH_2-50 wt% $La_{23}Nd_{7.8}Ti_{1.1}Ni_{33.9}Co_{32.9}Al_{0.65}$

4.3 Desorption and Absorption Behavior of MgH_2-$La_{23}Nd_{7.8}Ti_{1.1}Ni_{33.9}Co_{32.9}Al_{0.65}$ Nanocomposite

4.3.1 TGA analysis

The effect of $La_{23}Nd_{7.8}Ti_{1.1}Ni_{33.9}Co_{32.9}Al_{0.65}$ with various concentration (x=10, 25 & 50 wt%) on the desorption temperature of MgH_2 was studied using the TGA method. Figure 4.4 (a) and (b) shows the TGA curves for hydrogen desorption of the nanocomposites.

The total relative weight loss of 10 hrs milled MgH_2 and MgH_2–x wt% $La_{23}Nd_{7.8}Ti_{1.1}Ni_{33.9}Co_{32.9}Al_{0.65}$is respectively about 7.3 wt%, 1.90 wt%, 1.27 wt%, and 2.40 wt% as shown in figure 4.4 (a).

The as-milled MgH_2 without the $La_{23}Nd_{7.8}Ti_{1.1}Ni_{33.9}Co_{32.9}Al_{0.65}$ starts to decompose at 220°C. The onset desorption temperature of as-milled MgH_2 is much lower compared to that of the as-received pure MgH_2 (T_{onset} =350°C) which is due to the effect of milling on particle and grain size reduction.

With the addition of alloy the starting temperature of hydrogen desorption decreases from 220°C to 192°C, 181°C and 173°C for 10, 25 and 50 wt% respectively. There is slight reduction in the desorption temperature as the concentration increase to 10 to 50 wt%.

The lowest onset temperature value is observed for the 50 wt.% alloy doped sample, followed by the10 wt% doped and the 25 wt% doped samples, while the pure MgH_2 sample gives the highest value.

It indicates that $La_{23}Nd_{7.8}Ti_{1.1}Ni_{33.9}Co_{32.9}Al_{0.65}$ significantly improves desorption properties of MgH_2.

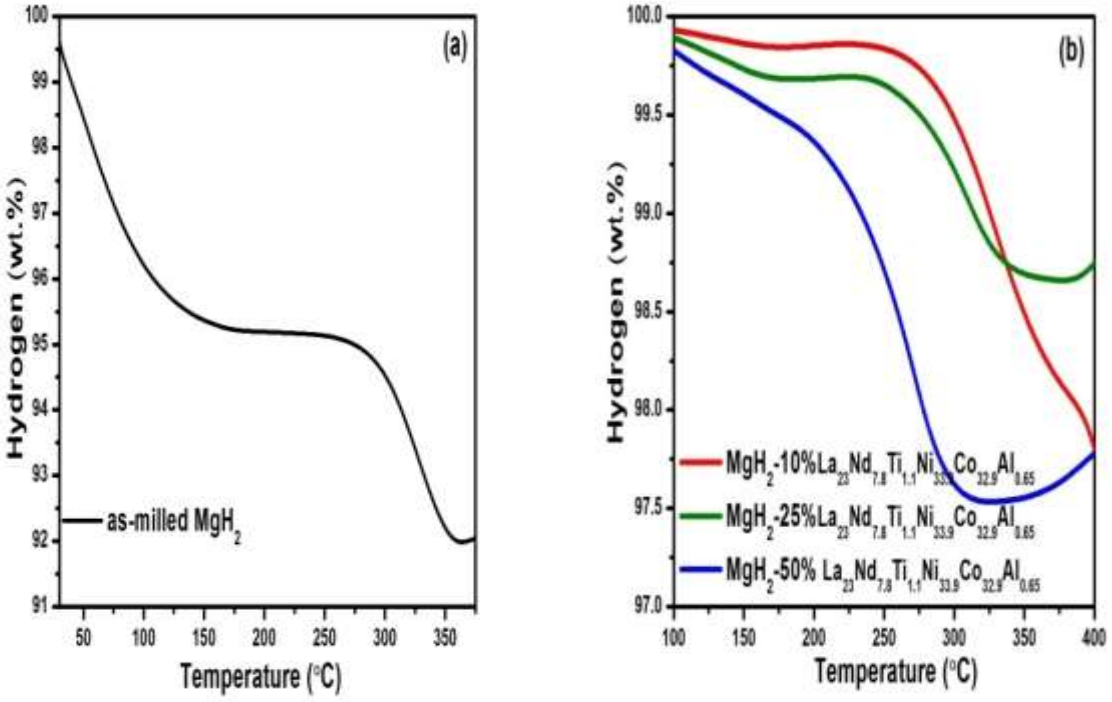

Figure 4.4.Hydrogen content measurement (a) as- milled MgH_2 (b) MgH_2- x wt% $La_{23}Nd_{7.8}Ti_{1.1}Ni_{33.9}Co_{32.9}Al_{0.65}$ alloy (x = 10, 25 & 50) nanocomposites

Activation energy of dehydrogenation reaction was also calculated to see the effect of $La_{23}Nd_{7.8}Ti_{1.1}Ni_{33.9}Co_{32.9}Al_{0.65}$ on the kinetics of MgH_2.DTA curve to analyze peak temperature of the as-milled MgH_2 and MgH_2-x wt% $La_{23}Nd_{7.8}Ti_{1.1}Ni_{33.9}Co_{32.9}Al_{0.65}$ nanocomposites.

Figure 4.5 shows the Kissinger plot of the hydrogen desorption reaction for as-milled MgH_2 and nanocomposites.

The activation energy can be calculated by plotting a curve between lnk and $1/RT_P$ using the following equation [138],

$$lnk = -\frac{E_a}{RT_P} + a$$

where, $k = \beta/T_P^2$

β = heating rate,

T_p= peak temperature

Ea = activation energy of desorption

R = gas constant

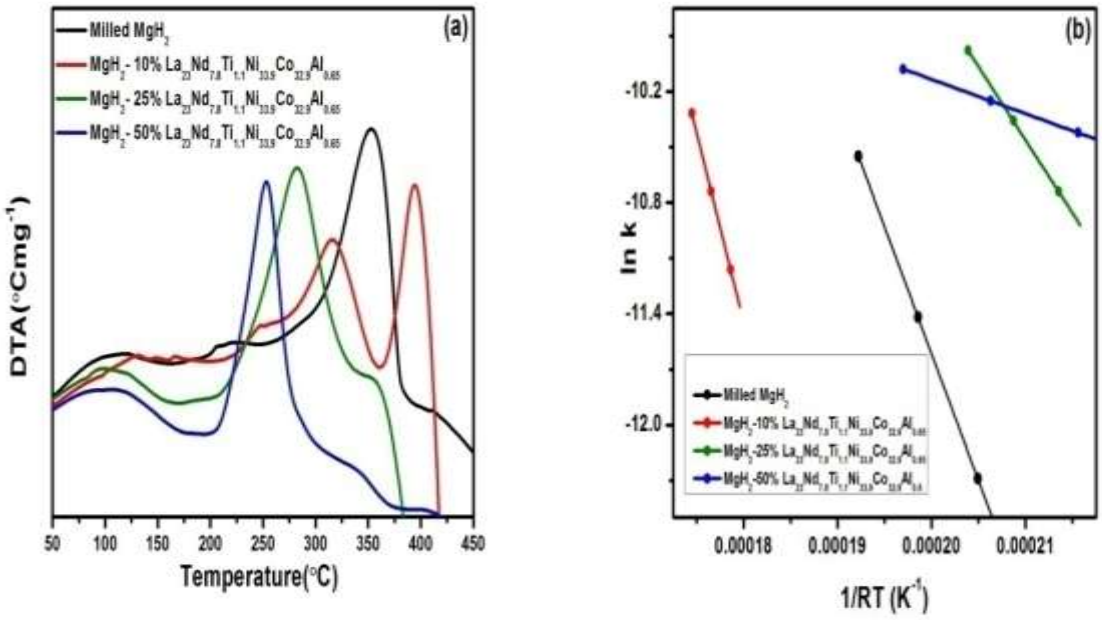

Figure 4.5. (a) DTA curve (b) Kissinger plot for dehydrogenation of the as- milled MgH_2 and MgH_2- x wt% $La_{23}Nd_{7.8}Ti_{1.1}Ni_{33.9}Co_{32.9}Al_{0.65}$ (x = 10, 25 & 50) nanocomposites

The activation energies were estimated from the slope of the straight line to be 177.90 KJ/mol for as-milled MgH_2, 204.65 KJ/mol for MgH_2-10 wt% $La_{23}Nd_{7.8}Ti_{1.1}Ni_{33.9}Co_{32.9}Al_{0.65}$,79.15 KJ/mol for MgH_2-25 wt% $La_{23}Nd_{7.8}Ti_{1.1}Ni_{33.9}Co_{32.9}Al_{0.65}$,185.29 KJ/mol MgH_2-50 wt% $La_{23}Nd_{7.8}Ti_{1.1}Ni_{33.9}Co_{32.9}Al_{0.65}$.

Table 4.3.Kinetics parameters for as milled MgH_2 and nanocomposites

Hydrogen (wt.%)	Activation energy(KJ/mol)	Peak Temperature (°C)	Heating rate (°C/min)	Sample
7	177.90 KJ/mol	353.38 352.76 337.66	5 10 15	Milled MgH_2
1.90	204.65 KJ/mol	394.65 404.82 414.19	5 10 15	MgH_2-10 wt% $La_{23}Nd_{7.8}Ti_{1.1}Ni_{33.9}Co_{32.9}Al_{0.65}$
1.27	79.15 KJ/mol	282.59 294.60 315.06	5 10 15	MgH_2-25 wt% $La_{23}Nd_{7.8}Ti_{1.1}Ni_{33.9}Co_{32.9}Al_{0.65}$
2.40	185.29 KJ/mol	282.59 294.60 315.06	5 10 15	MgH_2-50 wt% $La_{23}Nd_{7.8}Ti_{1.1}Ni_{33.9}Co_{32.9}Al_{0.65}$

4.3.2 DSC analysis

DSC investigations were carried out to investigate the effect of $La_{23}Nd_{7.8}Ti_{1.1}Ni_{33.9}Co_{32.9}Al_{0.65}$on hydrogen absorption behaviour of MgH_2 which is shown in figure 4.6 and is compared with as-milled MgH_2.Hydrogenation was performed at heating rate of $5^{\circ}Cmin^{-1}$ was maintained during DSC scan.

The addition of $La_{23}Nd_{7.8}Ti_{1.1}Ni_{33.9}Co_{32.9}Al_{0.65}$ reduce the onset temperature to 50°C for MgH_2-10 wt% $La_{23}Nd_{7.8}Ti_{1.1}Ni_{33.9}Co_{32.9}Al_{0.65}$ nanocomposites which further reduce to 20°C and 30°C for 25 wt% and 50 wt% $La_{23}Nd_{7.8}Ti_{1.1}Ni_{33.9}Co_{32.9}Al_{0.65}$ added MgH_2 indicating the positive effect of additive. However, increased amount of $La_{23}Nd_{7.8}Ti_{1.1}Ni_{33.9}Co_{32.9}Al_{0.65}$to 50 wt% reduces the peak height of peak at around 285°C. Even though complete hydrogenation could be achieved before the 10 hrs milled pure MgH_2 sample.

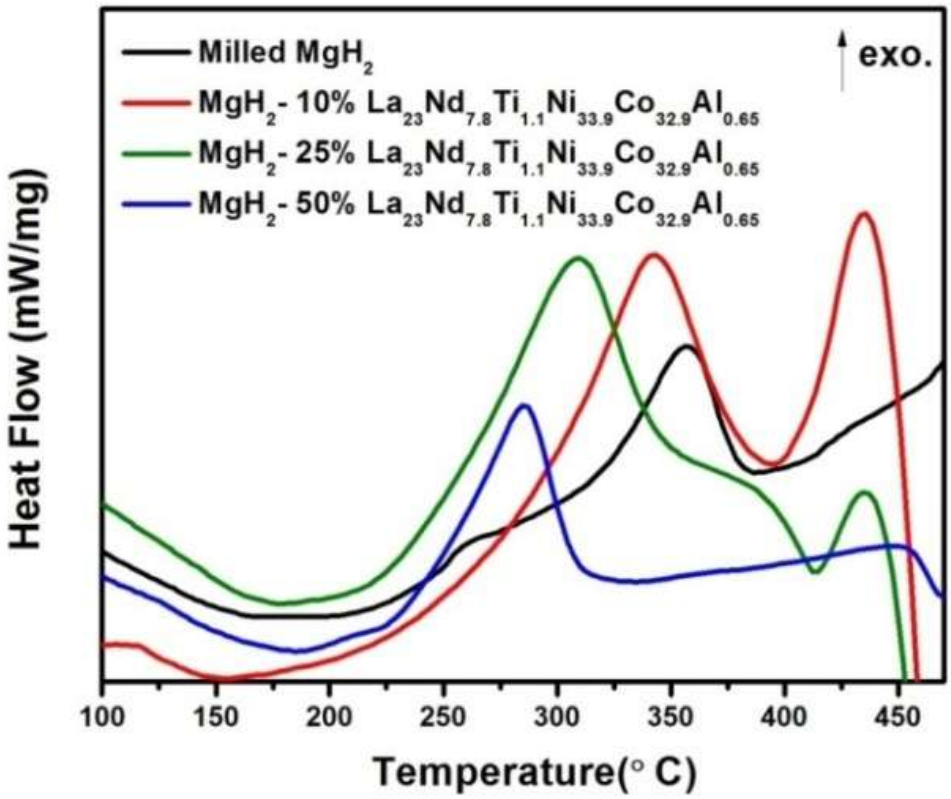

Figure 4.6. DSC curves for 10 hrs milled MgH_2 and MgH_2 –x wt% (10, 25 & 50) $La_{23}Nd_{7.8}Ti_{1.1}Ni_{33.9}Co_{32.9}Al_{0.65}$ nanocomposites

Chapter summary

- $La_{23}Nd_{7.8}Ti_{1.1}Ni_{33.9}Co_{32.9}Al_{0.65}$was synthesized first time by arc melting furnace and the effect of alloy content on hydrogenation properties of MgH_2 was studied.

- Compares the dehydrogenation characterization of MgH_2 with and without alloy showed that the 25 wt%$La_{23}Nd_{7.8}Ti_{1.1}Ni_{33.9}Co_{32.9}Al_{0.65}$doped MgH_2 powder decreases desorption temperature by about 60°C compare to the as-milled MgH_2.

- TGA result shows the activation energy is lower by about 98 kJ/mol compared to as-milled MgH_2. MgH_2-25 wt%$La_{23}Nd_{7.8}Ti_{1.1}Ni_{33.9}Co_{32.9}Al_{0.65}$ nanocompositesshows best result.

- SEM micrographs confirmed that activation pulverizes the alloy ingot into fine particles.

- DSC curves that 10 hrs milled MgH_2 consists of two exothermic peaks at 260°C and 356 $^{\circ}$C with onset at around 220°C, which means that the hydrogenation could be started at as low as 220°C.

The next chapter presents the hydrogen kinetics studies of MgH_2-FeTi composites.

Chapter-5

HYDROGEN KINETICS STUDIES OF MgH_2-FeTi COMPOSITES

Introduction

In present work MgH_2 -FeTi composite has been studied. Such system with various weight fractions of both constituents were processed by ball milling which very effectively reduced the particle size and formed nanocrystalline grains within the powder particles. Hydrogen desorption was tested using a thermo Gravimetric Analysis (TGA) and DSC.

5.1 Microstructural and Morphological Characterization

5.1.1 Phase analysis of MgH_2-FeTi nanocomposites

The XRD patterns of the MgH_2-x wt% FeTi (x=10, 25 & 50) composites after milling confirms that the microstructure comprises primarily MgH_2 and FeTi with a small amount of minority intermetallic Fe_2Ti is shown in figure 5.1.

The formation of Fe_2Ti is related to inhomogeneous structure of ingot obtained during casting process. It allows as to assume that FeTi intermetallic phase will not act only as a catalytic additive but also forming $FeTiH_x$ hydride might play the role as composite constituent.

The average crystallite size was calculated using Debye Scherer formula:

$$\boldsymbol{D = \frac{0.9\lambda}{\beta \cos\theta}}$$

Where, λ = X-ray wavelength

β = line broadening at half the maximum intensity in radian

θ = Bragg angle.

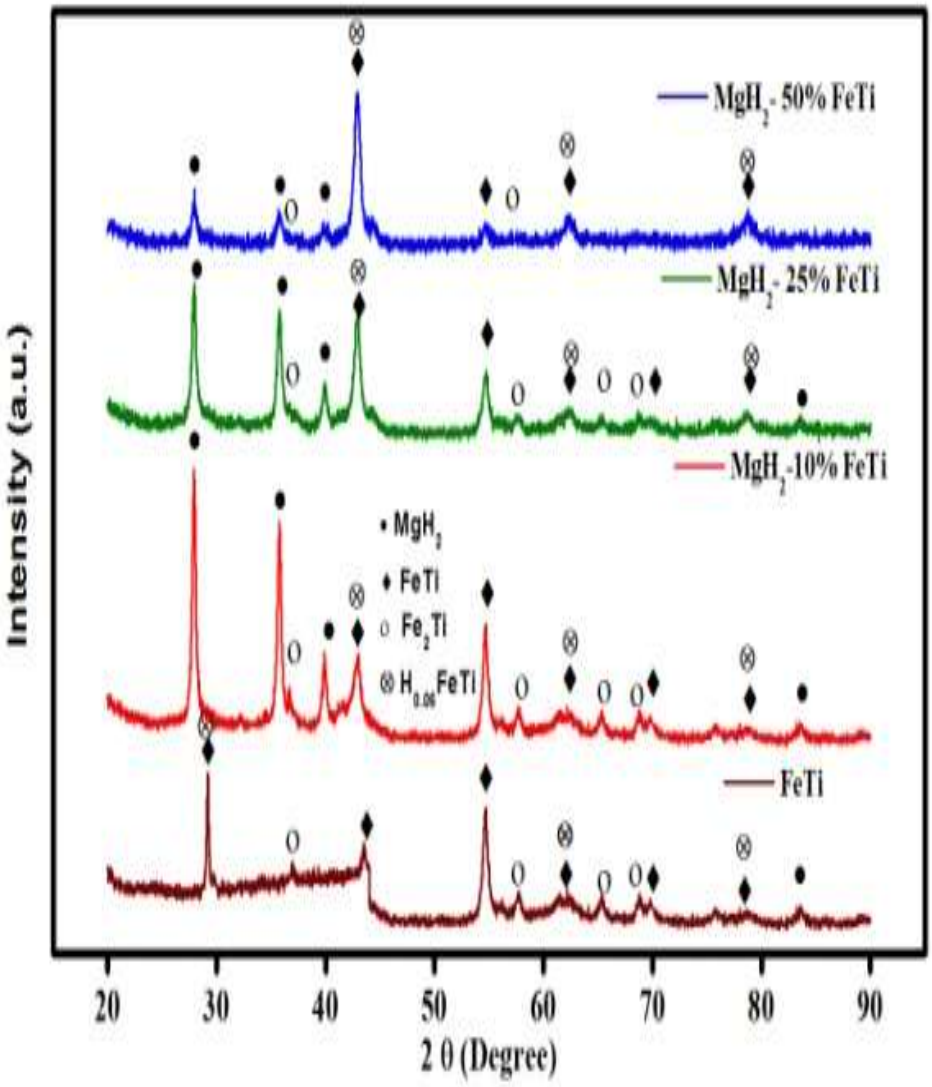

Figure 5.1. XRD patterns of MgH_2-x wt% FeTi (x=10, 25 & 50) nanocomposites

The average crystallites size for the MgH_2-x wt% FeTi (x=10,25 &50) nanocomposites are estimated to be about 43.5 nm, 50.1 nm and 26.1 nm respectively as shown in Table 5.1.

Table 5.1.The crystallographic data for MgH_2-x wt% FeTi (x =10, 25 & 50) nanocomposites

Sample	Phase	Space group (No.)	Lattice parameters *a*[Å] *c*[Å]	Volume V[Å ^{3}]	D_{avg} (nm)
x=10	MgH_2 FeTi Fe_2Ti $H_{0.06}FeTi$	$P4_2/mnm$ (136) Pm3m (221) P63/mmc (194) Pm3m (221)	4.517 3.020 2.975 2.975 4.785 7.799 2.979 2.979	61.63 26.33 154.64 26.44	43.5
x=25	MgH_2 FeTi Fe_2Ti $H_{0.06}FeTi$	$P4_2/mnm$ (136) Pm3m (221) P63/mmc (194) Pm3m (221)	4.517 3.020 2.975 2.975 4.785 7.799 2.979 2.979	61.63 26.33 154.64 26.44	50.1
x=50	MgH_2 FeTi Fe_2Ti $H_{0.06}FeTi$	$P4_2/mnm$ (136) Pm3m (221) P63/mmc (194) Pm3m (221)	\ 4.517 3.020 2.975 2.975 4.785 7.799 2.979 2.979	61.63 26.33 154.64 26.44	26.1

5.1.2 Morphological analysis of nanocomposites

The elemental composition of the alloy has been checked by EDS technique at different sites of the ingots and thee elemental composition was found almost same at all the sites.

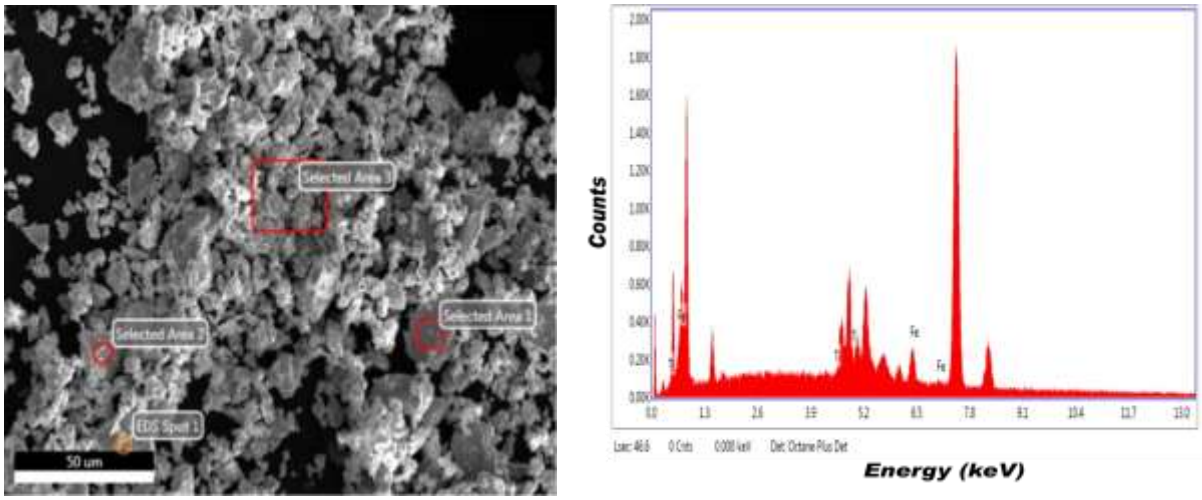

FIGURE 5.2.EDS analysis of the FeTi

The elemental percentage is shown in Table 5.2.

Table 5.2. Elemental composition in the FeTi by EDS analysis

Weight %		
Area	**Fe**	**Ti**
1	**65.96**	**34.04**
2	**68.93**	**31.07**
3	**67.03**	**32.97**
EDS spot 1	**69.10**	**30.90**
EDS confirms composition of material under study		

The morphology of the MgH_2 - x wt% FeTi (x= 10, 25 & 50) composites as shown in Figure 5.3.

It is clearly seen that ball milling reduced significantly the original particle size of MgH_2. There is no visible influence of FeTi content in various composites on their powders particle size and morphology.

At higher magnification rather smooth edges of particles can be seen,indicating the effect of mechanical treatment, cracks and gaps can be observed at higher magnification as well.

On the basis of the microscopic observation one could conclude that the surface of all powders synthesized is highly developed due to the high energy milling as the composites milled.

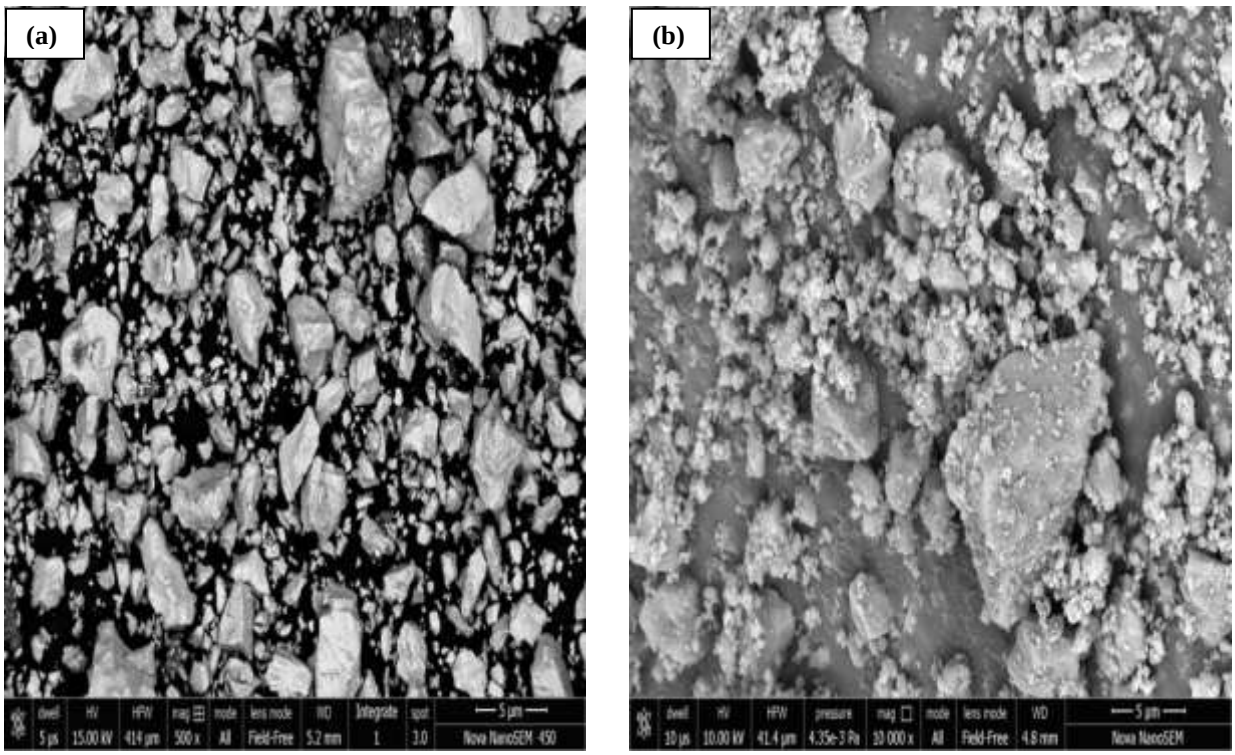

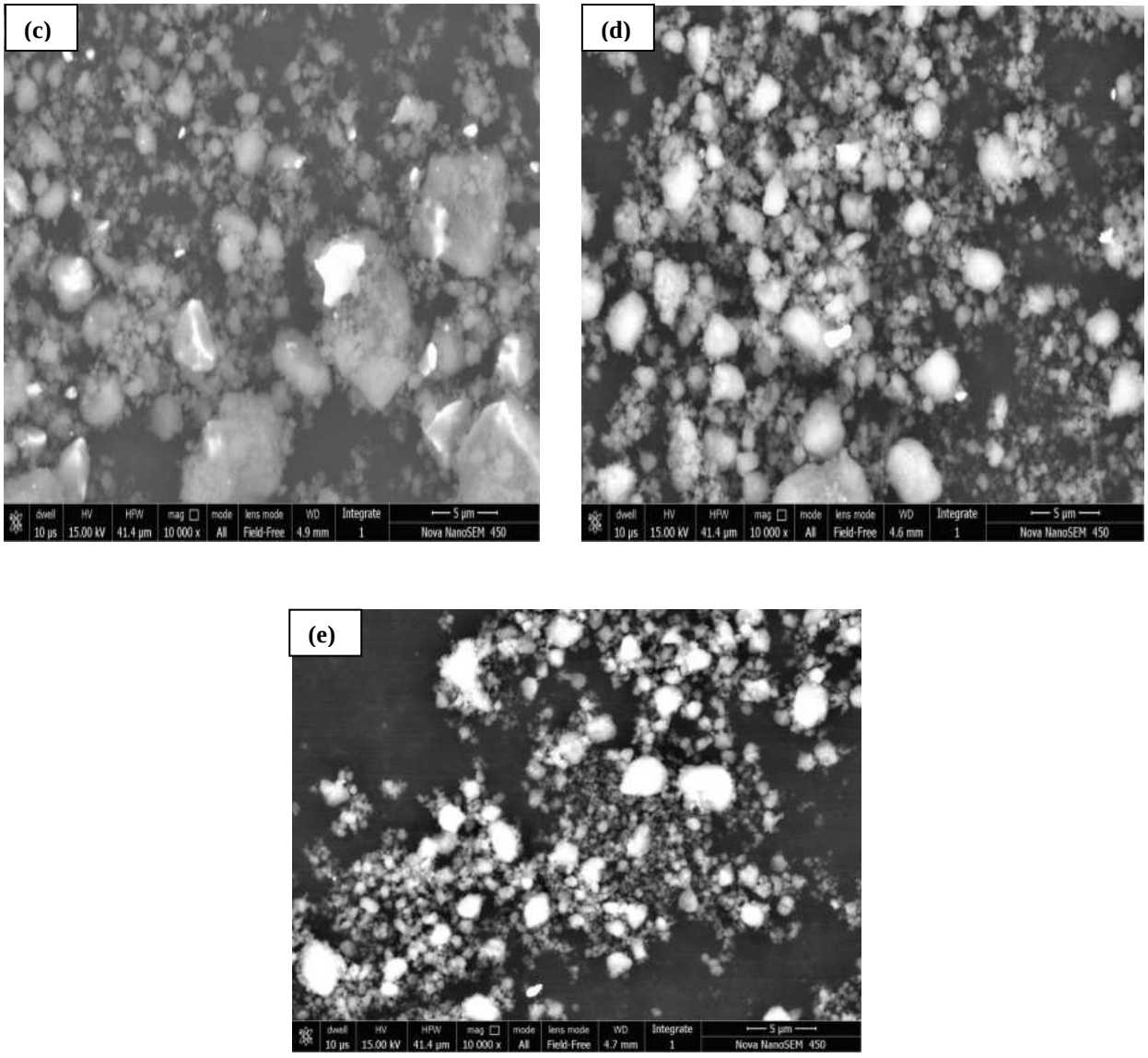

Figure 5.3.SEM analysis (BSE images) for the nanocomposites: (a) FeTi (b) as milled MgH_2 (c) MgH_2-10 wt.% FeTi (d) MgH_2-25 wt.% FeTi (e) MgH_2-50 wt.% FeTi

5.2 Desorption and Absorption Behaviour of MgH_2-FeTi Nanocomposites

5.2.1 TGA analysis

In present studies TGA studies were undertaken at a heating rate of 5, 10 & 15°C/min under 0.1

MPa Ar atmospheres. The total relative weight loss of as-milled MgH_2 and MgH_2-x wt% FeTi is respectively about 7.3 wt%, 1.02 wt%, 2.10 wt% and 2.84 wt% as shown in figure 5.4.

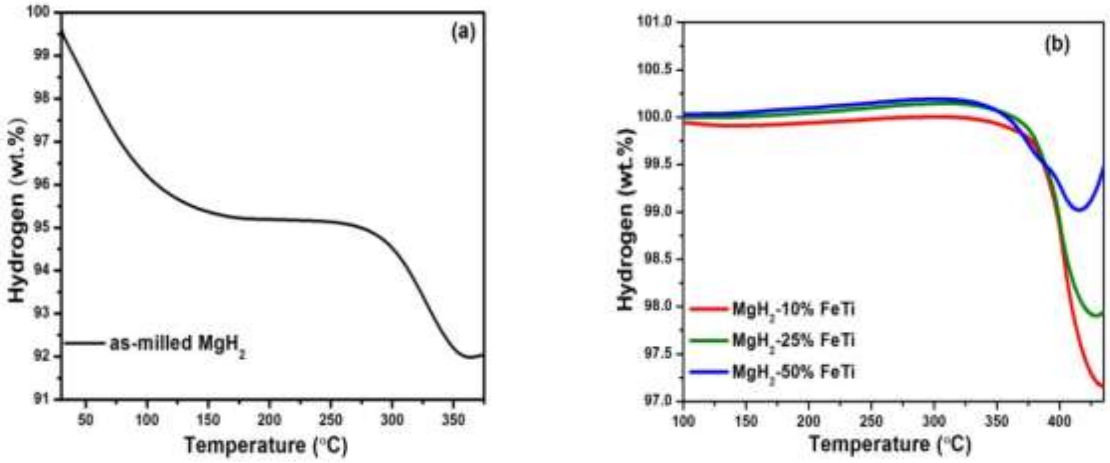

Figure 5.4. Hydrogen content measurement: (a) as- milled MgH_2 (b) MgH_2-x wt% FeTi (x = 10, 25 & 50) nanocomposites

DTA curve were undertaken to analyse peak temperature of the as-milled MgH_2 and MgH_2-x wt% FeTi samples under various heating rate (5,10 &15°C/min) and are shown in figure 5.5 (a). A curve plotting between lnK *vs* $1/RT_p$ helps in calculating the activation energy of the Mg composite.

In order to see the effect of alloy on kinetics of MgH_2 a systematic study of activation energy of the dehydrogenation reaction was also calculated. Figure 5.5 (b) is a Kissinger plot of the hydrogen desorption reaction for as-milled MgH_2 and MgH_2-x wt% FeTi (x=10, 25 & 50) composite. The activation energy has been calculated by following equation.

$$\boldsymbol{lnk = -\frac{E_a}{RT_P} + a}$$

Where, $k = \beta/T_p^2$

β = heating rate

T_p = Peak temperature

E_a = activation energy of desorption

R = Gas constant.

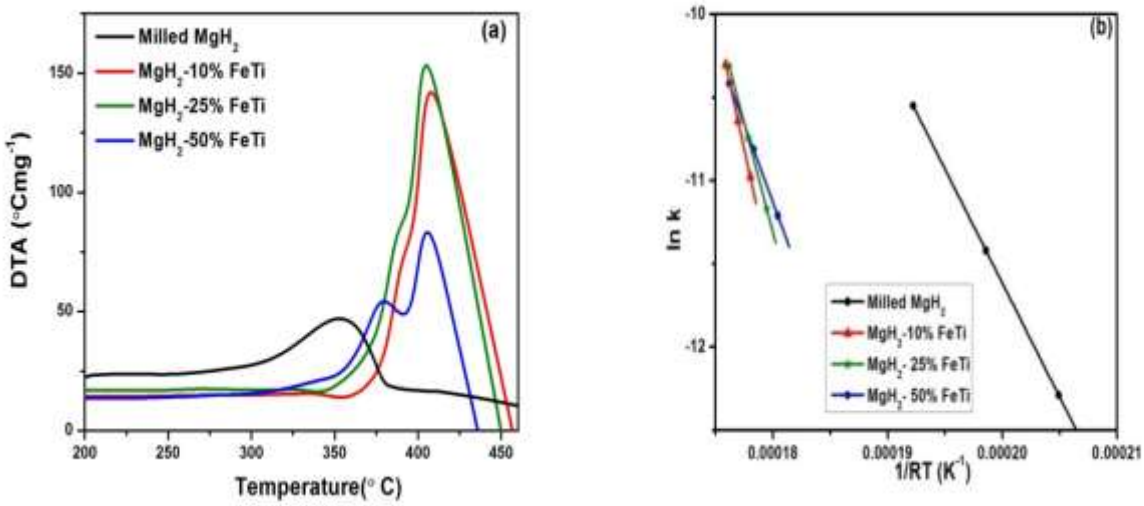

Figure 5.5. (a) DTA curve (b) Kissinger plot for dehydrogenation of the as- milled MgH_2 and MgH_2-FeTi nanocomposites

The activation energies obtained were 177.90 KJ/mol, 215.69 KJ/mol, 162.46 KJ/mol, 87.93 KJ/mol for 10hr milled MgH_2, MgH_2-10 wt% FeTi, MgH_2-25 wt% FeTi, MgH_2-50 wt% MgH_2 respectively.

It was found from Kissinger's plot that the activation energy (E_a) for the dehydrogenation of the MgH_2-50 wt% FeTi is much lower than as- milled MgH_2 indicating a significant improvement in dehydrogenation kinetics of MgH_2 by the addition of FeTi and MgH_2-25 wt% FeTi slightly lower than as-milled MgH_2.

It was found from Kissinger's plot that the activation energy (E_a) for the dehydrogenation of the MgH_2-50 wt% FeTi is much lower than as- milled MgH_2 indicating a significant improvement in dehydrogenation kinetics and for MgH_2-25 wt% FeTi is slightly lower than as-milled MgH_2.

Table 5.3.Kinetic Parameters for as-milled MgH_2 and MgH_2-x wt% FeTi

Hydrogen (wt %)	Activation energy (KJ/mol)	Peak Temperature (°C)	Heating rate (°C/min)	Sample
7.3	177.90 KJ/mol	353.38 352.76 337.66	5 10 15	Milled MgH_2
1.02	215.69 KJ/mol	398.66 399.85 408.71	5 10 15	MgH_2-10 wt% FeTi
2.10	162.46 KJ/mol	392.24 400.89 407.48	5 10 15	MgH_2-25 wt% FeTi
2.84	87.93 KJ/mol	387.84 403.08 407.48	5 10 15	MgH_2-50 wt% FeTi

5.2.2 DSC analysis

The above nanocomposites were then employed for DSC measurements to study the effect of FeTi on the hydrogen absorption behaviour of MgH_2. Figure 5.6 show a compilation of DSC curves for the MgH_2-x wt% FeTi (x=10, 25 & 50 wt%) compared to the DSC curve for milled

MgH_2. Hydrogenation was performed under 2 MPa hydrogen pressure and a heating rate of 15 $^{\circ}C\ min^{-1}$ was maintained during DSC scan.

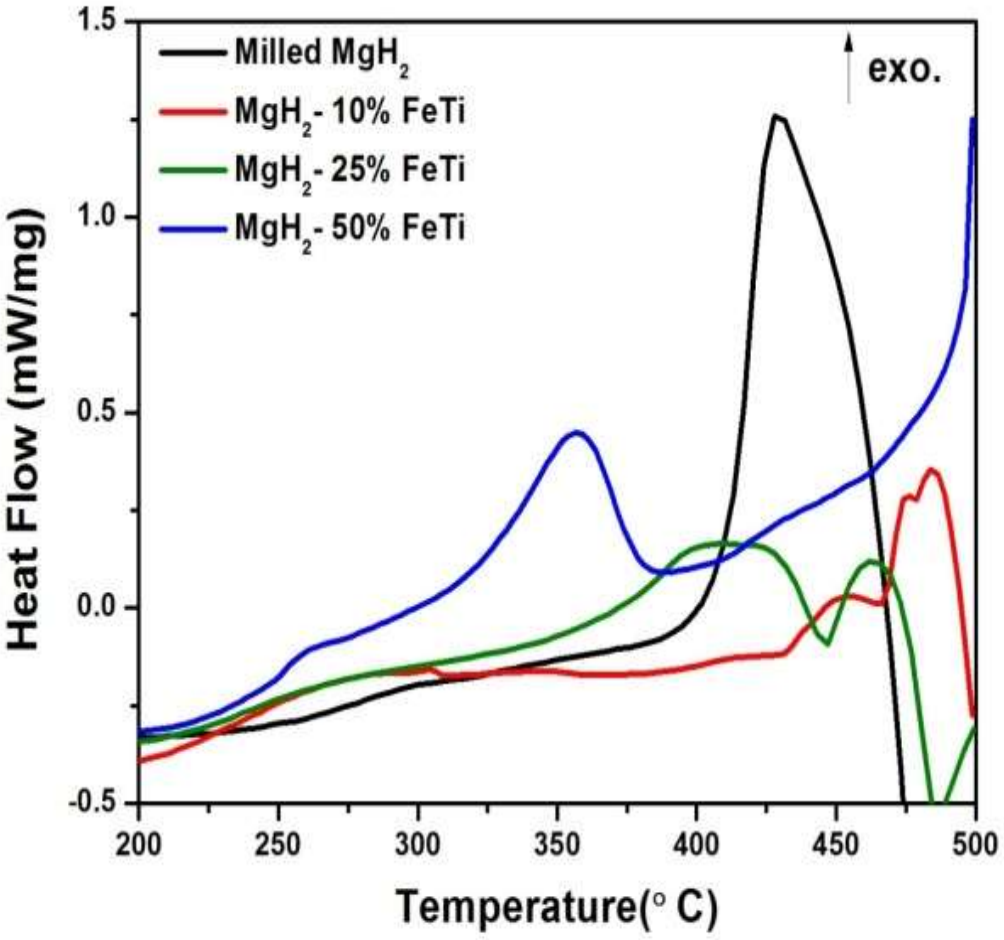

Figure 5.6. DSC curves for 10 hrs milled MgH_2 and MgH_2-FeTi nanocomposites.

It was observed from DSC traces that 10 hrs milled MgH_2 consists of two exothermic peaks at 260°C and 356°C with onset at around 250°C showing that the hydrogenation could be started at as low as 250°C. The appearance of multiple peaks in the DSC may be attributed to the presence of activated and non-activated part of the sample.

The additions of FeTi reduce the onset temperature to 25°C for MgH_2-25 wt% FeTi sample. On increasing the concentration of FeTi 25 to 50 wt% the onset temperature remains same. However, increased amount of FeTi to 25 wt% reduces the peak height of peak at around 440°C. Even though complete hydrogenation could be achieved before the 10 hrs milled pure MgH_2 sample.

Chapter Summary

- FeTi was synthesized first time by arc melting furnace and the effect of FeTi content on hydrogenation properties of MgH_2 was studied.

- Comparing the Dehydrogenation characterization of MgH_2 with and without FeTi showed that the 25 wt% FeTi doped MgH_2 powder decreases desorption temperature by about 60°C compare to the as-milled MgH_2.

- TGA result indicated that the activation energy is lower by about 89 kJ/mol for MgH_2-50 wt% FeTi compared to as-milled MgH_2 showing 50 wt% added alloy sample shows better results. SEM micrographs confirmed that activation pulverizes the alloy ingot into fine particles.

- DSC studies showed that 10h milled MgH_2 consists of two exothermic peaks at 260°C and 356°C with onset at around 250°C, which means that the hydrogenation could be started at as low as 250 °C. It is shown that the hydrogen desorption temperature and activation energy of the MgH_2-FeTi composites decreases linearly with increasing weight fraction of FeTi.

The next chapter presents the improved dehydrogenation kinetics of MgH_2 due to NiMnAl.

*****

Chapter-6

IMPROVED DEHYDROGENATION KINETICS OF MgH_2 DUE TO NiMnAl

Introduction

Composites formed by Ni, Mn and Al with MgH_2 results in fairly good hydrogen storage material but no clear explanation on the effect of NiMnAl on $MgH_2$for hydrogenation properties is found in literature. Motivated by this situation the aim of the present work is to study the effect of NiMnAl on hydrogen sorption kinetics of MgH_2. The hydrogenation behavior of the composite was examined through differential scanning calorimetry (DSC) and thermogravimetric analysis (TGA).

6.1 Structural Characterization by XRD

Figure 6.1.shows XRD patterns of the Mg-based nanocomposites containing 10, 25, 50 wt% NiMnAl as additive after 10h of ball milling.

When alloying with Ni, the hydrides transform from MgH_2 to Mg_2NiH_4 and the enthalpy of Mg_2NiH_4 is 64 kJ/mol H_2 which is lower than that of MgH_2. In these XRD patterns various phases were identified e.g. MgH_2, Mg_2Ni and Mg_2NiH_4.

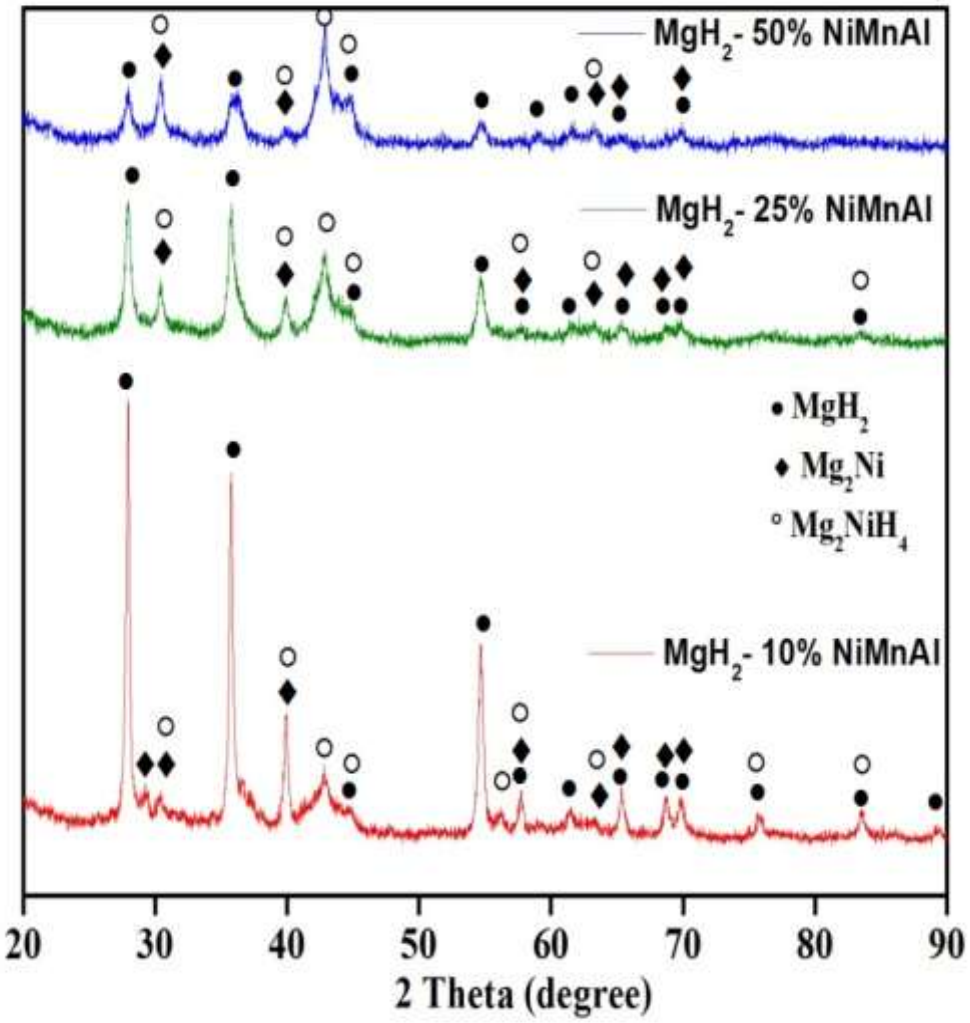

Figure 6.1. XRD pattern of MgH_2-x wt% (10, 25 & 50) NiMnAl nanocomposites

The increase in unit cell volume on activation is due to hydrogen absorption which decreases density of alloy resulting in decrease in lattice constant. Hydrogen absorption increases volume of alloy resulting in decrease in density as shown in figure 6.2, resulting in increase in lattice constants.

While desorption of hydrogen the material takes original shape, showing the increase in density that is decrease in lattice constant.

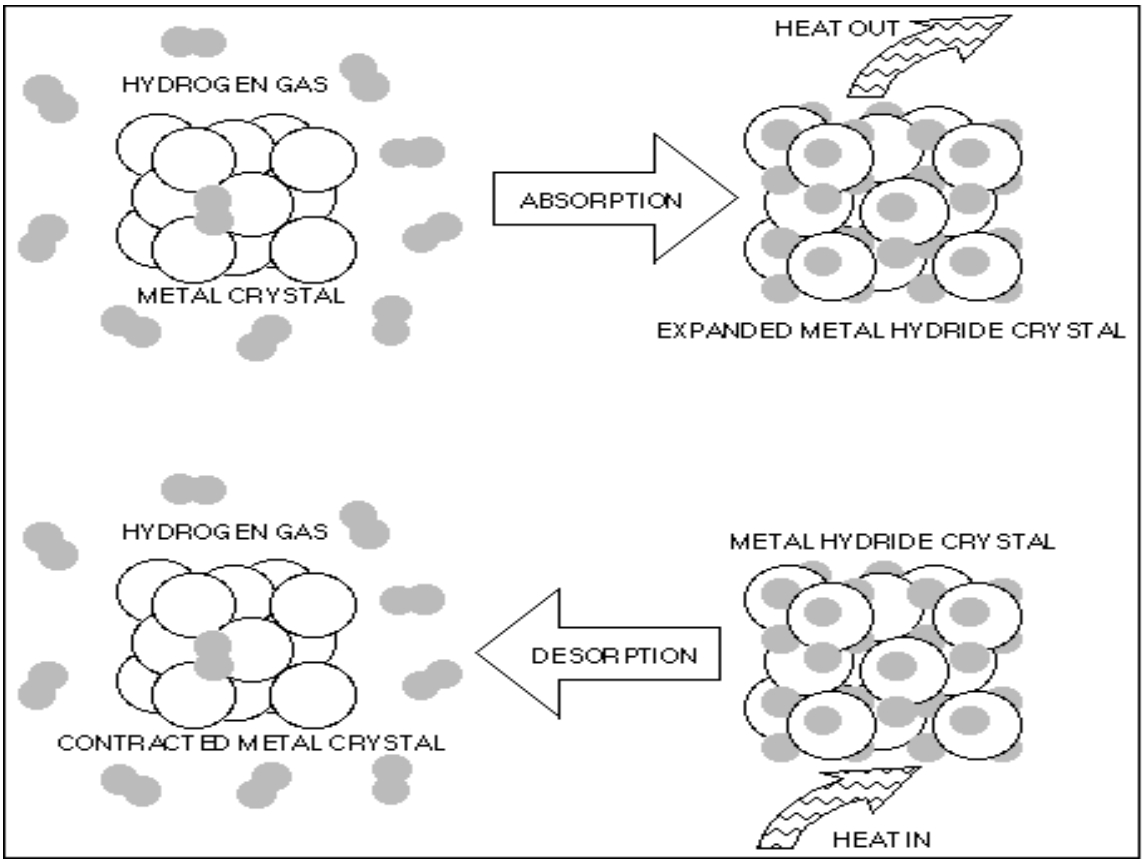

Figure 6.2.Hydrogen absorption desorption mechanism

The peak intensities decrease with the broadening of peaks which indicates accumulation of mechanical strains and reduction in particle size during milling .The average crystallite size was calculated using Debye Scherer formula:

$$\boldsymbol{D = \frac{0.9\lambda}{\beta \cos\theta}}$$

Where λ is the X-ray wavelength, β is the line broadening at half the maximum intensity in radian, θ is the Bragg angle. Values of average crystallites size for the MgH_2-x wt% NiMnAl (x=10,25,50) nanocomposites are estimated to be about 54 nm, 42 nm, and 43 nm respectively as shown in Table 6.1.

Table 6.1.The crystallographic data for MgH_2-x wt% NiMnAl (x =10, 25 & 50) nanocomposites

Sample	Phase	Space group (No.)	Lattice parameters *a*[Å]	*c*[Å]	Volume V[Å ^{3}]	D_{avg} (nm)
x=10	MgH_2 Mg_2Ni Mg_2NiH_4	$P4_2/mnm$(136) $P6_222$ (180) Cc (9)	4.517 5.205 15.0374	3.0205 13.236 6.4932	61.63 310.55 548.75	54
x=25	MgH_2 Mg_2Ni Mg_2NiH_4	$P4_2/mnm$(136) $P6_222$ (180) Cc (9)	4.517 5.205 15.0374	3.0205 13.236 6.4932	61.63 310.55 548.75	42
x=50	MgH_2 Mg_2Ni Mg_2NiH_4	$P4_2/mnm$(136) $P6_222$ (180) Cc (9)	4.517 5.205 15.0374	3.0205 13.236 6.4932	61.63 310.55 548.75	43

6.2 Morphological characterization by SEM

The chemical composition of the NiMnAl alloyhas been studied by EDS technique at different sites of the ingots was found almost same at all the sites as shown in figure 6.3.

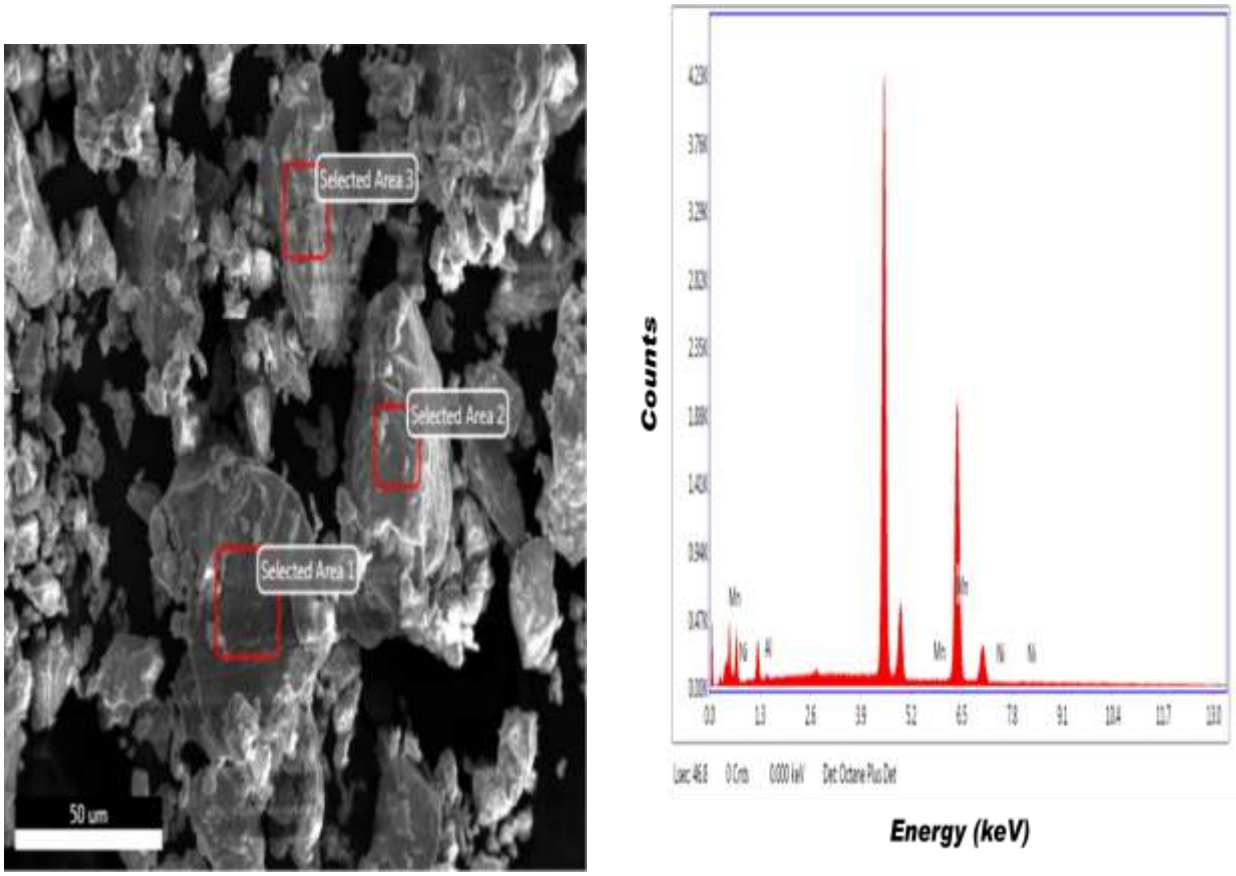

Figure 6.3: EDS analysis of the NiMnAl

The elemental percentage of the alloy is shown in Table 6.2.

EDS analysis confirmed that bright spots represent Mg_2NiH_4 phase while the dark areas represent MgH_2/Mg. It is clearly evident from the figure that the alloy is homogeneously dispersed in the MgH_2/Mg matrix.

Table 6.2. Chemical composition of the NiMnAl alloys at various area by EDS

Weight %			
Area	**Ni**	**Mn**	**Al**
1	**43.77**	**41.17**	**15.06**
2	**42.33**	**39.17**	**18.50**
3	**42.55**	**41.33**	**16.12**
EDS confirms composition of material under study			

SEM images obtained in back-scattered electrons (BSE) mode for the nanoocmposites containing milled MgH_2,pure NiMnAl and MgH_2- x wt% NiMnAl (10, 25 &50) alloy are shown in figure 6.4.

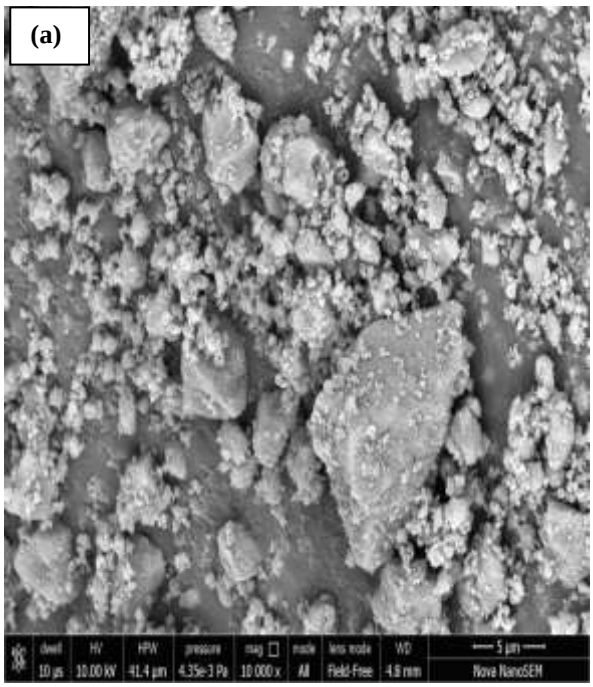
(a)
dwell HV HFW pressure mag mode lens mode WD
10 µs 10.00 kV 41.4 µm 4.35e-3 Pa 10 000 x All Field-Free 4.8 mm
5 µm
Nova NanoSEM

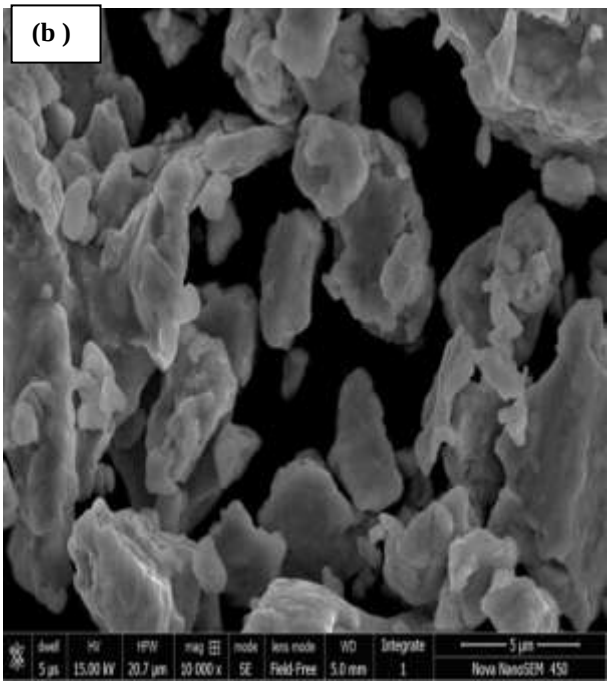
(b)
dwell HV HFW mag mode lens mode WD Integrate
5 µs 15.00 kV 20.7 µm 10 000 x SE Field-Free 5.0 mm 1
5 µm
Nova NanoSEM 450

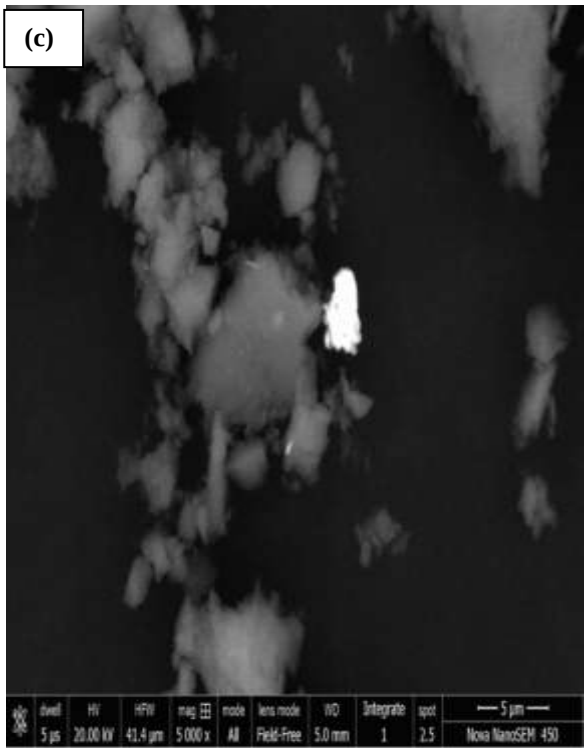
(c)
dwell HV HFW mag mode lens mode WD Integrate spot
5 µs 20.00 kV 41.4 µm 5 000 x All Field-Free 5.0 mm 1 2.5
5 µm
Nova NanoSEM 450

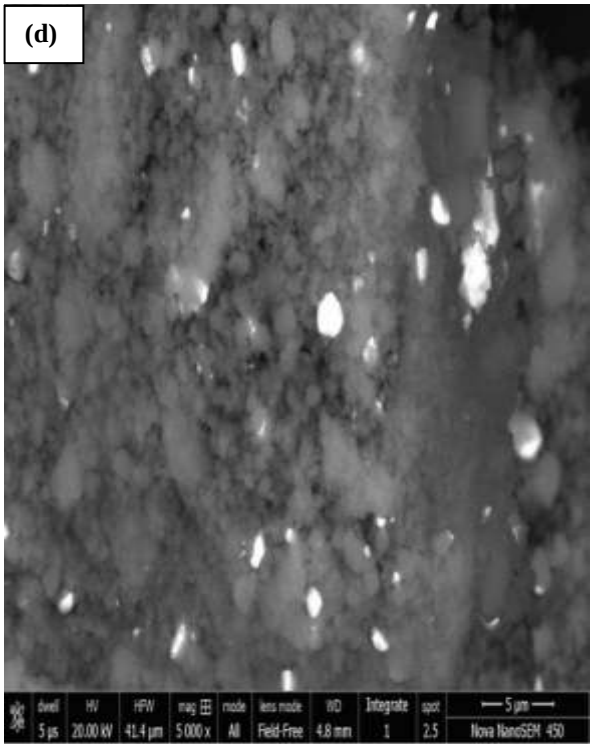
(d)
dwell HV HFW mag mode lens mode WD Integrate spot
5 µs 20.00 kV 41.4 µm 5 000 x All Field-Free 4.8 mm 1 2.5
5 µm
Nova NanoSEM 450

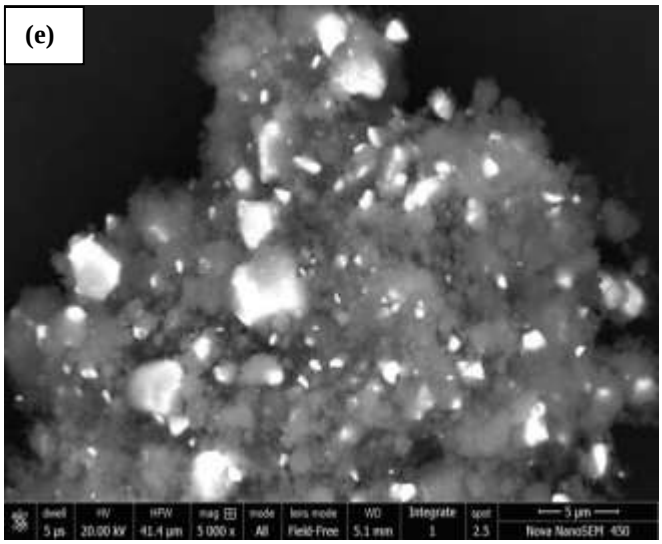

Figure 6.4: Morphological analysis of (a) milled MgH_2 (b) NiMnAl (c) MgH_2-10 wt% NiMnAl (d) MgH_2-25 wt% NiMnAl (e) MgH_2-50 wt% NiMnAl.

These images reveal morphology of alloy in the form of very fine agglomerates containing particles with different formats having planar and spherical faces. There is no notable differences was found using additive type confirming that the milling time (10 hrs) was not only enough to reduce Mg but also to result in a good level of mixing and homogeneity.

6.3 Kinetic Study of the Dehydrogenation/Hydrogenation Process

6.3.1 TGA analysis

Desorption behavior of MgH_2-x wt% NiMnAl (x=10, 25 & 50) is observed using TGA technique under 0.1 MPa Ar atmosphere. Figure 6.5 presents the TG performances of as-milled $MgH_2$and the MgH_2 doped with x wt% NiMnAl at the heating rate of 15˚C/min.

From the TG curves, it can be seen clearly that the addition of 10 wt% of NiMnAl the onset temperature drops significantly from 260°C to 210°C and decreases gradually as the wt % of NiMnAl additive further increased.

Most noticeable result is for MgH_2-50 wt% NiMnAl system which starts releasing hydrogen at 196°C temperature and total amount was found to be 2.3 wt%. Alloying can moderate the desorption temperature to a certain degree at the cost of reduced hydrogenation capacity.

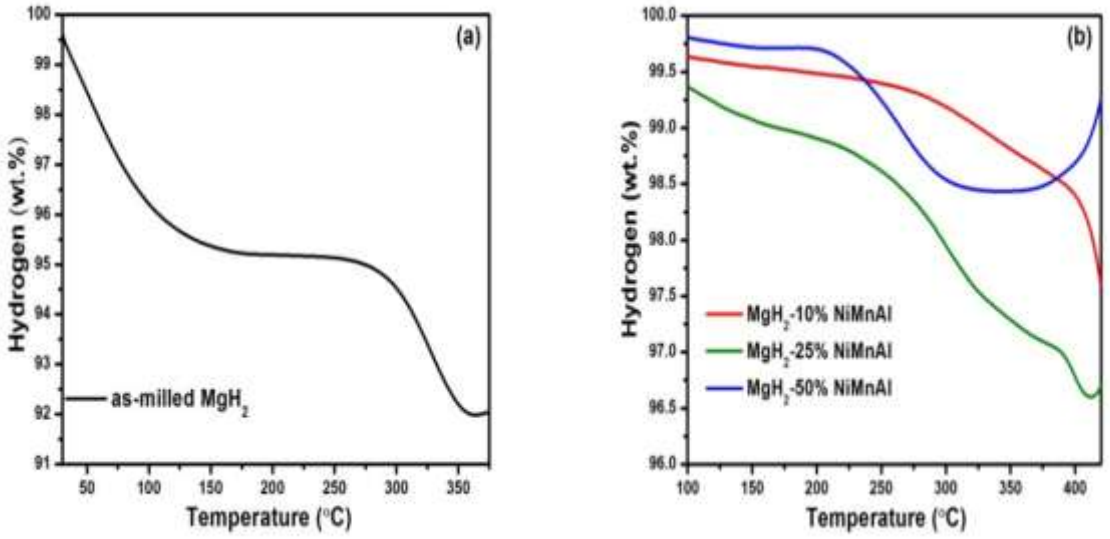

Figure 6.5.(a) Hydrogen content measurement (a) as- milledMgH_2 (b) MgH_2- x wt% NiMnAl (x = 10, 25 & 50) nanocomposites

DTA curve to analyze peak temperature of the as-milled MgH_2 and MgH_2-x wt% NiMnAl samples under different heating rate 5, 10 & 15 °C/min are shown in Figure 6.6 (a).

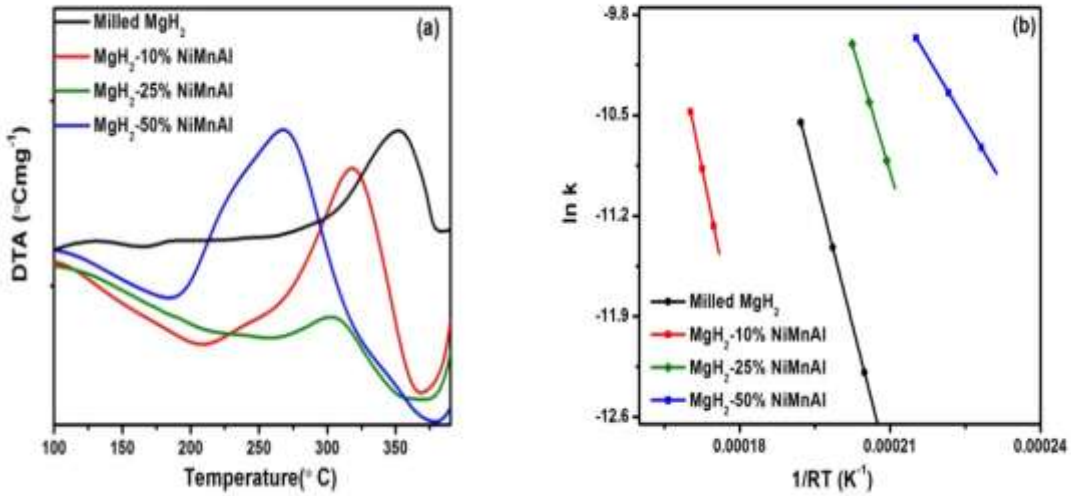

Figure 6.6 (a) DTA curve (b) Kissinger plot for dehydrogenation of the as- milled MgH_2 and MgH_2- x wt% NiMnAl (x = 10, 25 & 50) nanocomposites

Activation energy of the dehydrogenation reaction was also calculated to see the effect of alloy on kinetics of MgH_2. Figure 5(c) Shows Kissinger plot of the hydrogen desorption reaction for as-milled MgH_2 and MgH_2- x wt% NiMnAl (10,25 & 50) nanocomposite. The activation energy was calculated by plotting a curve between ln k and $1/RT_p$ using the following equation [138]:

$$\boldsymbol{lnk = -\frac{E_a}{RT_P} + a}$$

Where $k = \beta/T_p^2$,

β =Heating rate

T_p= Peak temperature

E_a = Activation energy of desorption

R = Gas constant

The activation energies were estimated to be 177.90 KJ/mol for as-milled MgH_2, 173.09 KJ/mol, 117.62 KJ/mol, 58.66 KJ/mol for MgH_2-x wt% NiMnAl (x=10,25 & 50) respectively. With increasing concentration of alloy activation energy decreases.

It is observed from Figure 5(c) that the activation energy (E_a) for the dehydrogenation is lowered by 4.81, 60.28, 119.24 KJ/mol for MgH_2-x wt% (x= 10, 25 & 50) NiMnAl and the 50 wt% doped MgH_2 has much lower activation energy than as- milled MgH_2. These results indicate a significant improvement in dehydrogenation kinetics of MgH_2 by the addition of alloy.

It can be seen that using whichever methods [139], increasing Ni content brings on a decrease in the hydrogen desorption activation energy which shows that Ni can facilitate the improvement of the hydrogen desorption kinetics of alloys. The reason that increasing Ni content improves the hydrogen absorption and desorption kinetics of the nanocomposite may be because it creates high catalytic alloy surface for the hydrogen reactions during mechanical milling [140].

This study on effect of NiMnAl alloy on MgH_2 has significantly decreased the hydrogen desorption temperature, improved kinetics and moderate content of hydrogen of nanocomposite as shown in Table 6.3.

Table 6.3. Kinetic parameters for as milled MgH_2 and MgH_2-x wt% (10, 25 &50) NiMnAl nanocomposite

Hydrogen (wt %)	**Activation energy (KJ/mol)**	**Peak Temperature (°C)**	**Heating rate (°C/min)**	**Sample**
4.2	177.90 KJ/mol	353.38 352.76 337.66	5 10 15	Milled MgH_2
2.40	173.09 KJ/mol	394.65 404.82 414.19	5 10 15	MgH_2-10 wt% NiMnAl
3.54	117.62 KJ/mol	282.59 294.60 315.06	5 10 15	MgH_2-25 wt% NiMnAl
1.62	58.66 KJ/mol	282.59 294.60 315.06	5 10 15	MgH_2-50 wt% NiMnAl

6.3.2 DSC analysis

DSC investigations were carried out to investigate effect of NiMnAl (10, 25 & 50) on the MgH_2 hydrogen absorption behaviour which is shown in figure 6.7 and is compared with as-milled MgH_2.

Hydrogenation was performed under 2 MPa hydrogen pressure and a heating rate of 15°C min^{-1} was maintained during DSC scan.

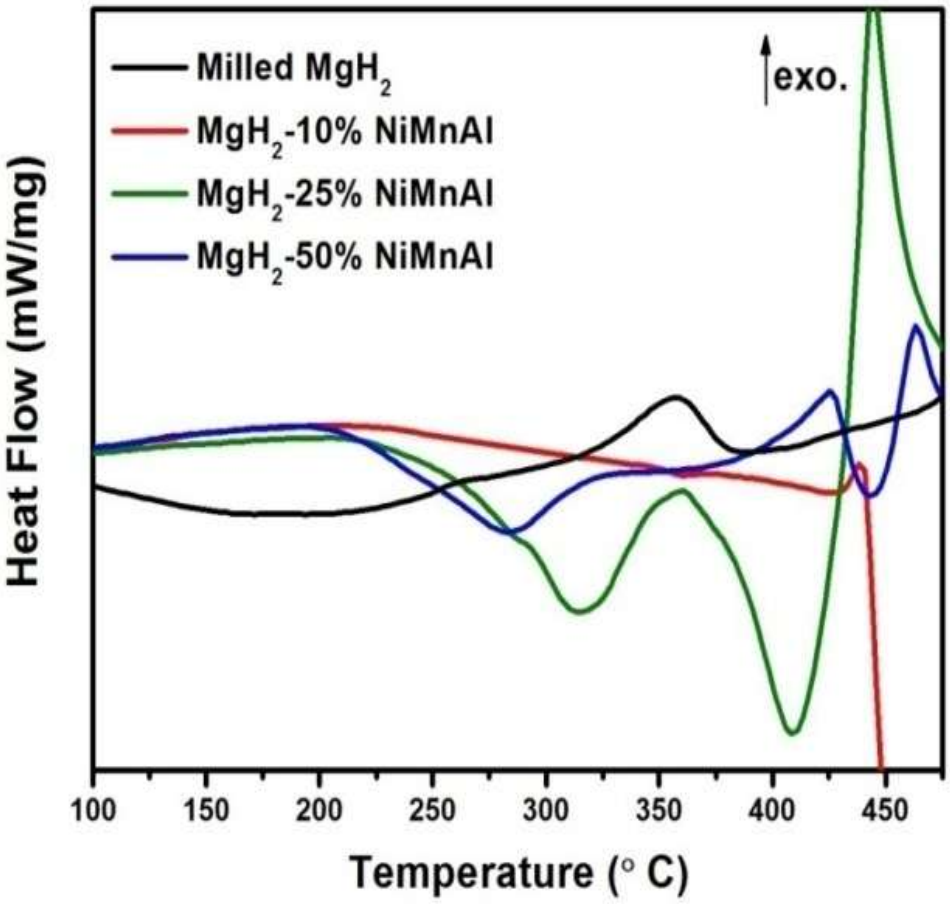

Figure 6.7: DSC curves for 10 hrs milled MgH_2 and MgH_2 -xwt% NiMnAl nanocomposites

It is observed from DSC curve that 10 hrs milled MgH_2 consists of one exothermic peak at 356 $^{\circ}$C with onset at around 320 $^{\circ}$C which means that hydrogenation could be started at as low as 320 $^{\circ}$C.

These peaks may be attributed to the presence of activated and non-activated species in the sample. The onset temperature was found to be same for nanocomposite having 25 wt% NiMnAl and it decreases about 40°C for 50 wt% indicating the positive effect of additive.

Chapter Summary

- NiMnAl alloy was synthesized first time by arc melting furnace and the effect of NiMnAl content on hydrogenation properties of MgH_2 was studied. In Nanocomposites, the presence of the Mg_2Ni, MgH_2 and Mg_2NiH_4 with good level of homogeneity was observed.

- NiMnAl alloy content significantly improves the hydrogen desorption behaviour of MgH_2 in comparison with as-milled MgH_2.

- Dehydrogenation characterization of MgH_2 with and without alloy showed that 50 wt% NiMnAl doped MgH_2 powder decreases desorption temperature by about 64°C compare to the as-milled MgH_2. TGA result shows the activation energy is lower by about 119.24 KJ/mol compared to as-milled MgH_2.

- DSC studies of as-milled MgH_2 consists of one exothermic peak at 356°C with onset at around 320°C which means that the hydrogenation could have been started at as low as 320°C. Improvement in kinetics could be associated to: (a) Refined microstructure (b) Good level of mixing and (c) Effect of alloy additives during desorption processes.

The next chapter presents the role of $NiMn_{9.3}Al_{4.0}Co_{14.1}Fe_{3.6}$ alloy on dehydrogenation kinetics of MgH_2.

*****

Chapter-7

ROLE OF $NiMn_{9.3}Al_{4.0}Co_{14.1}Fe_{3.6}$ ON DEHYDROGENATION KINETICS OF MgH_2

Introduction

The current chapter discussed the results based on study the influence MgH_2-x wt% $NiMn_{9.3}Al_{4.0}Co_{14.1}Fe_{3.6}$ (x=10, 25 & 50) additive on the hydrogenation properties of ball milled MgH_2 with various concentrations. Nanocomposites were characterized by x-ray diffraction (XRD), scanning electron microscopy (SEM) with EDS analysis, differential scanning calorimetry (DSC) and thermo gravimetric analysis (TGA).

7.1 Structural Characterization by XRD

Figure7.1 shows XRD patterns of the Mg-based nanocomposites containing 10, 25 %50 wt% $NiMn_{9.3}Al_{4.0}Co_{14.1}Fe_{3.6}$ as additive after 10 h of ball milling.

In these XRD patterns various phases were identified e.g. MgH_2, Mg_2NiH_4 and $Al_{60}Mn_{11}Ni_4$.The presence of MgO hydride phases containing additives species were not observed in the XRD patterns of the powder mixtures processing.

It was observed that the broadening of peak in as-milled MgH_2 samples and it could be attributed to the refinement of crystallite size and the presence of lattice strain.
The average crystallite size was calculated using Debye Scherer formula,

$$\boldsymbol{D = \frac{0.9\lambda}{\beta \cos\theta}}$$

Where, λ =X-ray wavelength,

β = Line broadening at half the maximum intensity (radian)

θ = Bragg angle

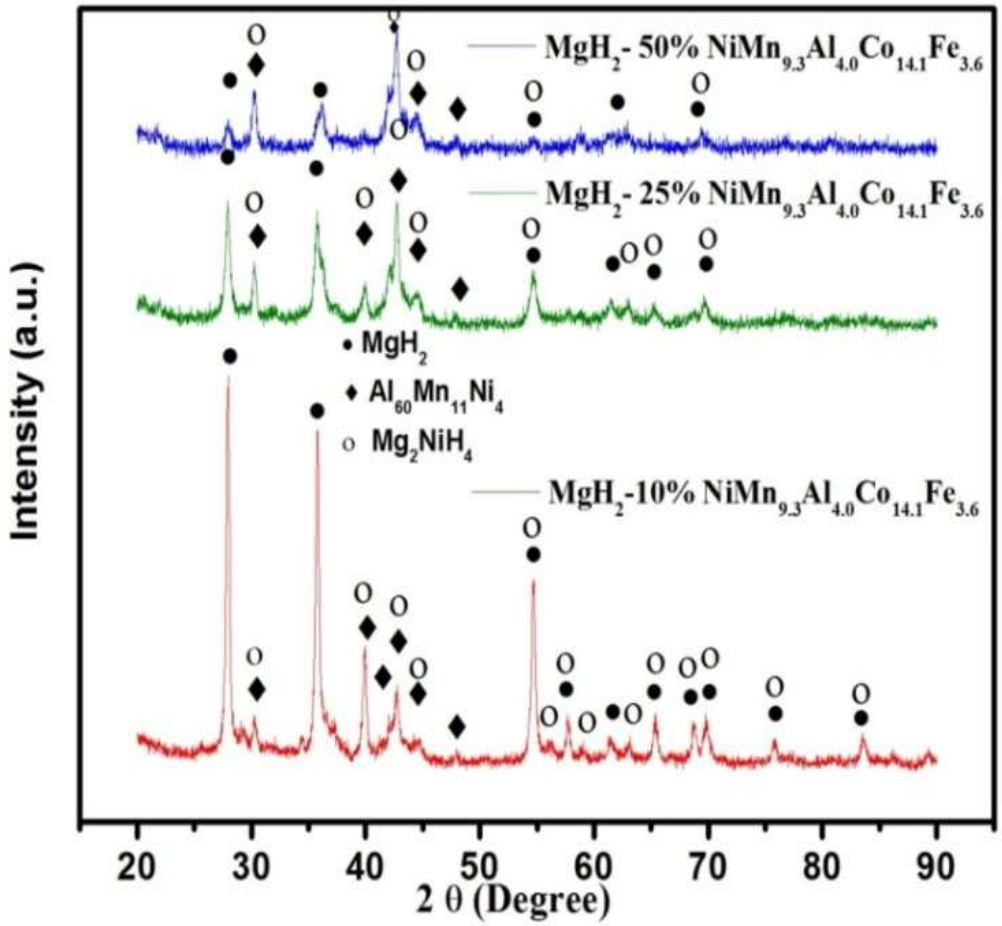

Figure 7.1. XRD pattern of MgH_2-x wt% (10, 25, 50) $NiMn_{9.3}Al_{4.0}Co_{14.1}Fe_{3.6}$

The increase in unit cell volume on activation is due to hydrogen absorption which decreases density of alloy resulting in decrease in lattice constant. Hydrogen absorption increases volume of alloy which may be 15 to 35% resulting in decrease in density as shown in figure 7.2 results in

increasing lattice constants. While desorption of hydrogen the material takes original shape showing the increase in density that is decrease in lattice constant. The peak intensities decrease with the broadening of peaks which indicates accumulation of mechanical strains and reduction in particle size during milling [141].

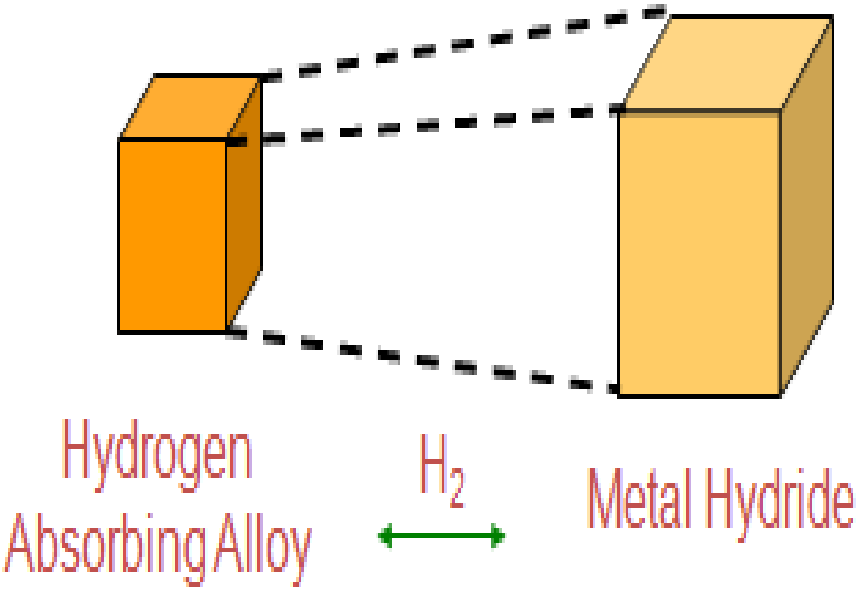

Figure 7.2. Expansion & Contraction Effects due to hydrogen.

Using Debye Scherer formula, the values of average crystallites size for the MgH_2-x wt% alloy (10, 25, 50) nanocomposites are estimated to be about 32 nm, 33 nm and 36 nm respectively (Table 7.1)

Table 7.1: Characteristics of the phases in the MgH_2-x wt% (10, 25, 50) $NiMn_{9.3}Al_{4.0}Co_{14.1}Fe_{3.6}$

Sample	Phase	Space group (No.)	Crystal Structure	Lattice parameters		Volume	D_{avg} (nm)
				a[Å]	*c*[Å]	V[Å ^{3}]	
x=10	MgH_2	$P4_2/mnm$(136)	Tetragonal	4.517	3.0205	61.63	

	$Al_{60}Mn_{11}Ni_4$ Mg_2NiH_4	Amam (63) Cc (9)	Orthorhombic Monoclinic	12.5 15.0374	7.55 6.4932	2246.13 548.75	32
x=25	MgH_2 $Al_{60}Mn_{11}Ni_4$ Mg_2NiH_4	$P4_2/mnm$(136) Amam (63) Cc (9)	Tetragonal Orthorhombic Monoclinic	4.517 12.5 15.0374	3.0205 7.55 6.4932	61.63 2246.13 548.75	33
x=50	MgH_2 $Al_{60}Mn_{11}Ni_4$ Mg_2NiH_4	$P4_2/mnm$(136) Amam (63) Cc (9)	Tetragonal Orthorhombic Monoclinic	4.517 12.5 15.0374	3.0205 7.55 6.4932	61.63 2246.13 548.75	36

7.2 Morphology of nanocomposite by SEM

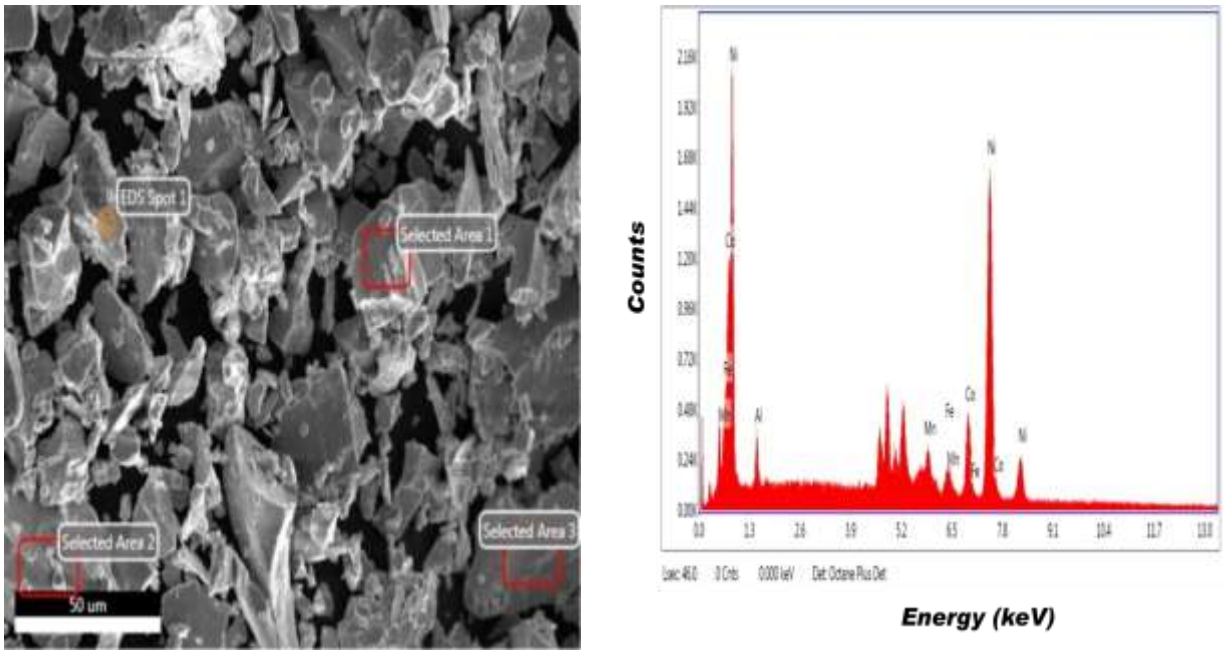

Figure 7.3: EDS analysis of the $NiMn_{9.3}Al_{4.0}Co_{14.1}Fe_{3.6}$

The elemental composition of the alloy has been checked by EDS technique at different sites of the ingots and thee elemental composition was found almost same at all the sitesas shown in Figure 4.The elemental percentage is shown in Table 2.

Table 7.2. Chemical composition in the alloy by EDS analysis

Weight %					
Area	**Ni**	**Mn**	**Al**	**Co**	**Fe**
1	68.99	9.26	4.04	14.14	3.57
2	67.44	11.61	2.64	13.89	4.43
3	64.04	13.72	1.55	14.77	5.92
EDS Spot 1	65.97	14.35	1.64	13.24	4.80
EDS confirms composition of material under study					

The morphology of the $NiMn_{9.3}Al_{4.0}Co_{14.1}Fe_{3.6}$ alloy observed by Scanning Electron Microscopy is shown in figure7.3.

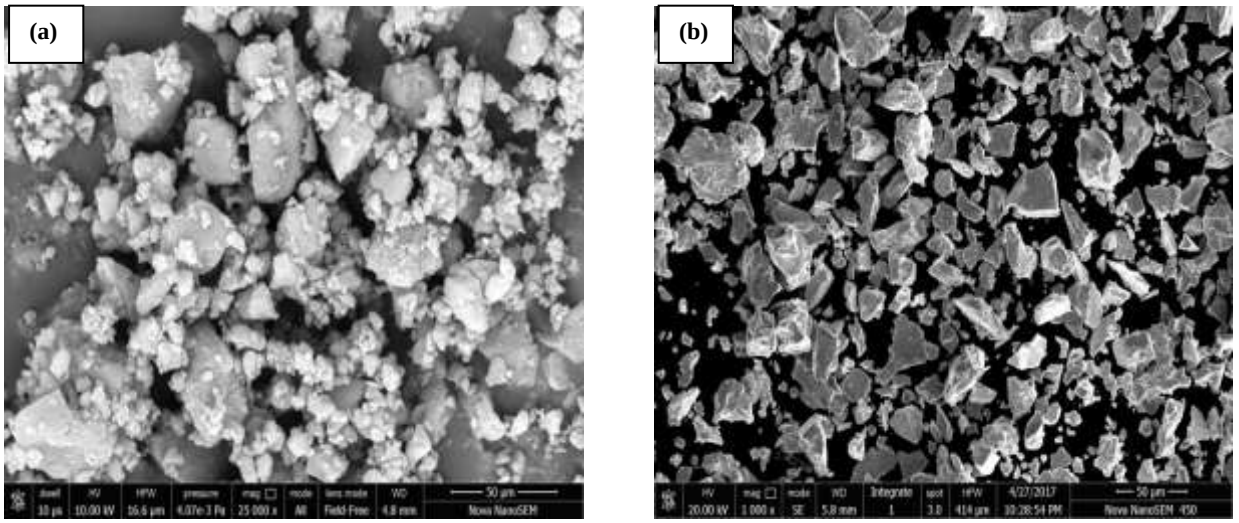

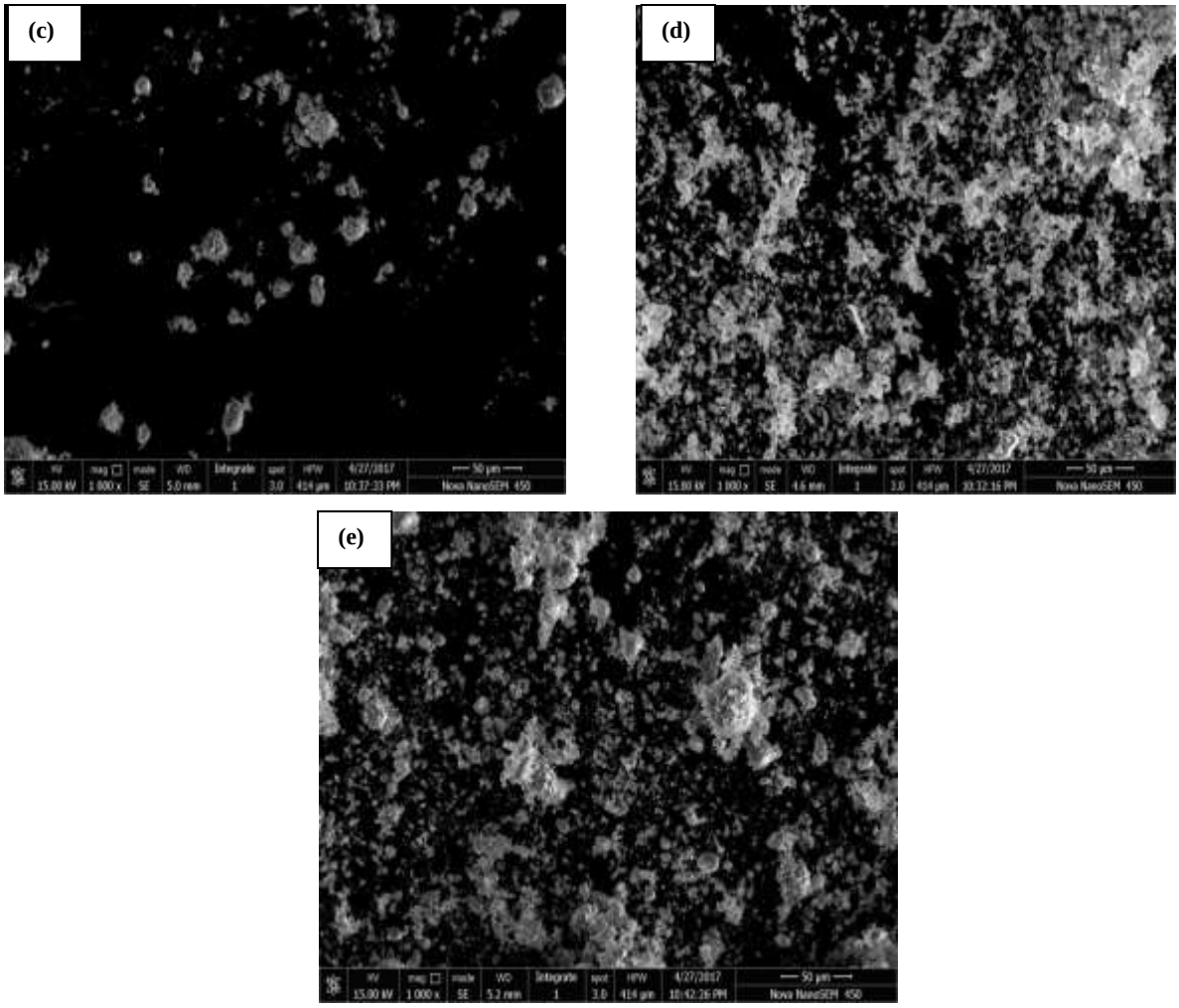

Figure 7.4. SEM image of (a) as-milled MgH_2 (b) pure $NiMn_{9.3}Al_{4.0}Co_{14.1}Fe_{3.6}$ (c) MgH_2-10 wt% $NiMn_{9.3}Al_{4.0}Co_{14.1}Fe_{3.6}$ (d) MgH_2-25 wt% $NiMn_{9.3}Al_{4.0}Co_{14.1}Fe_{3.6}$ (e) MgH_2-50 wt% $NiMn_{9.3}Al_{4.0}Co_{14.1}Fe_{3.6}$

The morphology of the $NiMn_{9.3}Al_{4.0}Co_{14.1}Fe_{3.6}$ observed by Scanning Electron Microscopy is shown in figure 7.4. It is obvious that increasing the concentration from 10 wt% to 50 wt% alloy content increases. Mechanical milling is effective in decreasing the size of particles and providing more fresh active surface. It has been reported that the kinetics of MgH_2 can be enhanced by decreasing the particle size which can lead to a reduction in the hydrogen diffusion pathway [142].

The inhomogeneous contact of the powders and steel balls during the ball-milling process could be the cause of this inhomogeneous particle size distribution [143]. It can be observed that the addition of alloy to the MgH_2 and 10 hrs of ball milling reduce the particle size which can have the benefit of more free surface and probably result in increased hydrogen desorption [144]. It is seen that the alloy powder consisted of particles varying in size 10-30 mm with irregular shapes and relatively smooth surfaces.

The change in the structure of particle metal powders is due to the different sizes of all the substituted elements. The emergence of nano-sized particles in the sample shows that high-energy ball milling is an ideal method to decrease the particle size of the powder particles down to the nano-scale and, consequently, increase the surface area and potential sites of hydrogen desorption.

7.3 Kinetic Study of the Dehydrogenation/Hydrogenation Process

7.3.1 TGA analysis

TGA studies on as-milled MgH_2 resulted in release of 7.3 wt% at 360°C hydrogen with onset temperature of 260°C. Figure 7.5(a) shows the TGA profiles of as-milled and MgH_2-x wt% alloy (x=10, 25 & 50) nanocomposite at a heating rate of 10°C/min under 0.1 MPa Ar atmospheres. The total relative weight loss of 10 h milled MgH_2 and MgH_2–x wt% alloy is respectively about 7.3 wt%, 5.4 wt%, 3 wt% and 2 wt% as shown in figure 7.5(a).

DTA curve to analyze peak temperature of the as-milled MgH_2 and MgH_2-x wt% $NiMn_{9.3}Al_{4.0}Co_{14.1}Fe_{3.6}$ nanocomposites under different heating rate 5, 10 &15 °C/min are shown in Figure 7.6 (a).

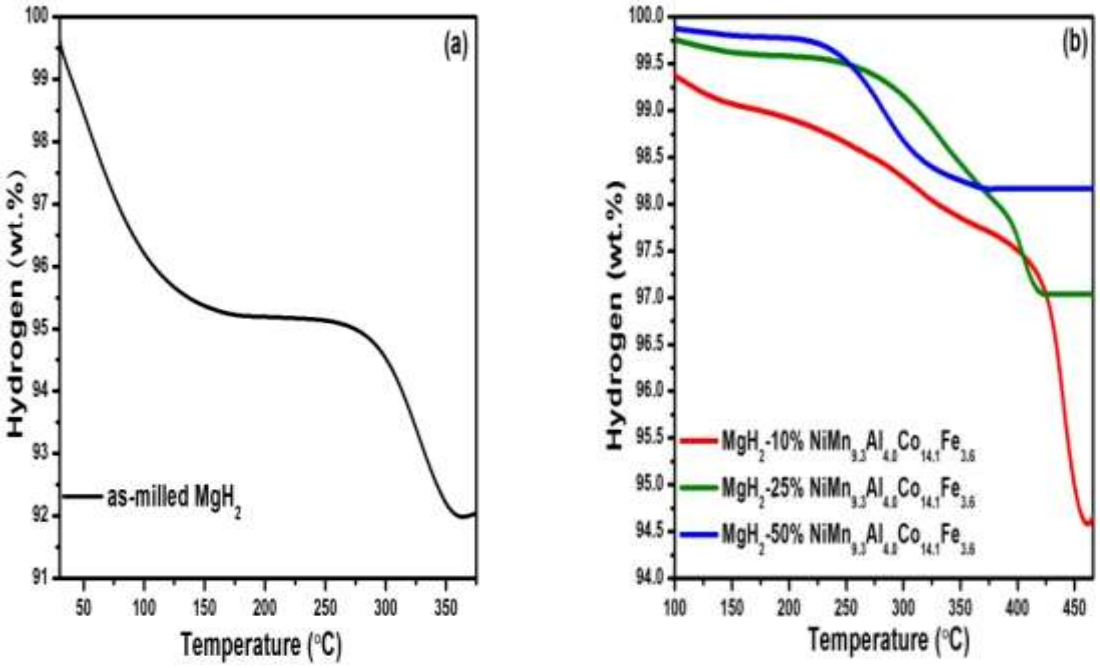

Figure 7.5: Hydrogen content measurement (a) as- milled MgH_2 (b) MgH_2- x wt% $NiMn_{9.3}Al_{4.0}Co_{14.1}Fe_{3.6}$ (x = 10, 25, 50) nanocomposites.

The as-milled MgH_2 without the catalysts starts to decompose at 260°C. With the addition of alloy the starting temperature of H_2 desorption decreases from 260°C to 220°C, 210°C and 180°C for 10, 25 and 50 wt% respectively.

There is slight reduction in the desorption temperature as the concentration increase to 25 to 50 wt%. The lowest onset temperature value is observed for the 50 wt% alloy doped sample, followed by the 10 wt% doped and the 25 wt% doped samples, while the pure MgH_2 sample gives the highest value.

It indicates that alloy significantly improves desorption properties of MgH_2.

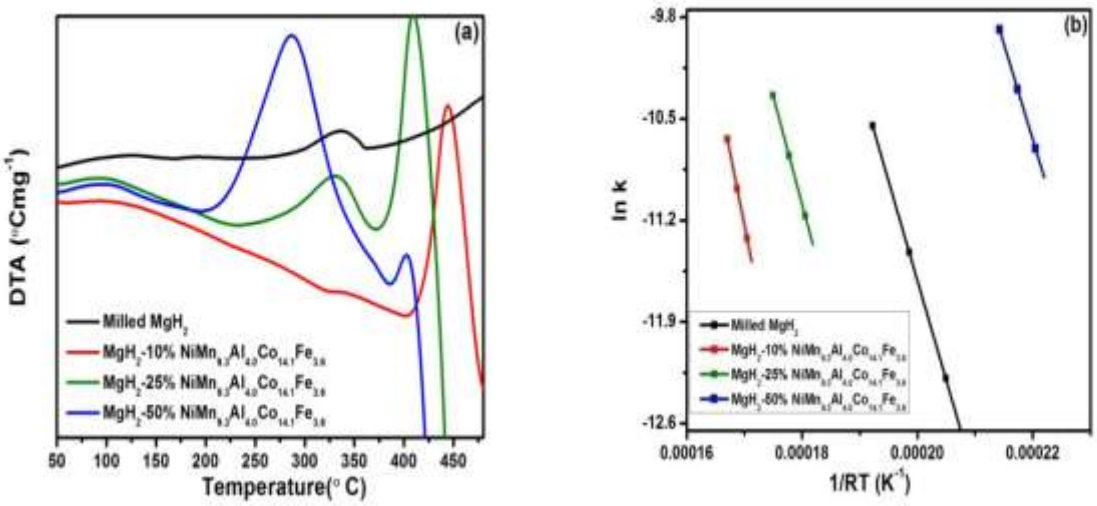

Figure7.6. (a) DTA curve (b) Kissinger plot for dehydrogenation of the as- milled MgH_2 and MgH_2- x wt% $NiMn_{9.3}Al_{4.0}Co_{14.1}Fe_{3.6}$ (x = 10, 25 & 50) nanocomposites.

The activation energy of dehydrogenation for the MgH_2-alloy systems was evaluated to understand the effect of alloy on the dehydrogenation of MgH_2. Calculating activation energy of dehydrogenation at three different heating rates (5, 10 & 15$^oCmin^{-1}$).

The activation energy can be calculated by plotting a curve between ln k and $1/RT_P$ using the following equation [28],

$$\boldsymbol{lnk = -\frac{E_a}{RT_P} + a}$$

Where, $k = \beta/T_P^2$

β = heating rate,

T_p= peak temperature

Ea=activation energy of desorption

R = gas constant

Figure7.6 (b) Shows Kissinger plot of the hydrogen desorption reaction for catalyzed MgH_2 samples. The activation energies were estimated from the slope of the straight line to be 177.90

KJ/mol for as-milled MgH_2, 200.62 KJ/mol, 148.85 KJ/mol, 131.34 KJ/mol for MgH_2-x wt% $NiMn_{9.3}Al_{4.0}Co_{14.1}Fe_{3.6}$ (x=10,25 & 50) respectively.

From the data, it is clear that the addition of alloy to MgH_2 lower its activation energy. It is thought that the activation energy is not directly related to the hydrogen desorption kinetics; it is a barrier that must be overcome to start the release of hydrogen. But the speed of hydrogen release also depends on other factors, such as alloy effect, surface area and particle size. There was also a slight correlation between activation energy and desorption temperature as well. Samples with high activation energies tended to have high thermal stabilities.

The above results indicate a significant improvement in dehydrogenation kinetics of MgH_2 by the addition of alloy. It is interesting to observe that increasing Ni content brings decreases hydrogen desorption activation energy facilitating the improvement of hydrogen desorption kinetics of nanocomposite. Ni may be creating high catalytic alloy surface for the hydrogen reactions during mechanical milling [145].

This study on effect of $NiMn_{9.3}Al_{4.0}Co_{14.1}Fe_{3.6}$ on MgH_2 has significantly decreased the hydrogen desorption temperature, improved kinetics and moderate content of hydrogen of nanocomposite as shown in Table 7.3.

Table 7.3. Kinetics parameters for MgH_2-$NiMn_{9.3}Al_{4.0}Co_{14.1}Fe_{3.6}$ nanocomposites

Hydrogen (wt %)	Activation energy (KJ/mol)	Peak Temperature (°C)	Heating rate (°C/min)	Sample
7.3	177.90	353.38 352.76 337.66	5 10 15	Milled MgH_2

5.4	200.62	427.09 444.82 444.41	5 10 15	MgH_2-10 wt% $NiMn_{9.3}Al_{4.0}Co_{14.1}Fe_{3.6}$
3	148.85	386.33 401.85 412.28	5 10 15	MgH_2-25 wt% $NiMn_{9.3}Al_{4.0}Co_{14.1}Fe_{3.6}$
2	131.34	267.16 275.81 286.65	5 10 15	MgH_2-50 wt% $NiMn_{9.3}Al_{4.0}Co_{14.1}Fe_{3.6}$

7.3.2DSC analysis

DSC investigations were undertaken to investigate the effect of (10, 25 & 50) wt% $NiMn_{9.3}Al_{4.0}Co_{14.1}Fe_{3.6}$ on hydrogen absorption in MgH_2 which is shown in figure 7.7 and is compared with as-milled MgH_2.

Hydrogenation was performed at heating rate of 15°C min^{-1} was maintained during DSC studies. It is observed from DSC curves that 10 h milled MgH_2 consists of two exothermic peaks at 260 $^{\circ}$C and 356°C with onset at around 220°C, which means that the hydrogenation could be started at as low as 220 °C.

These peaks may be attributed to the presence of activated and non-activated species in the sample. The addition of alloy reduce the onset temperature to 155°C for MgH_2-10 wt% alloy sample which further reduce to 17°C for 25 wt%.

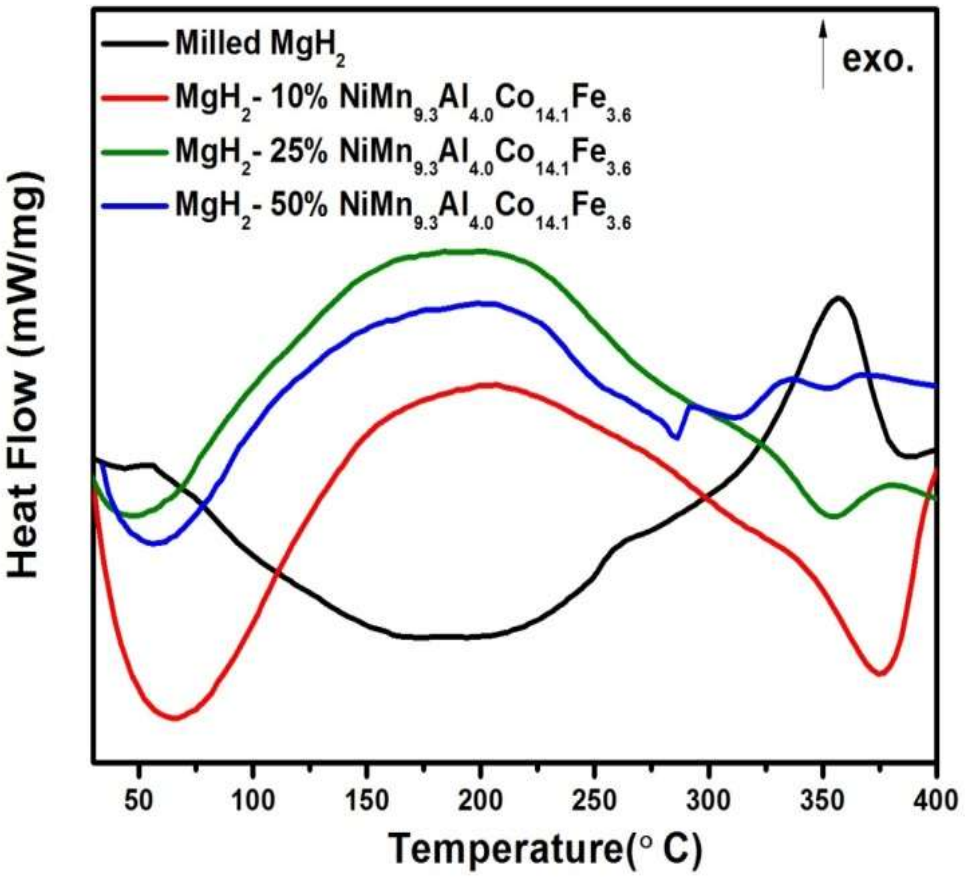

Figure7.7: DSC curves for 10 hrs milled MgH_2 and MgH_2 –x wt% $NiMn_{9.3}Al_{4.0}Co_{14.1}Fe_{3.6}$ nanocomposites

On increasing the concentration 25 wt% to 50 wt% alloy added MgH_2 the onset temperature remains same. After the addition of alloy a single broad exothermic peak was obtained between the temperature ranges 48°C-353°C.

Chapter Summary

- $NiMn_{9.3}Al_{4.0}Co_{14.1}Fe_{3.6}$ was synthesized first time by arc melting furnace and the effect of alloy content on hydrogenation properties of MgH_2 were studied.

- The average crystallites size for the MgH_2-x wt% $NiMn_{9.3}Al_{4.0}Co_{14.1}Fe_{3.6}$ (10, 25 & 50) nanocomposites were estimated to be about 32 nm, 33 nm and 36 nm.

- Dehydrogenation characterization of MgH_2 with and without $NiMn_{9.3}Al_{4.0}Co_{14.1}Fe_{3.6}$ showed that the 50 wt% $NiMn_{9.3}Al_{4.0}Co_{14.1}Fe_{3.6}$ doped MgH_2 powder decreases desorption temperature by about 80°C compare to the as-milled MgH_2.

- TGA result shows the activation energy of nanocomposite is lower by about 46.56 kJ/mol compared to as-milled MgH_2 and 50 wt% added alloy sample shows best result.

- DSC curves show that 10 h milled MgH_2 consists of two exothermic peaks at 260°C and 356°C with onset at around 220°C, which means that the hydrogenation could be started at as low as 220°C.

The next chapter presents the conclusion of the thesis work and scope for future work.

*****

Chapter-8

CONCLUSIONS

Following conclusions are drawn from the research work:

- The hydrogen decomposition of theMgH_2-x wt.% $La_{23}Nd_{7.8}Ti_{1.1}Ni_{33.9}Co_{32.9}Al_{0.65}$ takes place at a lower temperature in comparison to the as-milled MgH_2.

- The activation energy for the dehydrogenation of MgH_2-25 wt% $La_{23}Nd_{7.8}Ti_{1.1}Ni_{33.9}Co_{32.9}Al_{0.65}$ is 79.15 KJ/mol, which is much lower than the results determined for the as milled MgH_2 (177.90 KJ/mol).

- Desorption kinetics of MgH_2 is improved with the addition of different concentrations (10, 25 & 50) of FeTi. MgH_2-25 wt% FeTi nanocomposite has shown decreased desorption temperature by about 60°C compared to the as-milled MgH_2.

- Activation energy is lowered by about 89 kJ/mol for MgH_2-50 wt% FeTi compared to as-milled MgH_2 indicating 50 wt% added FeTi sample shows better results.

- Hydrogen desorption temperature and activation energy of the MgH_2-FeTi nanocomposites decreases linearly with increasing weight fraction of FeTi.

- Dehydrogenation characterization of MgH_2 with and without NiMnAl showed that addition of 50 wt% NiMnAl in MgH_2 powder decreased desorption temperature by 64°C compared to the as-milled MgH_2.

- Activation energy of MgH_2-50 wt% $NiMn_{9.3}Al_{4.0}Co_{14.1}Fe_{3.6}$nanocomposite is lowered by 46.56 kJ/mol compared to as-milled MgH_2.

- Dehydrogenation characterization of MgH_2 with and without $NiMn_{9.3}Al_{4.0}Co_{14.1}Fe_{3.6}$ shows that the 50 wt% $NiMn_{9.3}Al_{4.0}Co_{14.1}Fe_{3.6}$ doped MgH_2 powder decreased desorption temperature by 80°C compare to the as-milled MgH_2.

- The average crystallites sizes for the MgH_2-x wt% $NiMn_{9.3}Al_{4.0}Co_{14.1}Fe_{3.6}$ (x=10, 25 & 50) nanocomposites are estimated to be about 32 nm, 33 nm and 36 nm, respectively.

- Table 8.1 gives the comparsion of different nanocomposites prepared by subsequent arc melting followed by ball milling.

Table 8.1. Comparsion of present nanocomposites

Sample	H_2 (wt %)	Activation Energy (KJ/mol)	Onset temperature (°C)
MgH_2-25 wt% $La_{23}Nd_{7.8}Ti_{1.1}Ni_{33.9}Co_{32.9}Al_{0.65}$	1.27	137.29	181
MgH_2-25 wt% FeTi	2.10	162.46	250
MgH_2-25 wt% NiMnAl	3.54	117.62	196
MgH_2-25 wt% $NiMn_{9.3}Al_{4.0}Co_{14.1}Fe_{3.6}$	3.00	148.85	210

This table shows that MgH_2-25 wt% NiMnAl is better than the other nanoocmposites

The next chapter presents the suggestions for future work of the thesis.

*****

Chapter-9

SUGGESTIONS FOR FUTURE WORK

Following aspects are suggested for further studies:

1. The studies are mainly focused on kinetic properties of nanocomposites. However, few parameters may be introduced such as effect of change in concentration of the nanocomposites, ball to powder ratio and milling time.

2. Hydrogen storage studies are to be continued, using both experimental and theoretical tools, to find newer materials with suitable thermodynamics and kinetics properties, which can store higher amount of hydrogen.

3. P-C-T isotherm may be done for hydrogen storage capacity of absorption-desorption cycle.

4. Electrochemical properties and temperature programmed desorption (TPD) studies may be obtained for nanocomposites.

5. XPS studies may be undertaken to characterize the phase changes during milling and dehydrogenation.

REFERENCES:

[1] C.J. Winter and J. Nitsch, eds., Hydrogen as an energy carrier: technologies, systems, economy (Springer, Berlin, 1988).

[2] L. Schlapbach and A. Zuttel, Nature, 14 (2001) 353.

[3] J.M. Ogden, Physics Today, (April 2002) 69.

[4] R. Gross, M. Leach, A. Bauen, environ. Int.,29 (2003) 105.

[5] http://www.ornl.gov/divisions/ctd/march2.htm.

[6] A. Haavisto, M. Soininen, K. Varho, Maol Taulukot, Kemian Osa, Maolry and Kustannusosakeyhtio Otava, Finland 1978.

[7] New Hydrogen Technologies Neste Corporate R and D Project report: Evaluation of technologies, (Neste Oy, Finland 1992).

[8] Inc. www.qtww.com, webpage of quantum technologies.

[9] S. Sherif, T. Veziroglu, N. Zeytinoglu, Int. J. Hydrogen Energy, 22; 7 (1997) 683.

[10] U.S. Department of energy (DOE), Energy efficiency and renewable energy network, consumer energy information: EREC reference briefs. Hydrogen fuel (www.eren.doe.gov/consumerinfo/rebriefs/a10g.htm).

[11] W. Peschka, Liquid hydrogen fuel of the future, Springer-Verlag, Ny, USA, 1992.

[12] S. Aceves, J. Martinez-Frias, O. Garcia-villazana, Analytical and experimental evaluation of insulated pressure vessels for cryogenic hydrogen storage, Int. J. Hydrogen Energy, 25 (2000) 1075.

[13] H. Ewe, Selbach, the storage of hydrogen. In: A solar hydrogen energy system, Ed. Justi, Plenum Press, UK 1987.

[14] K. Yvon and P. Fischer, hydrogen in intermetallic compounds, Topics in applied physics, ed. L. schlapbach 1988 (Springer-Verlag, Berlin, 87).

[15] G. Sandrock, A. Panoramic overview of hydrogen storage alloys from a gas reaction pt. of view, J. Alloys and Compounds, 293-295 (1999) 877.

[16] K. Gross, G. Sandrock, G. Thomas, Hydride Development for hydrogen storage, Proc. of 2000 U.S. DOE hydrogen program review, USA 2000.

[17] A. Zaluska, L. Zaluski, and J. O. Strom-olsen, J. Alloys and Compounds, 298 (2000) 125.

[18] C.M. Jensen and K.J. Gross, Appl. Phys. A, 72 (2001) 213.

[19] S. Lee and Y. Lee, Appl. Phys. Lett., 76 (2000) 2877.

[20] Bae, J. Bok, Y.C. Choi, Y.G. Choi, T. Frauenheim, N. Kim, S.Y. Lee, Y. Lee, K. Nahm, K. Park, and S. Yu, Synthetic metals, 113 (2001) 209.

[21] S. An, T. Frauenheim, W. Kim, S. Lee, Y. Lee, Y. Park, G. Seifert, Synthetic metals,113 (2001) 1189.

[22] A. Chambers, C. Park, R.T.K. Baker, N.M. Rodrigue, J. Phys. Chem., 102 (1998) 4253.

[23] A.C. Dillon, K.M. Jones, T.A. Bekkedahal, C.H Kiang, D.S. Bethune and M.J. Heben, Nature, 386 (1997) 1997.

[24] M. Hirscher, M. Becher, U.D. Weglikowska, Abstract 2000 MRS Fall Meeting Session A 9.3, (2000) 17.

[25] M.B. Brzezinska, A. Czerwinski, J. Kleperis, M. Kopczyk, J. Skowrowski, G.Wojcik, J. solid state electrochem., 5 (2001) 29.

[26] Y. Ye, C.C. Ahn, C. Witham, B. Fultz, J. Liu, A.G. Rinzler, D. Colbert, K.A.Smith, R.E. Smalley, Appl. Phys. Lett., 74 (1999) 2307.

[27] C. Catlow, Zeolites: Structure, Synthesis, and properties – An Introduction. In: Modeling of structure and reactivity in zeolites, ed. Catlow, Academic press, UK 1992.

[28] S. Ernst, M. Fritz, J. Weitkamp, Int. J. Hydrogen Energy, 20:12 (1995) 967.

[29] D. Morgan, F. Sissine, Hydrogen: technology and policy, Congressional research service, Report for congress, USA 1995 (http://www.cnie.org/nle/eng-4.html)

[30] G. Eklund, O. Von Krusenstierna, Int. J. Hydrogen Energy, 8 (1983) 463.

[31] C. Padro, V. Putsche, Survey of the economics of hydrogen technologies, technical report, National Renewable Energy Laboratory, Colorado, USA (1999).

[32] T. Carter, L. Cornish, Hydrogen in metals, Engineering Failure Analysis, 8(2001)113.

[33] P. Fischer, K. Yvon, Crystal and magnetic structures of ternary metal hydrides: A comprehensive review, In: hydrogen in intermetallic compounds I, ed. Schlapbach, Springer-verlag, Germany 1988.

[34] Billur Sakintuna, Benno Weinberger, Farida Lamari-Darkrim, Michael Hirscher, Dogan Bilal, Metal hydride materials for solid hydrogen storage: a review. Int J Hydrogen Energy 32 (2007)1121-1140.

[35] Y. Fukai, The metal –hydrogen system, basic bulk properties, Springer series in materials science; 1993.

[36] P. Adelhelm , Petra E. de Jongh, The impact of carbon materials on the hydrogen storage properties of light metal hydrides, Journal of Materials Chemistry, 21 (2011) 2417-2427.

[37] http://www.ifam.fraunhofer.de/en/Dresden/HydrogenTechnology/hydrides/applications of-metal-hydrides.html.

[38] www.intechopen.com

[39] J. Bloch, Journal of Alloys and Compounds 312(2000) 135-153.

[40] C.S. Wang, X. H. Wang, Y.Q. lei, C.P Chen and Q. D Wang, Int. J. Hydrogen Energy 21 (1996) 471-478.

[41] M. Bououdina, D. Grant, and G. Walker, Int. J. Hydrogen Energy 31(2006) 177-182.

[42] V. Berube, G. Radtke, M. Dresselhaus, G.Chen, Size effects on the hydrogen storage properties of nanostructured metal hydrides: a review, Int. J. Energy Res 31(2007) 637-663.

[43] M. Dornheim , S. Doppiu, G. Barkhordarian, U. Boesenberg, T. Klassen, O. Gutfleisch, et al, Hydrogen storage in magnesium-based hydrides and hydride composites, Scr Mater 56 (2007) 841-846.

[44] A. Zuttel, P. Wenger, S. Rentsch , P. Sudan, Ph Mauron, Ch Emmenegger, $LiBH_4$ a new hydrogen storage material, J. Power Sources 118 (2003)1-7.

[45] A. Andreasen, Hydrogenation properties of Mg–Al alloys,Int. J. Hydrogen Energy 33 (2008) 7489–7497.

[46] I.P. Jain, Y.K. Vijay, L.K. Malhotra, K.S. Upadhyay, Hydrogen storage in thin film metal hydride-a review, Int. J. Hydrogen Energy 13 (1988)15-23.

[47] I.P. Jain , B. Devi, P. Sharma , A. Williamson , Y.K. Vijay , D.K. Avasthi, et al. Hydrogen in FeTi thin films by ERDA with Ag107 ions, Int. J. Hydrogen Energy 25 (2000) 517-21.

[48] W.C. Conner, J.L. Falconer, Spillover in Heterogeneous Catalysis, Chem. Rev. 95 (1995) 759–788.

[49] M. Beltowska-Brzezinska, A. Czerwinski, J. Kleperis, M. Kopczyk, J. Skowrouski, J. Solid State Electrochem., 5 (2001) 229.

[50] http://hydpark.ca.sandia.gov, Metal Hydride Internet Database, constructed by DOE, International Energy Agency (IEA), and Sandia National Laboratories.

[51] K. Jang, D. Kim, J. Lee, J. Alloys and Compounds, 293-295 (1999)583.

[52] I.P. Jain, M.I.S. Abu Dakka, Hydrogen absorption–desorption isotherms of $La_{(28.9)}Ni_{(67.55)}Si_{(3.55)}$ Int. J. of Hydrogen Energy 27 (2002) 395–401.

[53] H.H. Cheng, H.G. Yang, S.L. Li, X. X. Deng, D. M. Chen, K. Yang, Effect of hydrogen absorption/desorption cycling on hydrogen storage performance of $LaNi_{4.25}Al_{0.75}$, J. Alloys and Compounds, 453 (2008) 448-452.

[54] V. Roman, Denys, A. Volodymyr. Yartys, Effect of magnesium on the crystal structure and thermodynamics of the $La_{3-x}Mg_xNi_9$ hydrides J. Alloys and Compounds, 509 (2011) S540-S548.

[55] S.L. Li , W. Chen , G. Luo , X.B. Han , D.M. Chen , K. Yang , W.P. Chen. Effect of hydrogen absorption/desorption cycling on hydrogen storage properties of a $LaNi_{3.8}Al_{1.0}Mn_{0.2}$ alloy, Int. J. Hydrogen Energy 37 (2012) 3268-3275.

[56] A. Andrey, Poletaev, V. Roman. Denys, Jan Petter Maehlen and V. A. Yartys. Nanostructured rapidly solidified $LaMg_{11}Ni$ alloy: Microstructure, crystal Structure and hydrogenation properties. Int. J. Hydrogen Energy 37 (2012) 3548-3557.

[57] Zhu Yunfeng, Yang Yang, Wei Lingjun, Zhao Zelun, Li Liquan. Hydrogen storage properties of Mg–Ni–Fe composites prepared by hydriding combustion synthesis and mechanical milling, Journal of Alloys and Compounds, 520 (2012) 207-212.

[58] Gao Zhijie, Kang Long and Luo Yongchun. Microstructure and electrochemical hydrogen storage properties of La–R–Mg–Ni-based alloy electrodes, New J. Chem. 37(2013) 1105.

[59] He-xin Chen, Zhongmin Wang, Huai-ying Zhou , Qing-rong Yao, Hydrogen storage properties and thermal stability of amorphous $Mg_{70}(RE_{25}Ni_{75})_{30}$ alloys, J. Alloys and Compounds 563 (2013) 1–5.

[60] Xilin Zhu,Lichao Pei, Ziyang Zhao, Baozhong Liu, Shumin Han, Ruibing Wang**.** The catalysis mechanism of La hydrides on hydrogen storage properties of MgH_2 inMgH_2 + *x* wt% LaH_3 (*x* = 0, 10, 20 &30) composites, J. Alloys and Compounds577 (2013) 64-69.

[61] Zareii, Hadi Arabi**,** Faiz Pourarian. Synthesis, Characterization and hydrogen storage properties of Mm(Ni,Co,Mn,Al)$_5$alloy , Iranian journal of hydrogen & fuel cell, 2(2014) 83-94.

[62] L.Z. Ouyang, Z.J. Cao, L.L. Li , H. Wang , J.W. Liu , D. Min ,Y.W. Chen , F.M. Xiao , R.H. Tang , M. Zhu, Enhanced high-rate discharge properties of $La_{11.3}Mg_{6.0}Sm_{7.4}Ni_{61.0}Co_{7.2}Al_{7.1}$ with added graphene synthesized by plasma milling, Int. J. Hydrogen Energy, 39 (2014)12765 -12772.

[63] Xia Li, Tai Yang, Yanghuan Zhang , Dongliang Zhao, Huiping Ren. Kinetic properties of La_2Mg_{17}–x wt% Ni (x = 0–200) hydrogen storage alloys prepared by ball milling. Int. J. of Hydrogen Energy 39 (2014) 13557-13563.

[64] Christoph Frommen, Michael Heere, Marit D. Riktor, Magnus H. Sorby , Bjorn C. Hauback Hydrogen storage properties of rare earth (RE) borohydrides (RE = La, Er) in composite mixtures with $LiBH_4$ and LiH, J. Alloys and Compounds 645 (2015) S155–S159.

[65] Wei Lv, Yufan Shi, Wanpeng Deng, Jianguang Yuan, Youhua Yan, Ying Wu. Effect of Mg substitution for La on microstructure, hydrogen storage and electrochemical properties of $La_{1-x}Mg_xNi_{3.5}$ (x = 0.20, 0.23 &0. 25 at.%) alloys, Progress in Natural Science: Materials International 26 (2016) 177–181.

[66] Chaker Briki, Sihem Belkhiria, Mohamed Houcine Dhaou, Patricia de Rango, Abdelmajid Jemni, Experimental study of the influences substitution from Ni by Co, Al and Mn on the hydrogen storage properties of $LaNi_{3.6}Mn_{0.3}Al_{0.4}Co_{0.7}$ alloy, Int.J. Hydrogen Energy 42 (2017) 10081-10088

[67] Na Zhou, Wen-Bo Du, Pei-Long Zhang, Yong-Guo Zhu, Zhao-Hui Wang, Ke Liu, Shu-Bo Li, Microstructure and electrochemical properties of $La_{0.8-x}MM_xMg_{0.2}Ni_{3.1}Co_{0.3}Al_{0.1}$ (x = 0, 0.1, 0.2 & 0.3) alloys, Rare Metals 36 (2017) 645-650.

[68] P. Mandal, O.N. Srivastava, Hydrogenation behavior of the new composite storage material Mg-xwt% FeTi,J. Alloys and Compounds, 205, Issues 1–2 (1994) 111-118.

[69] Liang Guoxian, Wang Erde, Fang Shoushi, Hydrogen absorption and desorption characteristics of mechanically milled Mg- 35 wt% $FeTi_{1.2}$ powders, J. Alloys and Compounds223,1(1995) 111-114.

[70] P. Wang, A.M. Wang, B.Z. Ding, Z.Q. Hu, Mg–$FeTi_{1.2}$ (amorphous) composite for hydrogen storage, J. Alloys and Compounds 334 (2002) 243–248.

[71] R. Vijay, R. Sundaresan, M.P. Maiya, S. Srinivasa Murthy, Y. Fu, H.-P. Klein, M. Groll, Characterization of Mg–*x* wt% FeTi (*x* = 5–30) and Mg–40 wt% FeTiMn hydrogen absorbing materials prepared by mechanical alloying, J. Alloys and Compounds 384 (2004) 283–295.

[72] Shu-ke Peng, Xue-zhang Xiao, Rui-juan Xu, Li-xin Chen, Hydrogen storage behaviors and microstructure of MF_3 (M=Ti, Fe)-doped magnesium hydride, Transactions of Nonferrous Metals Society of China, 20 (2010) 1879-1884.

[73] Z. Zaranski, T. Czujko, The influence of ball milling process on hydrogenation properties of MgH_2–$FeTiH_x$ composites, J. Alloys and Compounds, 509S (2011) S608– S611.

[74] Babak Shalchi Amirkhiz, Beniamin Zahiri, Peter Kalisvaart,David Mitlin, Synergy of elemental Fe and Ti promoting low temperature hydrogen sorption cycling of magnesium, Int. J. Hydrogen Energy, 36, 11 (2011) 6711-6722.

[75] Chhagan Lal, I.P. Jain, Effect of ball milling on structural and hydrogen storage properties of Mg - x wt% FeTi (x=2 & 5) solid solutions, Int. J Hydrogen Energy 37 (2012) 3761 -3766.

[76] Robert A. Varin, Zbigniew Zaranski , Tomasz Czujko , Marek Polanski , Zbigniew S. Wronski,The composites of magnesium hydride and iron-titanium intermetallic, Int. J. of hydrogen energy, 36 (2011) 1177 -1183.

[77] Stefano Deledda, Ana Vassileva Borissova,Christianne Poinsignon, Thomas Klassen, H-Sorption in MgH_2 nanocomposites containing Fe or Ni with Fluorine, ChemInform 37,10 (2006) .

[78] Sunil Kumar Pandey, Anchal Srivastava, O.N. Srivastava, Improvement in hydrogen storage capacity in $LaNi_5$ through substitution of Ni by Fe, Int. J. Hydrogen Energy, 32, 13 (2007) 2461-2465.

[79] Jun Lu, Joon Choi Young, Zak Fang Zhigang, Yong Sohn Hong, Ewa Ronnebro, Hydrogen storage properties of nanosized MgH_2-0.1TiH_2 prepared by ultrahigh-energy-high-pressure milling, J. American Chemical Society 131, 43 (2009) 15843-15852.

[80] R.V. Denys, I. Yu Zavaliy, V. Paul-Boncour, V.V. Berezovets, I.V. Koval chuk, A.B. Riabov, New Mg-Mn-Ni alloys as efficient hydrogen storage materials, Intermetallics 18 (2010) 1579-1585.

[81] Haizhen Liu, Xinhua Wang, Yongan Liu, Zhaohui Dong, Guozhou Cao, Shouquan Li and Mi Yan, Improved hydrogen storage properties of MgH_2 by ball milling with AlH_3: preparations, de/rehydriding properties, and reaction mechanisms, J. Mater. Chem. A, 1 (2013) 12527.

[82] Ali Motavalli, Mohammad Rajabi ,Hydrogen desorption properties of MgH_2-5 at% Ni_3FeMn composite via combined vacuum arc remelting and mechanical alloying Articles in Press, Accepted manuscript (2014).

[83] M. Ismail, The hydrogen storage properties of destabilized MgH_2–AlH_3 (2:1) system, Materials Today: Proceedings 3S (2016) S80 – S87.

[84] G. Liang, J. Huot, S. Boily, A. Van Neste, R. Schulz, Catalytic effect of transition metals on hydrogen sorption in nanocrystalline ball milled MgH_2 –Tm (Tm=Ti, V, Mn, Fe and Ni) systems, J. Alloys and Compounds 292 (1999) 247–252.

[85] Ewa Ronnebro, Dag Noreus, Surface sensitivity of Mg_2NiH_4 leading to a profound color change, Applied Surface Science, 228, 1–4 (2004) 115-119.

[86] S. Li, G.L. Pan, X.P. Gao, J.Q. Qu, F. Wu, D.Y. Song, The electrochemical properties of $MmNi_{3.6}Co_{0.7}Al_{0.3}Mn_{0.4}$ alloy modified with carbon nanomaterials by ball milling, J. Alloys Compounds 364 (2004) 250-256.

[87] M. Ben Moussa,M. Abdellaoui, C. Khaldi, H. Mathlouthi, J. Lamloumi, A. Percheron Guegan, Effect of substitution of Mm for La on the electrochemical properties of the $LaNi_{3.55}Mn_{0.4}Al_{0.3}Co_{0.75}$ compound, J. Alloys and Compounds, 399, 1–2 (2005) 264-269.

[88] Peter Delchev, Tsveta Himitliiska, Tony Spassov, Microstructure and hydriding properties of ball-milled Mg–10 at% $MmNi_5$ (Mm = La, Ce-rich mischmetal) composites, J. Alloys and Compounds417, 1–2 (2006) 85-91.

[89] Mohammad Ismail, Y. Zhao, Xuebin Yu, S. X. Dou ,The hydrogen storage properties and reaction mechanism of the MgH_2–$NaAlH_4$ composite system, Fuel and Energy 36(15) (2011) 9045-9050.

[90] D.J. Cuscueta, L. Corso , A. Arenillas , P.S. Martinez , A.A. Ghilarducci , H.R. Salva, Electrochemical effect of carbon nanospheres on an AB_5 alloy, Int. J. Hydrogen Energy 37 (2012) 14978-14982.

[91] Rohit R. Shahi, Anandprakash Tiwari, Mohammad Shaz and O.N. Srivastava, Studies on de/rehydrogenation characteristics of nanocrystalline MgH_2 co-catalyzed with Ti, Fe and Ni.Int. J. Hydrogen Energy 38 (2013) 2778–2784.

[92] Yana Liu, Jianxin Zou, Xiaoqin Zeng, Xiaomei Wu, Dejiang Li, and Wenjiang Ding,Hydrogen storage properties of a Mg–Ni nanocomposite coprecipitated from solution, J. Phys. Chem. C, 118 (2014) 18401–18411. DOI: 10.1021/jp504918x.

[93] V. Khodaparast, M. Rajabi, Hydrogen desorption properties of MgH_2-5 Wt% Ti-Mn-Cr composite via combined melt spinning and mechanical alloying procedia materials science 11 (2015) 611 – 615.

[94] Sumita Srivastava, Kuldeep Panwar, Effect of transition metals on ball-milled $MmNi_5$ hydrogen storage alloy, Mater Renew Sustain Energy (2015) 4:19. DOI: 10.1007/s40243-015-0062-9.

[95] Stephen D. House, John J. Vajo, Chai Ren, Angus A. Rockett, Ian M. Robertson, Effect of ball-milling duration and dehydrogenation on the morphology, microstructure and catalyst dispersion in Ni-catalyzed MgH_2 hydrogen storage materials, Materials Science and Engineering 86 (2015) 55-68.

[96] Xuezhang Xiao, Chenchen Xu, Jie Shao, Liuting Zhang, Teng Qin, Shouquan Li, Hongwei Ge, Qidong Wang and Lixin Chen, Remarkable hydrogen desorption properties and mechanisms of the Mg_2FeH_6-MgH_2core–shell nanostructure, Journal of Materials Chemistry A, Issue 10 (2015).

[97] Wajid Ali, Mingyang Li, Pengyue Gao, Chong He Li, Hydrogenation properties of Ti-Fe-Mn alloy with Cu and Y as additives, Int. J. Hydrogen Energy, 42(4) (2016).

[98] Mukesh Jangir, Ankur Jain , Shotaro Yamaguchi , Takayuki Ichikawa, Chhagan Lal, I.P. Jain, Catalytic effect of TiF_4 in improving hydrogen storage properties of MgH_2,Int. J. Hydrogen Energy 41 (2016) 14178-14183.

[99] Ziying Zhang, Jiarui Jin, Huizhen Zhang, Xiao xiao Qi, Yang Bian, Hui Zhao,First-principles calculation of hydrogen adsorption and diffusion on Mn-doped Mg_2Ni (010) surfaces, Applied Surface Science 425(2017) 148-155.

[100] L. Guoxian, W. Erde, F. Shoushi, Hydrogen absorption and desorption characteristics of mechanically milled Mg–35 wt% FeTi1.2 powders, J Alloys Compds 223 (1995) 111–4.

[101] G. Liang, S. Boily, J. Huot, A.V. Neste, R. Schulz, Hydrogen absorption properties of a mechanically milled Mg–50 wt.% $LaNi_5$ composite, J Alloys Compds. 268 (1998) 302–7.

[102] G. Liang, S. Boily, J. Huot, A.V. Neste, R. Schulz, Mechanical alloying and hydrogen absorption properties of the Mg–Ni system, J Alloys Compds. 267 (1998) 302–6.

[103] M. Zhu, H. Wang, L.Z. Ouyang, M.Q. Zeng, Composite structure and hydrogen storage properties in Mg-based alloys, Int J Hydrogen Energy 31 (2006) 251–57.

[104] M. Zhu, W.H. Zhu, C.Y. Chung, Z. X. Chea, Z. X. Lia, Microstructure and hydrogen absorption properties of nano-phase composite prepared by mechanical alloying of MmNi(CoAlMn) and Mg, J Alloys Compds. 293–295 (1999) 531–5.

[105] A. Zaluska, L. Zaluski , J.O. Strom-Olsen, Synergy of hydrogen sorption in ball-milled hydrides of Mg and Mg_2Ni, J Alloys Compds. 289 (1999) 197–206.

[106] B. Bogdanovic, A. Reiser, K. Schlichte, B. Spliethoff, B. Tesche, Thermodynamics and dynamics of the Mg–Fe–H system and its potential for thermochemical thermal energy storage, J Alloys Compds.345 (2002) 77–89.

[107] K.S. Jung, E.Y. Lee, K.S. Lee, Catalytic effects of metal oxide on hydrogen absorption of magnesium metal hydride, J Alloys Compds.421 (2005) 179–84.

[108] H. Imamura, K. Masanari, M. Kusuhara, H. Katsumoto, T. Sumi, Y.Sakata. High hydrogen storage capacity of nanosized magnesium synthesized by high energy ball-milling. J Alloys Compds. 386 (2005) 211–6.

[109] L. Fabing, J. Lijun, D. Jun, W. Shumao, L. Xiaopeng, Z. Feng, Synthesis and hydrogenation properties of Mg–La–Ni–H system by reactive mechanical alloying, Int J Hydrogen Energy (2006) in press.

[110] N.E. Tran, S.G. Lambrakos, M.A. Imam, Analyses of hydrogen sorption kinetics and thermodynamics of magnesium–misch metal alloys, J Alloys Compds. 407 (2006) 240–8.

[111] https://www.energy.gov/eere/fuelcells/doe-technical-targets-onboard-hydrogen-storage-light-duty-vehicles

[112] S. Xiangqian, C. Yungui, T. Mingda, W. Chaoling, D. Gang, K. Zhenzhen K, The structure and 233K electrochemical properties of MgH_2-$La_{0.8-x}Nd_xMg_{0.2}Ni_{3.1}Co_{0.25}Al_{0.15}$($x$ = 0.0–0.4) hydrogen storage alloys, Int. J Hydrogen Energy, 34 (2009) 2661–9.

[113] Z. Hang, X. Xiao, K. Yu, S. Li, C. Chen, L. Chen, Influence of Fe content on the microstructure and hydrogen storage properties of MgH_2-$Ti_{16}Zr_5Cr_{22}V_{57-x}Fe_x$($x$ = 2–8) alloys. Int J Hydrogen Energy, 35 (2010) 8143–8.

[114] H. Shi, S. Han, Y. Jia, Y. Liu, X. Zhao, B. Liu, Investigation on hydrogen storage properties of MgH_2-$LaMg_{8.52}Ni_{2.23}M_{0.15}$(M = Ni,Cu, Cr) alloys, J Rare Earth,31 (2013) 79.

[115] https://en.wikipedia.org/wiki/Glovebox.

[116] D. Sun, H. Enoki, F. Gingl, E. Akiba, J. Alloys Compounds 285 (1999) 279.

[117] J.S. Benjamin, Sci Am J.L. Bobet 40 (1976) 234.

[118] T. Spassov, P. Solsona, S. Surinach and M.D. Baro, J. Alloys and Compounds 349 (2003) 242-254.

[119] A. Takasaki, V.F. Huett and F.K. Kelton, Materials Transacations 43(2002) 2165- 2168.

[120] C. Suryanarayana, Prog Mater Sci 46 (2001)1.

[121] D. M. Moore and R. C. Reynolds, Jr. 1997, X-Ray diffraction and the identification and analysis of clay minerals. 2nd Ed. Oxford University Press, New York.

[122] prism.mit.edu/x-ray/Basics of XRD.ppt.

[123] X-ray diffraction, http://en.wikipedia.org/wiki/X-ray diffraction.

[124] Barbara L Dutrow, Louisiana state university christine M. Clark, astern michigan university.

[125] Proc. of national workshop on advanced methods for material characterization (NWMC-2004), BARC, Mumbai.

[126] http://en.wikipedia.org/scanning electron microscope.

[127] Willwin Edara (I/II MPharm Chips), Differential Thermal Analysis and Differential Scanning Calorigraphy.

[128] T. Hatakeyams and F.X. Quinn, Thermal analysis fundamental and application to polymer science: Thermogravimetry,John willey and sons publications 2nd Ed, 45-71(1999).

[129] T. P. Blach, E.M.Gray, J. Alloys Compd. 2006:doi:10.1016/J,Jallcom.2006 12.06.

[130] G. Sandrock, J Alloys Compd 877 (1999) 293-295.

[131] U. Eberle, G. Arnold, R.von Helmholt, J. Power Sources 154 (2006) 456.

[132] C.A. Dillon, K.M. Jones, T.A. Bekkedahl, C. H. Kiang, D.S. Bethune, M. J. Haben, Nature 386(1997) 377.

[133] N. Mahmoudi, A. Kaflou and A. Simchi, J. Power Sources, 196 (2011), 4604–4608.

[134] X. B. Yu, Z. X. Yang, H. K. Liu, D. M. Grant and G. S. Walker, Int. J. Hydrogen Energy 35 (2010) 6338–6344.

[135] H. Reule, M. Hirscher, A. Weisshardt and H. Kronmuller, J. Alloys Compd., 305 (2000) 246–252.

[136] S. Agarwal, A. Aurora, A. Jain, I. P. Jain and A. Montone, Int. J. Hydrogen Energy, 34 (2009) 9157–9162.

[137] S. Kato, A. Borgschulte, M. Bielmann and A. Zuttel, Phys. Chem. Chem. Phys., 14 (2012) 8360–8368.

[138] V. Berube, G. Chen, M.S. Dresselhaus, Impact of Nanostructuring on the Enthalpy of Formation of Metal Hydrides. Int. J. Hydrogen Energy 33 (2008) 4122−4131.

[139] M. Cabo, S. Garroni, E. Pellicer, C. Milanese, A. Girella, A. Marini, E. Rossinyol, S. Surinach and M. D. Baro, Int. J. Hydrogen Energy 36 (2011) 5400–5410.

[140] A. Patah, Takasaki and J. S. Szmyd, Int. J. Hydrogen Energy, 34 (2009) 3032–3037.

[141] Rafi-ud-din, X. H. Qu, P. Li, Z. Lin, M. Ahmad, M. Z. Iqbal, M. Y. Raque and M. H. Farooq, RSC Adv., 2 (2012) 4891–4903.

[142] R. Yavari, A. LeMoulec, F. R. de Castro, S. Deledda, O. Friedrichs, W. J. Botta, G. Vaughan, T. Klassen, A. Fernandez and A. Kvick, Scr. Mater., 52 (2005) 719–724.

[143] C.C. Nwakwuo, C. Pistidda, M. Dornheim, L. L. Hutchison and J. M. Sykes, Int. J. Hydrogen Energy, 37 (2012) 2382–2387.

[144] S. X. Tao, P. H. L. Notten, R. A. van Santen and A. P. J. Jansen, Phys. Rev. B: Condens. Matter Mater. Phys., 82 (2010) 125448.

[145] S.A. Jin, J. H. Shim, J. P. Ahn, Y. W. Cho and K. W. Yi, Acta Mater.,55 (2007) 5073–5079.

[146] M.W. Rahman, A. Castellero, S. Enzo, S. Livraghi, E. Giamello and M. Baricco, J. Alloys Compd., 509 (2011) S438–S443.

[147] P. Vermeulen, H. J. Wondergem, P. C. J. Graat, D. M. Borsa, H. Schreuders, B. Dam, R. Griessen and P. H. L. Notten, J. Mater. Chem. 18 (2008) 3680–3687.

[148] J.H. Dai, Y. Song and R. Yang, J. Phys. Chem. C, 114 (2010) 11328–11334.

[149] G.Liang, J. Huot, S. Boily, A. Van Neste and R. Schulz, J. Alloys Compd., 292 (1999) 247–252.

[150] D. Moser, D.J. Bull, T. Sato, D. Noreus, D. Kyoi, T. Sakai, N. Kitamura, H. Yusa, T. Taniguchi, W. P. Kalisvaart and P. Notten, J. Mater. Chem., 19 (2009) 18150–8161.

[151] Bassetti, E. Bonetti, L. Pasquini, A. Montone, J. Grbovic and M.V. Antisari, Eur. Phys. J. B, 43 (2005) 19–27.

[152] M.O.T. Conceicao, M.C. Brum, C. S. Guimaraes and D.S. dos Santos, J. Alloys Compd. 536 (2012) S255–S258.

[153] Shivani Agarwal, Annalisa Aurora, Ankur Jain, Jain IP, Amelia Montone , Catalytic effect of ZrCrNi alloy on hydriding properties of MgH_2, Int. J. Hydrogen Energy 34 (2009) 9157 – 9162.

[154] H.E. Kissinger. Anal. Chem. 29 (1957) 1702–1706.

[155] Sakintunaa Billur, Lamari-Darkrimb Farida, Hirscherc Michael, Metal hydride materials for solid hydrogen storage: A review, Int. J. Hydrogen Energy 32 (2007) 1121–1140.

[156] Xuan Quy Tran, Stuart D. McDonald, Qinfen Gu, Tomokazu Yamamoto, Koji Shigematsu, Kohei Aso, Eishi Tanaka, Syo Matsumura, Kazuhiro Nogita, In-situ investigation of the hydrogen release mechanism in bulk Mg_2NiH_4, J. Power Sources. 341 (2017) 130-138.

[157] Y.S. Au, M.K. Obbink, S. Srinivasan, P.C. Magusin, K.P. Jong, P.E. Jongh, The size dependence of hydrogen mobility and sorption kinetics for carbon-supported MgH_2 particles, Adv. Funct.Mater.24 (2014) 3604-3611.

[158] G. Liu, K. Wang, J. Li, Y. Wang, H. Yuan, Enhancement of hydrogen desorption in magnesium hydride catalyzed by grapheme nanosheets supported Ni-CeO_x hybrid nanocatalyst, Int. J. Hydrogen Energy 41 (2016) 10786-10794.

[159] Hosseini-Gourajoubi, M. Pourabdoli, D. Uner, S. Raygan, Effect of process control agents on synthesizing nano-structured 2Mg-9Ni-Y catalyst by mechanical milling and its catalytic effect on desorption capacity of MgH_2, Adv. Powder Technol.26 (2015) 448-453.

[160] Xuan Quy Tran, Stuart D. McDonald, Qinfen Gu, Tomokazu Yamamoto, KojiShigematsu, Kohei Aso, Eishi Tanaka, Syo Matsumura, Kazuhiro Nogita, In-situ investigation of the hydrogen release mechanism in bulk Mg_2NiH_4, Journal of Power Sources, 341 (2017) 130-138.

PUBLICATIONS

List of publications based on the research presented in this thesis

A. List of Publications in Journals

1. **Priyanka Meena**, Mukesh Jangir, Arun Kumar, Ramvir Singh, V.K. Sharma, I.P. Jain, "Improved dehydrogenation kinetics of MgH_2 due to NiMnAl" Published in Mater. Res. Express 4 (2017) 116520 (**Chapter 6**).
2. **Priyanka Meena**, Mukesh Jangir, Ramvir Singh, V.K. Sharma, I.P. Jain, "Synthesis and hydrogen storage of $La_{23}Nd_{7.8}Ti_{1.1}Ni_{33.9}Co_{32.9}Al_{0.65}$ alloys" Published in J Mater Res Technol. 7(2) (2018) 173–179 (**Chapter 4**).
3. **Priyanka Meena**, Ramvir Singh, V.K. Sharma, I.P. Jain, "Role of $NiMn_{9.3}Al_{4.0}Co_{14.1}Fe_{3.6}$ alloy on dehydrogenation Kinetics of MgH_2" Published in journal of Magnesium and alloys 000 (2018) 1–8 **(Chapter 7)**.
4. **Priyanka Meena**, Mukesh Jangir, Ramvir Singh, V.K. Sharma, I.P. Jain, "Hydrogen Kinetics Studies of MgH_2-FeTi Composites", AIP Conference Proceedings 1953, 030010 (2018); doi: 10.1063/1.5032345 **(Chapter 5)**.
5. **Priyanka Meena**, Ramvir Singh, V.K. Sharma, I.P. Jain, "Effect of $LaNi_5$ type alloy doping in MgH_2 for hydrogen storage" under review **(Chapter 4)**.

B. List of Publication in conferences

1. **Priyanka Meena**, Mukesh Jangir, Ramvir Singh, V.K. Sharma, I.P. Jain. "Hydrogen Kinetics Studies of MgH_2-FeTi Composites" 2017, 2nd International Conference on Condensed Matter and Applied Physics, Bikaner, India
2. **Priyanka Meena**, Mukesh Jangir, Ramvir Singh, V.K. Sharma, I.P. Jain. "Mg-based nanocomposites for hydrogen storage containing $La_{23}Nd_{7.8}Ti_{1.1}Ni_{33.9}Co_{32.9}Al_{0.65}$ alloys as additives" 2017, International Conference on Nanotechnology, IIT Roorkee, India.

C. Other Publications

1. Mukesh Jangir, **Priyanka Meena**, I.P. Jain. "Improved hydrogen storage properties of MgH_2 catalyzed with TiO_2", AIP Conference Proceedings 1953, 030059 (2018); doi: 10.1063/1.50323

Brief Bio-Data of the author

Ms. Priyanka Meena has done B.Tech. and M.Tech. in the year 2013 in Nanotechnology from Centre for Converging Technologies, University of Rajasthan, Jaipur.

She is an active research scholar since January 2015 of the department of Metallurgical and Materials Engineering, Malaviya National Institute of Technology, Jaipur. During her course of research she published four research papers in SCI journals, a few in journals of repute and presented some research papers in national and international conferences.

She worked for her Ph.D. under the guidance of Prof. I.P.Jain, Emeritus Professor, Centre for Non Conventional Energy Resources, University of Rajasthan, Jaipur.

Her area of interest is Hydrogen storage in materials needed for mobile and stationary applications of hydrogen energy which is the fuel for 21st century.

*****